UNIVERSITEIT VAN PRETORIA
UNIVERSITY OF PRETORIA
YUNIBESITHI YA PRETORIA

CHARACTERISATION OF FISCHER-TROPSCH WAX/LINEAR LOW-DENSITY POLYETHYLENE (LLDPE) BLENDS

by

Thobile Mhlabeni

Submitted in partial fulfilment of the requirements for the degree

Doctor of Philosophy in Chemical Technology

in the

Department of Chemical Engineering

Faculty of Engineering, Built Environment and Information Technology

University of Pretoria

Republic of South Africa

August

2023

DECLARATION

I, Thobile Mhlabeni, student No. 19409088, do hereby declare that this research is my original work and that to the best of my knowledge and belief, it has not been previously in its entirety or in part been submitted and is not currently being submitted either in whole or in part at any university for a degree or diploma, and that all references are acknowledged.

SIGNED August 2023

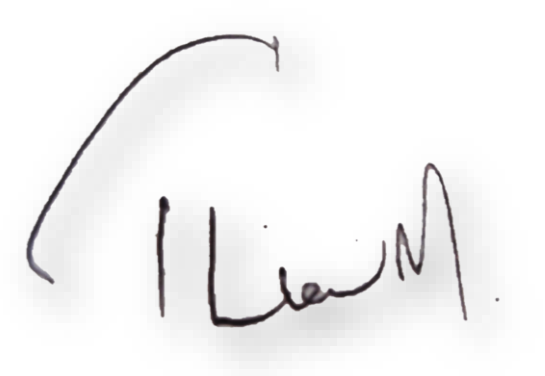

Thobile Mhlabeni

CHARACTERISATION OF FISCHER-TROPSCH (F-T) WAX/LINEAR LOW-DENSITY POLYETHYLENE (LLDPE) BLENDS

Author: Thobile L. Mhlabeni

Supervisor: Prof. Walter W. Focke

Co-Supervisor: Dr. Shatish Ramjee

Degree: PhD Chemical Technology

Department: Chemical Engineering

SYNOPSIS

Wax is often used as a processing additive in polymer compounding, particularly in thermoplastic processing, due to its ability to improve processability. Wax acts as an external lubricant in the polymer melt, reducing the melt viscosity and increasing the melt flow rate. It's addition, in masterbatching operations, facilitates improved dispersion of additives and fillers, as well as easier mixing and extrusion. Furthermore, the addition of wax to the polymer can reduce the processing temperature, leading to energy savings and reduced wear on processing equipment. However, the effectiveness of wax as a processing additive is strongly dependent on the type and amount of wax used, as well as the specific polymer being processed and its processing conditions. This study investigated the flow behaviour and compatibility characteristics of Fischer-Tropsch (F-T) wax blended with linear low-density polyethylene (LLDPE), for its possible application as a processing aid package for highly filled pigment masterbatches. The samples were prepared by melt blending using extrusion. The blends were prepared in predetermined quantities of the F-T wax

and LLDPE in increments of 10 wt-%. This study provides a survey of characterisation methods and principles using rheology, differential scanning calorimetry (DSC), and hot stage polarised optical microscopy (POM). Both sample preparation and characterisation work were conducted in a temperature range of 120 – 180 °C. Rheological behaviour of the F-T wax/LLDPE blends were measured using the cone-and-plate configuration. The results showed that small additions of LLDPE to F-T wax increased the viscosity of the blend significantly. The composition dependence of the zero-shear melt-viscosity of the blends was adequately represented by the Friedman and Porter mixing rule: $\eta_o = \left(w_p \eta_p^{1/\alpha} + w_w \eta_w^{1/\alpha}\right)^{\alpha}$ with α = 3.4. This is equivalent to the expression in which the viscosity is calculated via the weight-average molecular mass of the mixture, i.e., $\eta_0 = KM^{\alpha}$. This implies that the zero-shear melt viscosity was dominated by polymer chain entanglement. The activation energy for viscous flow was found to be insensitive to blend composition. A linear relationship in all the Han plots, i.e., the plots of the logarithm of the storage modulus (G') against the logarithm of the loss modulus (G'') was observed. Within the experimental uncertainty, they were essentially unaffected by variations in blend composition, temperature and the applied angular frequency. Additionally, the Cole-Cole plots supported the notion that the wax/LLDPE blends were miscible in the molten state. These results suggest full miscibility of the F-T wax/LLDPE blend system down to temperatures as low as 120 °C. The melting and crystallisation behaviour were studied using hot-stage optical microscopy and differential scanning calorimetry (DSC) in isothermal and dynamic modes. DSC results revealed significant LLDPE melting point depression increasing with increasing wax content. Optical microscopic monitoring of isothermal crystallisation, of the LLDPE phase, showed that adding wax decreased the size of the polymer spherulites. Beyond 50 wt-% wax, it was not possible to distinguish the spherulites at the magnification applied (25×). Overall, it was found that increasing the wax content delayed the onset of crystallisation, decreased the overall crystallinity, and reduced the size of the crystallites of the LLDPE-rich phase. The results from both techniques were consistent with partial co-crystallisation of the two components. In summary, all the results indicate full miscibility of the wax and the LLDPE in the melt and partial co-crystallisation in the solid state. Furthermore, in the dynamic DSC scans, the near complete absence of a wax-like melting peak for the blend containing 10 wt-% wax suggests complete miscibility at that concentration.

DEDICATIONS

To my son,

SIHLE LUTHANDO MHLABENI

and my parents

BASHITEGILE and MOSASEKHI MHLABENI

ACKNOWLEDGEMENTS

I would like to convey my sincerely gratitude to my supervisor Prof. Walter W. Focke for his support, patience, and encouragement throughout my time at the University of Pretoria. The insight and guidance you provided is truly appreciated!!!

I would also like to thank Dr. Shatish Ramjee for the discussions and guidance with this work.

I would also like to express gratitude to the following colleagues and friends for their assistance with instrumental operations, numerous discussions about life in general, words of encouragement, and their companion during this chapter of my life:

Dr. Isbe van der Westhuizen

Thabang Mphateng

Farirai Ashly Matshaba

Shane Lehlogonolo Tabane

Mahlako Mary

Fundiswa Madziba

Phethile Dzingai

Dr. António Benjamin Mapossa

Dennis Moyo

I would also like to appreciate the financial support from Sasol South Africa, research grant agreement SAP No# 126/20 GT

Special thanks to Dr. Basanda Nondlazi for making it seem possible. Thank you for your companion and the discussions as I strived to understand many things during this time.

I would also like to extend my most sincere gratitude and appreciation for the patience my son, Sihle Mhlabeni, has shown in my pursuit for a Ph.D. My most sincere gratitude my family, Bashitegile Mhlabeni, Mosasekhi Mhlabeni, Tommy Mhlabeni, Athalia Mhlabeni and Brain Mhlabeni for their outmost support.

Last but not least, I would like to give thanks to God in heaven "*But by the grace of God I am what I am: and his grace which was bestowed upon me was not in vain*". This work couldn't have been completed by my strength alone.

TABLE OF CONTENTS

LIST OF FIGURES

LIST OF TABLES

LIST OF ACRONYMS, ABBREVIATIONS AND DEFINITIONS

ACRONYM/ABBREVIATION	DEFINITION
Cp	heat capacity
DSC	differential scanning calorimetry
GL	generalized logistic function
DGL	time-derived generalized logistic function
FTIR	Fourier transform infrared spectroscopy
HDPE	high-density polyethylene
HF	specific heat flow
LLDPE	linear low-density polyethylene
LDPE	low-density polyethylene
LVER	linear viscoelastic region
MFI	melt flow index
POM	polarised optical microscopy
sf	scale factor
TGA	thermogravimetric analyser

LIST OF SYMBOLS

SYMBOL	DEFINITION	UNITS
A	Avrami & Hill models's proportionality factor	J g^{-1}
b	rate factor which depends on temperature	s^{-1}
b	mean spherulite diameter	µm
c	area of the crystallisation peak	J g^{-1}
G^*	complex modulus	Pa
G'	storage modulus	Pa
G''	loss modulus	Pa
ΔH	change in enthalpy	J g^{-1}
M	consistency index power law for viscosity	Pa s^{-n}
k	Herschel Bulkley consistency index	Pa s^{n}
K	Avrami constant	—
M	weight average molecular mass	Da/g mo^{-1}
M_n	number average molecular mass	mol^{-1}
n	Avrami index	—
n	flow behaviour index for viscosity	—
$\dot{q}$	heat flux	W g^{-1}
T	temperature	°C or K

T_c	crystallisation temperature	°C
T_g	glass transition temperature	°C
T_m	melting temperature	°C
T_{cent}	the temperature at which the maximum rate	°C
T_{hwhm}	the half width at height maximum	°C
t	time	min or s
t_{apm}	time at the peak maximum	s
t_{cryst}	crystallisation time	s
t_{ind}	induction time	min
w_i	weight fraction of i^{th} component	—
X_c	degree of crystallisation	%
x	mole fraction of i^{th} component	—

Greek

α	exponent for zero-shear viscosity relationship	—
α	DGL conversion factor	—
β	Parameter Lederer viscosity equation	—
β	lamellar thickness ratio	—
γ	strain amplitude	—
δ	phase angle	rad
$\dot{\gamma}$	shear rate	s^{-1}
η	shear viscosity	Pa s

η_o	zero shear viscosity	Pa s
η^*	complex viscosity	Pa s
η'	real viscoelastic component	Pa s
η''	imaginary viscoelastic component	Pa s
η_{12}	viscosity of mixture	Pa s
χ	Flory-Huggins interaction parameter	—
ϕ_i	volume fraction of i^{th} component	—
τ	shear stress	Pa
τ	crystallisation exotherm symmetry factor	—
τ	Avrami & Hill characteristic time constant	min
ω	angular frequency	rad s^{-1}

THESIS OUTLINE

The thesis comprises five chapters, references and appendices. An outline of each chapter is as follows,

Chapter 1 consists of the summarized introduction to the study, a brief background, and details of the materials under study, the characterisation methods applied, the research hypothesis and the objectives of the study.

Chapter 2 consists of an extended literature review focusing on the wax and polyethylene components. This chapter expands on the review of wax and polyethylene materials in their pure states and as blends in their application as processing additives. The review covers various aspects related to these components and their blends. One key aspect covered in the chapter is the characterisation techniques used to analyse the experimental data of the F-T wax/LLDPE blends. The chapter provides a detailed review of these techniques, along with their respective theoretical concepts. These characterisation techniques are essential for understanding the properties and behaviour of wax and polyethylene blends. Additionally, the chapter breaks down the general characteristic features of wax/polyethylene blends found in the existing literature. It particularly emphasizes the aspect of compatibility between the two materials.

Chapter 3 consists of an in-depth description of the raw materials, preparations of polymer materials, methods of analysis and instrumental characterisation techniques.

Chapter 4 delivers the results and discussions of the properties of F-T H-wax/H-LLDPE and L-Wax/L-LLDPE blends. *Section 4.1* presents the characterisation of H-Wax /H-LLDPE blends, where H- and L- represents high and low molecular mass, respectively. In this section of the chapter, the focus is on discussing various viscosity and viscoelastic components related to wax and polyethylene materials, both in their pure states and as blends. This section aims to provide a comprehensive understanding of the rheological properties of wax and polyethylene blends. It explores how these parameters are influenced by various factors including composition, temperature, shear rate, frequency. Also presented in this section are the insights into

the thermal behaviour, phase transitions, and stability of wax and polyethylene blends under different conditions i.e., composition and temperature. *Section 4.2* presents the characterisation of L-Wax/L-LLDPE blends. In this section of the chapter, the focus is on discussing various thermophysical properties of wax and polyethylene materials, both in their pure states and as blends. This section aims to provide a comprehensive understanding of their compatibility in their solid state. It explores how these parameters are influenced by various factors including composition and temperature. Also presented in this section, are the insights gained into the rheological behaviour of wax and LLDPE blends under different conditions i.e., composition, temperature, shear rate.

Chapter 5 summarises the key findings and outcomes of the study and then finally provides recommendations for possible future work.

The references section provides a comprehensive list of the sources consulted and cited during this study, which was also used to elucidate the findings of the study.

The appendices present all the complementary and additional data produced during the study.

CHAPTER 1

1 INTRODUCTION

1.1 BACKGROUND TO THE STUDY

Polyethylene is a key member of the polyolefin family of plastics and is the most used plastic in the world; hence, it's large-scale production. Its popularity and diversity in application are owed to its sophisticated characteristics. These characteristics include a simple molecular structure, ease of production and good electrical, chemical, and mechanical properties, including excellent impact resistance, heat resistance and stiffness. However, the stiffness of the polyethylenes is low because the glass transition temperature of the amorphous portions is extremely low.

Calcium carbonate ($CaCO_3$) is commonly used as an inexpensive inorganic filler in polyethylene compounds to increase its impact toughness and modulus and heat deflection temperature (Elleithy et al., 2011, Tanniru and Misra, 2005). However, due to their polar nature, when added to polymer matrix, the $CaCO_3$ particles tend to form agglomerates instead of being uniformly dispersed (Hostomsky and Jones, 1991). Filler agglomeration can have negative effects on the properties and performance of the polymer composite. One significant disadvantage of using $CaCO_3$ as a filler is that it negatively impacts the tensile strength and impact resilience properties of the solid material. Furthermore, the presence of $CaCO_3$ clumps within the polyethylene matrix reduces the apparent maximum volume fraction of the filler, leading to increased melt viscosity (Dangtungee et al., 2005).

In many respects, the viscosity and flow behaviour of any polymer has been linked to their molecular mass (Ferry, 1980, Dealy, 1991, Lodge et al., 1992, Watanabe, 1999). In general, as the molecular mass of a polymer increases, the melt viscosity also increases to the point where processing becomes difficult. This is because, beyond a critical molar

mass, the polymer chains become highly entangled. The motion of individual chains becomes severely restricted and is only possible in a cooperative sense. This means that it becomes more difficult for the chains to move past each other and flow freely. Hence, processing additives are often added to ensure the necessary flexibility and adequate flow properties. The benefits of processing additives are mainly seen in the melt phase of the polymer resin using conventional processing techniques including extrusion, injection moulding, film blowing machines, and others.

Currently, different classes of processing additives are used during thermoplastic melt-processing (Drobny, 2014, Morris, 2017, Hahladakis et al., 2018). However, this study only focuses on lubricants in particular polyethylene wax, paraffin wax, and hydrocarbon/alkane wax. Waxes are well-known lubricants commonly applied to improve the processability of a range of polymers, e.g., polyvinyl chloride (PVC) and polymethyl methacrylate (PMMA). They also act as internal lubricants for polyolefins, e.g., polyethylene and polypropylene. Although, there is little understanding on their lubrication mechanism during compounding, based on their compatibility with the host polymer, they are classified as either external lubricants or internal lubricants (King and Noël, 1972). External lubricants are substances that are incompatible and therefore tend to migrate to the surface of the polymer. The presence of a low viscosity phase between the main polymer melt and the metal surface results in a lubricating action, i.e., a reduced drag force between polymer melt and hot metal surface. In these cases, waxes are known to reduce the processing temperature while functioning as mould release agents during injection moulding. Internal lubricants are compatible with the matrix polymer and dissolve in them. This results in an overall lower viscosity of the blend compared to the neat polymer. Hartitz (1974) demonstrated that less polar molecules such as paraffin waxes, polyethylene wax, and oils work in this way due to their molecular interaction with the polymer matrix. This study suggested that in addition to the observed external lubrication features, there may be some chemical association between the polyethylene and the wax molecules. Owing to these factors, waxes have been utilised as suitable lubricants/processing additives for modifying polyethylene melt viscosity due to their similarities in chemical and structural properties.

Since then, the industry and academia have eagerly adopted wax to either provide lubrication and/or provide physical modification during polyethylene compounding. For instance, polyethylene waxes are commercially available and have been used for their excellent dispersive and distributive mixing properties in manufacturing colour pigment polyethylene masterbatches (Gale, 1997). The excellent dispersive and distributive mixing properties have been attributed to their inherently low molecular mass and melt viscosity when compared to their counterpart polyethylene polymers. For also these reasons, polyethylene waxes are also used for their ability to increase lubricity and improving the softening point of hot melt adhesives (Deshmukh et al., 2010, Gale, 1997, Motooka et al., 1986).

Recently, several studies successfully explored the use of various paraffin waxes as processing aids for linear low-density polyethylene (LLDPE) (Mpanza and Luyt, 2006), high-density polyethylene (HDPE) (Esmaeilzade et al., 2022) and ultrahigh-molecular-mass polyethylene (UHMWPE) (Bakshi and Ghosh, 2022) as base polymers. On the other hand, several studies investigated paraffin waxes mixed with different grades of polyethylene, however, for different applications (Salyer, 1996, Zalba et al., 2003, Krupa et al., 2007, Molefi et al., 2010, Mngomezulu et al., 2011). In all these studies, it was consistently found that due to the different lubrication effects, adding wax improves the flow properties of highly entangled polyethylene chains.

Likewise, Sotomayor et al. (2014) found that adding up to 50 wt-% wax significantly reduced the melt viscosity of HDPE by more than an order of magnitude during injecting moulding, see Figure 1.1. Furthermore, some studies investigating the flow rate (FR) concluded that the presence of wax reduced the melt viscosity of polyethylene substantially (Krupa and Luyt, 2001a, Mpanza and Luyt, 2006). In summary, the most pronounced effect in mixing wax and polyethylene is the improvement in the polymer processability and this a most desirable feature of a processing additive.

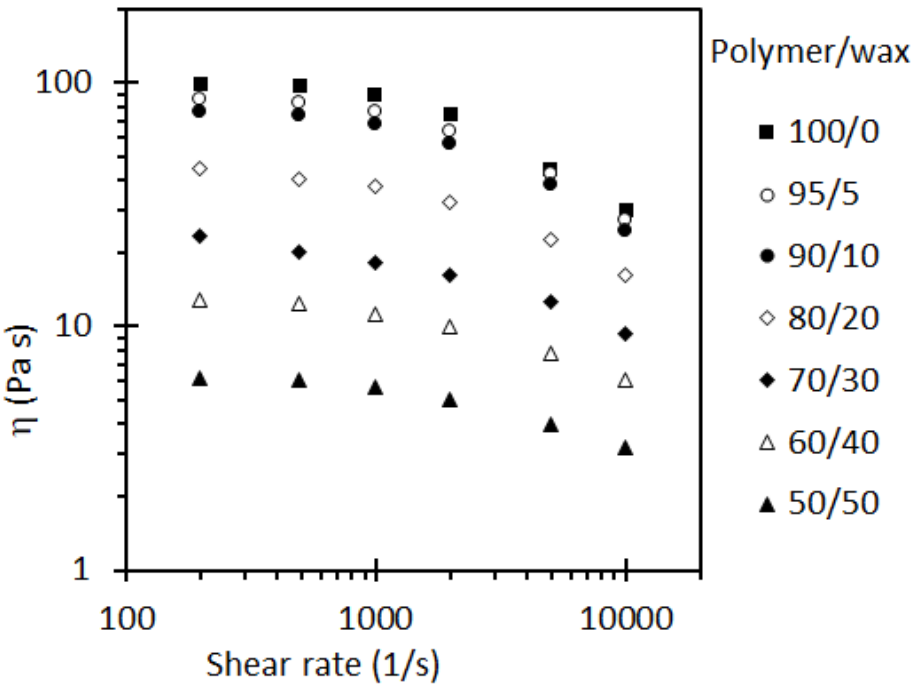

***Figure 1.1*:** Viscosity versus shear rate of paraffin wax/HDPE blends at 160 °C. Figure reproduced with permission (Sotomayor et al., 2014)

1.2 RESEARCH PROBLEM

Current practice in the polymer compounding industry is to use polyethylene wax as the preferred viscosity modifier for highly filled calcium carbonate compounds and pigment masterbatches. Anecdotal evidence suggests that the lower molar mass F-T wax, on its own, cannot be used as a replacement as it exacerbates the problem of die-drool. The present study formed part of a larger investigation focussed on the possibility of adapting the Fisher-Tropsch (F-T) wax by combining it with a low molar mass LLDPE. The hope was that a suitable combination could constitute as an alternative replacement for the polyethylene wax currently used in polymer compounding. Towards this problem the present study focussed on establishing the extent of the compatibility of the F-T wax with the LLDPE. In this context, a good understanding of the influence of the wax on the physical properties of the blend, e.g., the melt viscosity, was a critical requirement.

In terms of the viscosity, F-T wax was found to improve the melt flow of polyethylene without compromising other thermal properties (Mpanza and Luyt, 2006a, Esmaeilzade et al., 2022, Gudiño Rivera et al., 2022). However, there was a challenge encountered concerning compatibility with other polyethylene types especially when their molecular mass was high.

Die-lip drooling is a common issue in polymer extrusion operations, including those using virgin resins. Figure 1.2 shows die-lip drooling during neat HDPE polymer melt extrusion (Musil et al., 2011). Die-lip drooling refers to the accumulation of oxidized extrudate on the open face of the die. Die-lip drooling occurs when the complex shear field in the die landings of an extruder causes fractionation of a lower molar mass material. The fractionated materials migrate to the surface of the melt, and then deposits and accumulates on the extruder's die face, causing processing problems. Deposition and accumulation happens because the melt viscosity of such components is substantially lower than the polymer, and thus tend to migrate quicker towards the outer surfaces of the die (Chaloupková and Zatloukal, 2009). Die-lip drool can be exacerbated by the build-up of additives on the die's surface. Die-lip drool is a complicated phenomenon, and despite extensive research and understanding of polymer processing, its formation mechanism is not entirely understood yet. However, there is anecdotal evidence suggesting that low molecular mass waxes, such as F-T waxes, may contribute to die-lip build-up (Lee, 2002, Musil and Zatloukal, 2014, Chaloupková and Zatloukal, 2009).

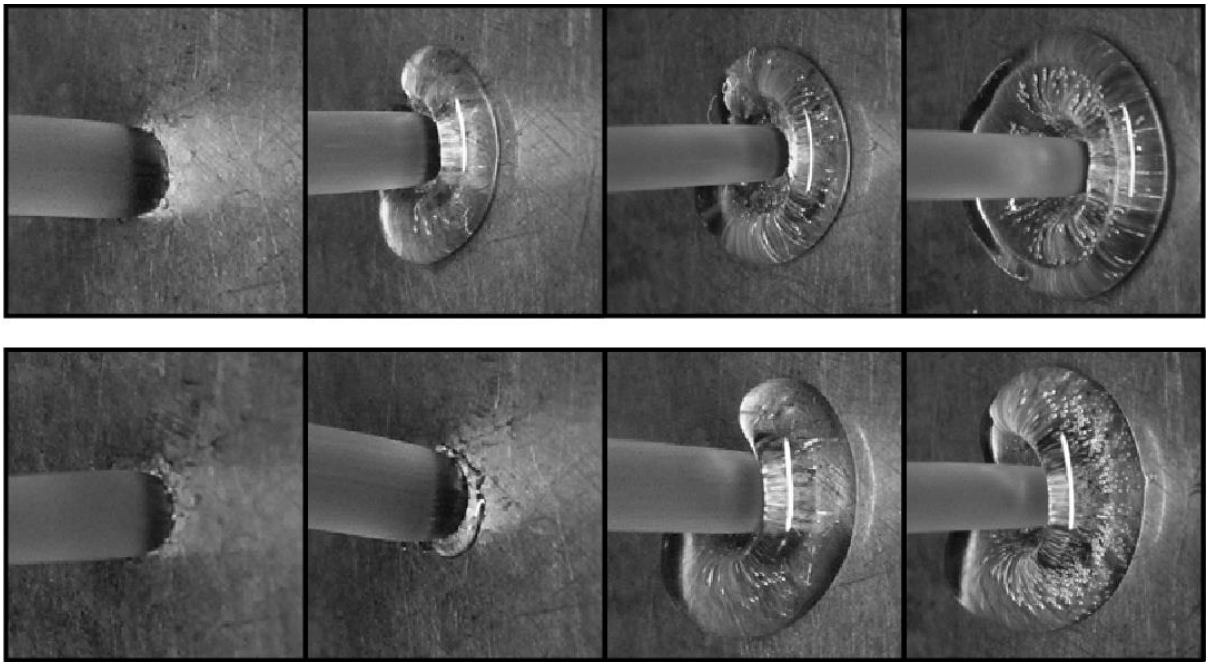

Figure 1.2: Die drool during HDPE polymer melt extrusion. Figure reproduced with permission (Musil et al., 2011)

Studies attributed die-lip drool to poor thermodynamic compatibility with the parent polymer (Koningsveld et al., 1974, Patterson and Robard, 1978). The lack of compatibility between additives and the polymer matrix strongly influences die-lip drooling in polymer extrusion. This is because when incompatibility is present, the low viscosity additive can migrate to the die landings during the extrusion process. This leads to the accumulation of the oxidized extrudate. Hence in case of poor compatibility between the F-T wax and polymer, the wax may have a higher tendency to migrate to the metal surfaces and contribute to additive build-up. Therefore, it is imperative to consider the extent of compatibility between the F-T wax and polymer, to help lessen die-lip drooling issues and improve the overall extrusion process.

Some studies investigated low molar mass liquid crystalline polymers, fluoro-elastomers and hyperbranched polymers to minimize extrudate surface irregularities including die swell and die drool (Lichkus and Harrison, 1992, Hull and Jones, 1996, Hong et al., 1999, Kharchenko et al., 2003). Similar to low molecular mass waxes, poor thermodynamic compatibility between the additive and parent polymer has also been reported (Hong et

al., 2000). There is a lack of clarity as to what controls the compatibility and stability of blends of F-T wax with polyethylene in the context of the shear-driven fractionation causing die-drool.

Both compounds belong to the same chemical family of linear saturated hydrocarbons. Perhaps, improving thermodynamic compatibility and increasing the average molar mass of the F-T wax could help to overcoming this limitation. Therefore, the hypothesis was that that the required compatibility can be achieved by appropriate blending of F-T waxes with low molecular mass linear low-density polyethylene (LLDPE) (Krupa and Luyt, 2001a, Chen and Wolcott, 2014, Gumede et al., 2016). The hypothesis is that small additions of low molecular mass LLDPE to F-T wax could yield high molecular mass chain distribution to reduce or even prevent die-lip drooling of the neat F-T wax while encouraging better compatibility with the base polymer. The aim is to moderately raise the melt viscosity and processing temperature of the F-T wax to achieve longer residence time in the polymer matrices during the exposure to high shear in the die of the extruders. The die-drool aspect of the larger research project was dealt with separately. The present study focussed on establishing the compatibility of the F-T wax with LLDPE and the effect on physical properties, in particular the rheology of such blends.

Polymer blending

Polymer blending is a common method widely used to enhance thermo-mechanical and thermo-physical properties of polymer mixtures or to create a material with new properties. Polyethylene blending involves physically mixing two or more polymer components with different molecular structure, or molecular configuration. It is of particular interest in this study due to its ease of preparation which is cost effective and its efficiency in improving many primary properties including melt viscosity. Because of these great properties' polymer blending has become an important research area for advanced polymer materials.

Viscosity of wax/polyethylene blends

Information on the rheology and phase behaviour of general wax/polyethylene blends is limited (Sotomayor et al., 2014, Esmaeilzade et al., 2022, Gudiño Rivera et al., 2022). Furthermore, there has not been an active area of study concerning the processability characteristics of F-T wax blended with LLDPE, particularly the rheological behaviour of these blends. Hence, knowledge of the melt viscosity and the overall rheological behaviour of these blends is an important aspect to consider.

Compatibility between wax and polyethylene blends

Earlier studies based on various wax/polyethylene blends showed that the extent of miscibility between the two components varies with (1) the molecular structure i.e., degree of branching and molecular mass distribution of the polyethylene and the wax used; and (2) the blend composition (Luyt and Brüll, 2004, Molefi et al., 2010). Regarding the former, earlier studies demonstrated that the Flory-Huggins interaction parameter can be used to estimate miscibility in a polymer solution/blend (Flory, 1941, Huggins, 1941, Ke, 1961, Coran and Anagnostopoulos, 1962, Nakajima and Hamada, 1965, Martínez-Salazar et al., 1996). The Flory-Huggins parameter considers polymer components that are chemically similar but differ greatly in chain length and structure. In the referenced studies, it was observed that amongst a wide range of *n*-alkane diluents, including waxes, mixed with polyethylene, the solubility of polyethylene increased with increasing molecular mass of the diluents. In these studies, a small positive and even negative values of the interaction parameter were noted suggesting partial miscibility to good miscibility, respectively. The lower the value of the interaction parameter, the greater the expected miscibility in the binary systems. Since then, the interaction quantity has been used as a reliable parameter to correlate miscibility within binary blends. Later on, Chen and Wolcott (2014) explored the Flory–Huggins's interaction parameter between paraffin wax and polyethylene. The study applied melting point depression analysis. In their study they obtained small positive values which were correlated to partially miscibility. The extent of miscibility was attributed to their similar chemical structures.

Other empirical studies investigated the miscibility of various paraffin waxes or alkanes combined with polyethylenes using thermal analysis. Thermal studies provide a rapid means of evaluating the miscibility/compatibility in polymer blends. The available literature indicates that, in both crystalline and melt states, alkanes/paraffin and F-T waxes are more compatible with LLDPE than with low-density polyethylene (LDPE) or HDPE (Krupa and Luyt, 2000, Krupa and Luyt, 2001a, Mpanza and Luyt, 2006a, Molefi et al., 2010, Chen and Wolcott, 2014, Chen and Wolcott, 2015, Gumede et al., 2017). Differential Scanning Calorimetry (DSC) results showed that LLDPE and wax may even be partially miscible in the crystalline phase (Krupa and Luyt, 2000). Miscibility of polyethylene and wax in the crystalline phase was confirmed by Crystallisation Analysis Fractionation (CRYSTAF) which showed co-crystallisation of waxes with LLDPE but not with HDPE and LDPE (Luyt and Brüll, 2004). Thus, it can be inferred that a F-T wax, with relatively high molecular mass, is likely to exhibit at least some partial miscibility with a low molecular mass linear low-density polyethylene.

Clearly, there is always some partial solubility of one polymer in another. It is also possible that the polymers can be miscible over the full composition range. If this is not the case, DSC results will reveal that some of these blends will differ with respect to their melting temperatures and degree of crystallinity. On the other hand, inconsistent results were found in literature concerning the miscibility of wax with polyethylenes. For instance, Mpanza and Luyt (2006a), reported one endothermic peak for LLDPE blended with EnHance, H1 and M3 waxes at wax content up to only 10 wt-%, while other studies observed similar endothermic responses with wax loadings up to 30 wt-% (Djoković et al., 2003, Krupa and Luyt, 2001, Mpanza and Luyt, 2006, Mtshali et al., 2003a). In these studies, partial miscibility was observed with further increase of wax concentration. Partial miscibility has also been associated with co-crystallisation. Hence, others focussed on co-crystallisation phenomena to establish the extent of solid-state miscibility. Gumede et al. (2016) observed that the co-crystallisation phenomenon is associated with shifts to lower temperatures of the melting and crystallisation temperatures of the LLDPE-rich phase. This occurrence could imply either solubility of the LLDPE in the wax-containing melt, or co-crystallisation, or both. Based on these observations, studying the fortification

of F-T waxes with low molecular mass LLDPE for ultimate use as processing additives is recommended.

1.3 AIMS AND OBJECTIVES

Literature has primarily focused on wax/PE blends, with polyethylene as the only major phase (Chen and Wolcott, 2014, Mngomezulu et al., 2010, Mtshali et al., 2003a, Mpanza and Luyt, 2006a). This suggests that attention was focussed on the advantage offered by wax operating independently as a processing aid for polyethylene. Instead, this study seeks to also explore blends of F-T wax and LLDPE over the entire composition range. Furthermore, literature on the influence of wax/PE composition on blend miscibility and crystallisation behaviour is not consistent. Moreover, it is seldomly reported that wax modified by blending with low molecular mass LLDPE can be used to improve the miscibility and viscosity properties of a polymer matrix.

This study probed blend compatibility considering the rheological of melts and the thermal properties and crystalline structure of solid samples of Fischer-Tropsch waxes blended with high flow grades of linear low-density polyethylenes (LLDPEs). The objectives of this study were pursued by:

1. Interpreting the results, concerning the miscibility status of the blends, by investigating thermal properties using DSC and the crystalline morphology using polarised optical microscopy (POM).
2. Assessing the rheological behaviour of the blends as a function of shear rate, composition and temperature.

Therefore, overall, this study set out to investigate the influence of the following effects and conditions;

1. Blend composition
2. Temperature
3. Shear rate (or shear stress) and the frequency of oscillation, and

4. To understand how these parameters, affect the chemical interaction, structure and compatibility of the two-component system in the molten-liquid state.

CHAPTER 2

2 LITERATURE REVIEW

2.1 BRIEF REVIEW OF PROCESSING ADDITIVES/AIDS

In polymer compounding, processing additives are substances used to improve the melt strength and flow properties of polymers. Some processing additives improve the general flow rate of the polymer melt by lowering the melt viscosity. Increasing the melt flow rate increases product output during polymer compounding. In most cases, processing additives also work by reducing the processing temperature. The reduction in processing temperature reduces polymer stress endurance in the barrel and energy consumption. Therefore, because of these features of processing additives, polymers are one of the most versatile, cost-efficient materials in the world. In fact, without processing additives, the general polymer products would not exist since many polymer materials are useless until they undergo processability modification process.

Processing additives can be categorised depending on their function and chemical nature. Some of the commonly used processing additives include fluoropolymers, heat stabilizers, lubricants, release and anti-slip agents, flow enhancers and viscosity reducers. These processing aids function uniquely from each other. For instance, heat stabilizers e.g., metal salt combinations function by preventing thermal degradation of polyvinyl chloride (PVC). They help to prevent unwanted chemical reactions, such as chain scission or crosslinking, which can lead to product defects. Heat stabilizers are mainly employed during PVC compounding. Fluoropolymer on the other hand, functions by building up on metal die surfaces thereby forming a slippery surface coating that increases the flow stability. Fluoropolymers are mostly used for copolymers of vinylidene fluoride and hexafluoropropylene. Lubricants are known to provide either internal or external lubrication effect for the general polyolefins. Lubricants are additives that reduce friction and help the polymer melt flow more easily. They are particularly useful in

preventing sticking of the melt to the processing equipment. Release agents are used to prevent the adhesion of the polymer melt to the mould surfaces. They help in easing the release of the finished product. Flow enhancers or viscosity reducers, improve the flow properties of the polymer melt or lower the viscosity of the polymer melt by reducing intermolecular forces between polymer chains. This improves the processability of the polymer by allowing it to flow more easily during processing.

It is important to make a good selection of the appropriate processing additives to ensure synergy between the additive and polymer. Furthermore, it is crucial to achieve a good balance of the concentration and optimum processing temperature between additive and polymer. In many respects, the concentration of processing additives is typically added in small amounts, usually in the range of 0.1 % to 5 % by mass, depending on the specific additive and application. They are often used in masterbatch formulations, which are highly concentrated mixtures of additives and/or pigments dispersed in a polymer carrier resin. In this application, the processing aid, typically a wax assists the break-down of particle agglomerates. This is achievable due to their known lubricating properties, which can reduce friction between particles while improving their rheological properties. Overall, processing additives such as wax play a critical role in polymer compounding by improving the processability and performance of polymers, ultimately leading to better product quality and production efficiency.

2.2 WAX AND WAX PROPERTIES

Wax is well-known for its ability to improve processability, particularly in thermoplastic e.g., polyethylene and polypropylene masterbatch processing (Gale, 1997). Due to its lubricating effect, wax is widely employed as a processing additive in polymer compounding. Wax can act as both internal and an external lubricant in the polymer melt, reducing the melt viscosity and increasing the melt flow rate (King and Noël, 1972). This results in improved dispersion of additives and fillers, as well as easier mixing and extrusion.

Wax is a general term covering a wide range of substances with different chemical structures sourced from nature and man-made industrial manufacturing processes. Naturally sourced wax results from biochemical processes whereas synthetic wax is derived from petroleum processes. The scope of this study is limited to polyethylene wax and F-T wax as man-made waxes, and paraffin wax which falls in the category of petroleum wax naturally sourced from minerals. Polyethylene wax is derived from polymerization of ethylene monomers following the same method as their parent polymers i.e., HDPE. F-T wax is a by-product of the coal chemical industry and can also be derived from natural gas. Paraffin wax is saturated hydrocarbons derived as by-products from the processing of petroleum oils. While polyethylene and paraffin wax are commercially available in different grades from the following producers: Clariant (Licowax), Dow chemical company (Insite™ catalyst), BASF (Luwax) and Mitsui (Excerex™ process) etc. (Bennett, 1944), F-T wax is mainly produced by Sasol, South Africa.

Classically, these waxes consist of a mixture of distinct chain molecules. For instance, paraffin wax is not only made-up of hydrocarbon mixture of *n*-paraffins (with a molecular formula of $CH_3(CH_2)_nCH_3$ where $n \geq 18$). This wax also contains iso-alkanes, alpha-olefins, alcohols and oxygenates in small amounts. Through processes such as thermal cracking or oxidative degradation, the long polymer chains of HDPE are broken down into shorter chains, resulting in polyethylene waxes with a range of molecular masses and lengths. Due the distinction in the chain molecules, these waxes vary widely in terms of molecular mass distribution. For example, polyethylene wax exhibits a broader molecular mass distributions with an average molecular mass up to 10000 g mol^{-1} while paraffin and F-T waxes may range from 200 to 1000 g mol^{-1} (Ciesińska et al., 2016). Their melting temperatures generally increase with increasing molecular mass. In addition, when exposed to moderate-high temperatures all wax turns into a low viscosity liquid over a melting range. Moreover, their crystallisation behaviour is also mainly influenced by their molecular mass (Retief and Le Roux, 1983, Liu et al., 2015, Shen et al., 2018, Bakshi and Ghosh, 2022, Rathod and Banerjee, 2013). Due to their predominantly straight chain molecules most waxes form a highly crystalline structure in the form of plates, needles, or malformed crystals (Jafari Ansaroudi et al., 2013).

2.3 WAX APPLICATIONS

Waxes in general are in high demand due to their variation in chemical composition and their ability to be tailored for various applications (Turner et al., 1955). Figure 2.1 shows the different sectors in which wax was applied in 2012 (Wei and Xiaoya, 2012). According to the global 2012 report, the packaging industry is the second dominating consumer of wax (Duru et al., 2013). Within packaging, waxes are generally used from the processing stage to coatings and as barrier systems. The scope of this study is limited to its function as a viscosity modifier for polyolefin masterbatch compounding.

Historically and presently, polyethylene wax and paraffin wax has been widely used as processing additives for a variety of plastics processing applications. Both type of waxes have been commonly used to enhance lubricity and softening point of polyethylene, polypropylene and hot melt additives (HMAs) during extrusion (Deshmukh et al., 2010, Gale, 1997, Motooka et al., 1986). Recently, several authors addressed the use of these waxes to enhance the processability of polyethylene (Liu et al., 2015, Shen et al., 2018, Bakshi and Ghosh, 2022). In many instances, it was shown that even small amounts of can significantly improve the flow behaviour of polyethylene. Moreover, a survey of the literature also reveals similar behaviour when considering a broad range of different paraffin wax used in combination with LDPE, LLDPE and HDPE (Esmaeilzade et al., 2022, Mpanza and Luyt, 2006, Mpanza and Luyt, 2006a).

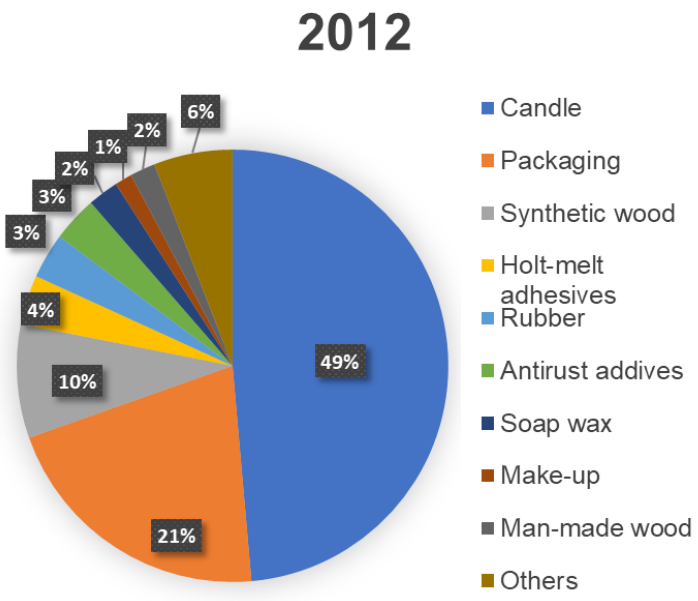

Figure 2.1: Worldwide applications of wax. Figure reproduced from (Wei and Xiaoya, 2012)

2.4 POLYETHYLENE AND ITS PROPERTIES

Like the polyethylene wax, the polyethylene polymer is formed from ethylene monomers sourced from natural gases and petroleum oil. The main difference between the two is the number of ethylene repeat units in the monomer which determines the molecular mass. The molecular mass of the polymer is higher ranging from 10,000g mol^{-1} to 6,000,000 g mol^{-1} (Bayat et al., 2013). Branching is also an important factor which directly affects the grade of polyethylene. Short-chain branching in polyethylene is obtained by the copolymerisation of ethylene with higher alpha olefins, e.g., 1-hexene, 1-octene and 1-butene (Boyron et al., 2019, Mülhaupt, 2003). Chain branching, in conjunction with molecular mass, can provide a variety of polyethylene molecular structures largely influencing physical properties i.e., density, crystallinity, ductility, colours, phase transition temperatures, yield strength etc.

Polyethylene is classified into several groups due to their densities. The density strongly depends on the degree of branching. Figure 2.2 shows the different chain branches of the three common polyethylenes (Ragaert et al., 2016). High-density polyethylene (HDPE) with a density between 0.93 to 0.97 g cm^{-3} has a few if any branches (Boyron et al., 2019). Low-density polyethylene (LDPE), 0.910 to 0.940 g cm^{-3}, features both long and short branches (Boyron et al., 2019). Linear low-density polyethylene (LLDPE), 0.91 to 0.925 g cm^{-3}, consists of numerous short branches of well-defined length, which are randomly placed along the main chain (Ragaert et al., 2016). Table 2.1 shows the common properties of HDPE, LLDPE and LDPE including the density.

Crystallinity is another inherent property of polyethylene also influenced by the degree of branching and molecular mass. Crystallinity has a direct bearing on the physical properties of the polyethylene. In fact, physical properties such as mechanical, thermal, optical, etc. properties strongly depend on the ability of polyethylene chain molecules to crystallise. High levels of branched chains hinder crystallisation. In general, polyethylene is semi-crystalline with the degree of crystallinity varying from about 30 to 90 % and these levels can even be found in clear or translucent thin films. Table 2.1 also shows some of the common properties (mainly influenced by the degree of crystallinity) of HDPE, LLDPE and LDPE.

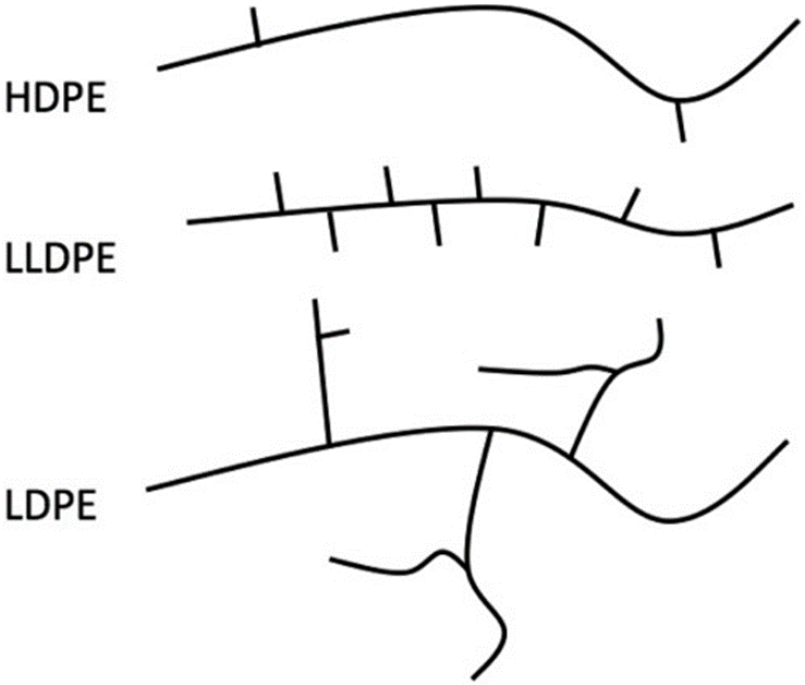

Figure 2.2: Molecular structure of HDPE, LLDPE and LDPE. Figure reproduced with permission (Ragaert et al., 2016)

Table 2.1: Common properties of HDPE, LLDPE and LDPE (Ogah, 2012, Bayat et al., 2013)

Properties	HDPE	LLDPE	LDPE
Density	0.93 - 0.97 g cm^{-3}	0.91 - 0.925 g cm^{-3}	0.91 - 0.94 g cm^{-3}
Crystallinity	Higher than LLDPE and LDPE	Higher than LDPE	Lower than LLDPE
Melting point	120 - 180 °C	110 - 130 °C	105 - 115 °C
Tensile strength and stiffness	High	High to medium	Low
Flexibility and impact resistance	Low	Moderate	High
Applications	Pipes, bottles, and containers	Stretch films, food packaging, and shrink films	Plastic bags, squeeze bottles, and toys

2.5 POLYETHYLENE APPLICATIONS

Polyethylene is amongst the most utilized plastics worldwide. According to a PlasticsSA report in 2020, there is a high demand for polyolefins such as polyethylene applicable for the packaging industry, refer to Figure 2.3. Herein, polyethylene is primarily used to manufacture packaging materials such as film, lamination film, stand-up pouch film, and medium and heavy-duty bag film, bottles etc, refer to Table 2.1 for specific applications for HDPE, LLDPE and LDPE. In general, polyethylene makes good packages due its good flexibility at room temperature, great processability, strength and toughness, chemical resistance, moisture barrier etc. In addition, it can be easily fabricated into clear or translucent thin films. Another added advantage is the low-cost production making it popular for usage in the plastics industry.

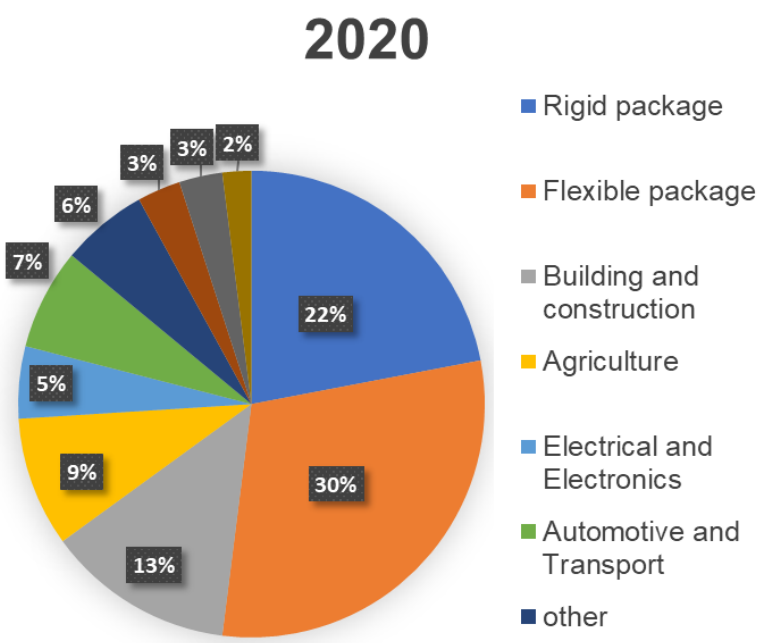

Figure 2.3: Different applications of plastics across SA. Figure reproduced from PlasticsSA annual report 2020/2021 (PlasticsSA, 2020/2021)

2.6 POLYMER BLENDS

Polymer blends refer to a mixture of two or more polymers that are physically mixed together to create a new material. The resulting material can have different physical and chemical properties than the individual polymers, depending on the composition of the blend and the processing methods used to create it. Polymer blends can be created using a variety of processing methods, such as solution blending, solid-state blending and melt blending. Solution blending involves dissolving the polymers in a solvent and then mixing them together, while solid-state blending involves mixing the polymers together. Melt blending is one of the most common methods and it involves melting the polymers together and mixing them while they are in a liquid state. Solution blending significantly enhances complete miscibility, solid-state processing guarantees processing simplicity

and upscaling, and melting blending can provide both advantages of solution blending and solid-state processing. Polymer blends can be used in a wide range of applications, including packaging, automotive parts, and medical devices. The properties of the blend can be tailored to suit the specific requirements of the application, such as mechanical strength, flexibility, and resistance to heat and chemicals.

2.7 BRIEF HISTORY OF POLYETHYLENE BLENDS

Polyethylene blends has remained a major topic in both industry and academia. They provide a wide range of benefits including: (1) enhancing original properties, (2) imparting new features, (3) improving processability to suit industrial applications, (4) reducing production costs and time, and (5) improving material recyclability as post-consumer waste (Munaro and Akcelrud, 2008, Schellenberg and Fienhold, 1998, Hay and Zhou, 1993, Shen et al., 2018). In industry, polymer blends can be used to create new materials with improved properties, such as increased strength and flexibility. These materials can be used in a wide range of applications, such as automotive parts, packaging, and medical devices. The ability to tailor the properties of polymer blends to meet specific application requirements has significant economic and technological implications. In academia, the study of polymer blends contributes to the understanding of the fundamental principles underlying the behaviours of polymers. This knowledge can be used to develop new theories, models, and computational tools for predicting the behaviours of general polymer blends and designing new materials. Furthermore, the world market for polymer blends including polyethylene blends is expected to continue to grow due to factors such as the rise in population, industrialization and improving technologies. Their demand is attributed to their versatile properties that offer high performance over their traditional counterparts and cost effectiveness. Consequently, the market value of polymer blends is predicted to grow to over USD 5.30 billion at a compound annual growth rate of 5.4 % in the forecast period of 2020-2025.

Overall, the impact and contribution of the study of polyethylene blends to both industry and academia is crucial in advancing our understanding of materials science and

developing new materials with improved properties for various applications. However, creating polymer blends can be a complex process, as the properties of the resulting material can be influenced by factors such as the compatibility of the polymers, the processing conditions, and the composition of the blend. Therefore, careful consideration and optimization of these factors are required to create a successful polymer blend.

Following are some key properties based on polyethylene blends demonstrating the advantages offered over their traditional components. Some studies showed that HDPE blended with LLDPE shows improved stress crack resistance (Munaro and Akcelrud, 2008, Schellenberg and Fienhold, 1998). In addition, Munaro and Akcelrud (2008) also observed a decrease in hardness and yield stress of HDPE with additions of LDPE and LLDPE. Other authors observed high melting temperatures, total crystallinity, yield stress and elongation at break when LLDPE with hexyl branches were blended with HDPE (Hay and Zhou, 1993). Other researchers observed that additions of HDPE in UHMWPE and low molecular mass polyethylene wax in UHMWPE facilitated easier melt processing of UHMWPE while improving Young's modulus and tensile strength (Lim et al., 2005, Shen et al., 2018).

2.8 MISCIBILITY IN POLYMER BLENDS

Achieving complete miscibility between polymer blend components can be a major challenge in studying polymer blends. The lack of miscibility can affect the final properties of the blend and thus, researchers have put a significant amount of effort into understanding how the two components mix. The solid-state morphology and physical properties of blends are often determined by miscibility in the melt phase. Therefore, studying the melt state of blends has become an important area of research (Hill et al., 1993, Vadalia et al., 1994). However, studying the thermodynamic equilibrium interactions in the melt state can be controversial due to the use of indirect methods and costly techniques that are not always accessible. As a result, researchers often rely on experiments carried out in the solid state to determine the miscibility of the blends. To overcome the challenge of achieving complete miscibility, researchers have used various techniques such as modifying the chemical structure of the polymer components, using

compatibilizers, and adjusting processing conditions. By carefully controlling these factors, researchers can improve the miscibility of polymer blends and create new materials with unique properties.

Generally, the Gibbs free energy (ΔG), entropy (ΔS), and enthalpy (ΔH) are fundamental thermodynamic parameters that govern the miscibility between the two components of a polymer blend. In the case of polymer blends, the Gibbs free energy of mixing must be reduced for the blend to be miscible. When the Gibbs free energy of mixing is zero or negative, the blend is in thermodynamic equilibrium and the two components are completely miscible. In this system governing conditions must be fulfilled as follows:

$$\Delta G_{mix} = \Delta H_{mix} - T\Delta S_{mix} < 0 \qquad (2.1)$$

Where ΔG_{mix} is the Gibbs free energy of mixing, ΔS_{mix} is the combinatorial entropy of mixing and ΔH_{mix} is the enthalpy of mixing.

When the two components of a blend are completely miscible, there is usually a small enthalpy of mixing, which can be positive or negative, depending on the specific components and conditions. However, for all polymer systems for which the interaction forces are of the van der Waals type, the enthalpy of mixing is always positive. The entropy is the state of molecular disorder or randomness. When two components of a blend are completely miscible, the disorder of the system increases, and the entropy of the system increases. This leads to a decrease in the Gibbs free energy of the system, making it more favourable for the two components to be miscible. Overall, the thermodynamic parameters of Gibbs free energy, entropy, and enthalpy are important in understanding and predicting the miscibility of polymer blends. By controlling these parameters through adjustments to the chemical structure of the components or processing conditions, researchers can improve the miscibility of polymer blends and create new materials with desired properties.

In polymer blends, there are three distinct mixing states: miscible, immiscible, and partially miscible (Hill et al., 1993, Vadalia et al., 1994, Martínez-Salazar et al., 1996, Crist and Hill, 1997). A miscible blend is also referred to as a homogeneous blend. In this type of blend, the two or more polymer components mix well to an extent that it appears as a

single-phase system. The blend exhibits zero interfacial tension between the components, and it displays average or deviated properties of the two components or a whole new set of properties. In contrast, an immiscible or heterogeneous blend consists of non-uniform and visibly distinct phases. The polymer components in this type of blend are incompatible due to high interfacial tension. A partially miscible blend is a blend that exhibits phase separation in a range of composition while appearing as a single-phase system in another range. Phase separation is mostly observed in the intermediate region, such as a 50/50 composition. A phase-separated morphology typically consists of a co-continuous morphology and a dispersed phase depending on the specific composition and interaction parameters. In the co-continuous morphology, both components form continuous networks that are interconnected and dispersed throughout the system, resulting in a bi-continuous phase structure. In the phase-separated morphology, the two components form separate domains or droplets within the blend. The partially miscible blends often exhibit unique properties that are different from either of the pure components or the miscible blends. The properties of the partially miscible blends can be tuned by adjusting the blend composition and processing conditions to control the morphology of the system.

Figure 2.4 shows the three distinct mixing states, conditions required, and typical graphs observed for this state. The graphs relate Gibbs free energy of mixing as a function of volume fraction of a binary system showcasing different degrees of miscibility states. For a miscible blend, the entropy of mixing is greater than the enthalpy of mixing and favours mixing condition shown in equation (2.2):

$$\Delta H_{mix} < T\Delta S_{mix}, \qquad \Delta G_{mix} < 0 \tag{2.2}$$

This condition is represented by the blue curve in Figure 2.4(a). On contrary, a polymer blend represented by the red curve defies the above-mentioned conditions and is said to be immiscible. With this type of a blend, the enthalpy of mixing dominates and is the deciding factor for miscibility, equation (2.3):

$$\Delta H_{mix} > 0, \quad \Delta G_{mix} > 0 \tag{2.3}$$

One of the reasons for immiscibility in polymer blends is the large difference in molecular masses of the components. This is because the size difference between the polymer chains affects their ability to mix and form a homogenous blend. The reason is to be found in the reduced entropy of mixing relative to the entropy of mixing when the components are of similar size. The entropy of mixing is not sufficient to overcome the positive enthalpy of mixing. This results in the formation of non-uniform, visibly distinct phases, i.e., the formation of a partially miscible blend. Another reason for immiscibility can be differences in the polarity or chemical nature of the polymer components. For example, chemically different polymers tend to be immiscible due to the differences in their intermolecular forces. Both cases are thermodynamically unfavourable because of the increase in free energy. Consequently, immiscible blends tend to phase separate over time as the system seeks to reach a more stable state, where the free energy is minimized.

In a partially miscible polymer blend, shown in Figure 2.4(b), a single phase can be observed at either end of the composition range (i.e., component A-rich phase or component B-rich phase) where the interaction between the two components is stronger. However, in the intermediate range, a two-phase morphology can be observed due to the presence of a balance between the interactions of the two components.

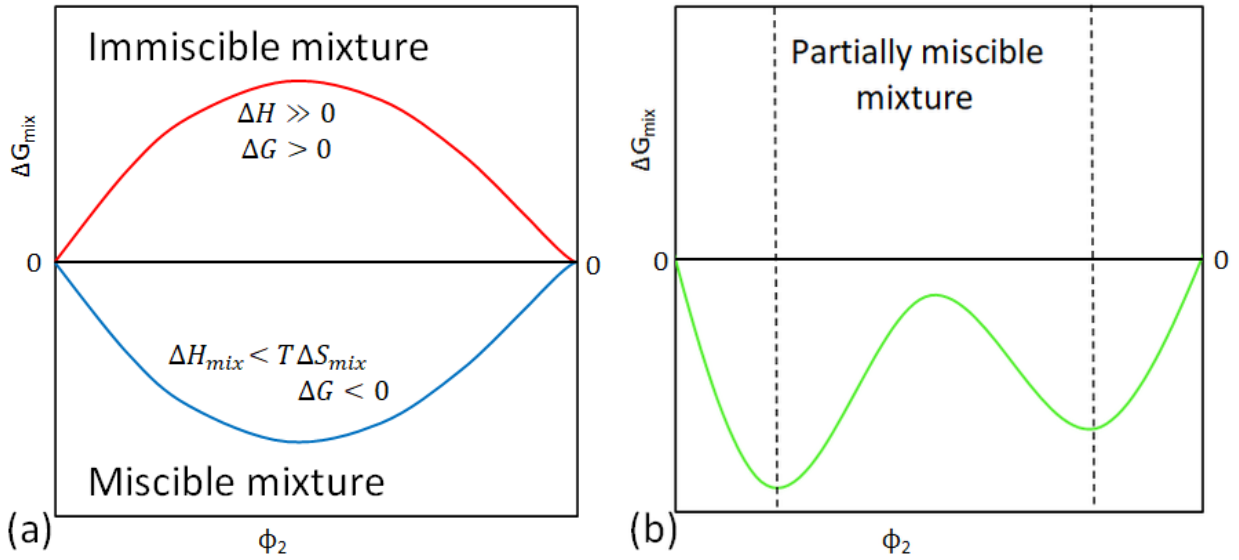

Figure 2.4: Variation of Gibbs energy of mixing, enthalpy of mixing and entropy of mixing with composition providing insights into the miscibility behaviour of a binary polymer blend. Figure adapted from (Higgins et al., 2010)

The Gibbs free energy of mixing curves obtained at a series of temperatures can be transformed to a temperature–composition phase diagram. This summarizes the phase behaviour of a binary mixture. Figure 2.5 shows the typical temperature-composition symmetrical phase diagram for a regular polymer solution. This phase diagram shows the presence of a miscibility gap for a special polymer-diluent solution. The figure shows two areas of immiscibility whose coexistence curve limits are defined by the upper critical solution temperature (UCST) and lower critical solution temperature (LCST). These points of curvature define the critical temperature points. The LCST point is the temperature below which the mixture is completely miscible. Similarly, the UCST is the temperature above which the mixture is completely miscible. The outer boundary of the miscibility gap represents a single-phase region, where the polymer solution is stable and completely miscible. The metastable region is located between the spinodal and binodal curves and it is prone to fluctuations in composition and temperature. Within the metastable region, phase separation is governed by nucleation and growth processes. Finally, the unstable region between the spinodal lines indicates that any small fluctuation in composition can lead to phase separation by spinodal decomposition.

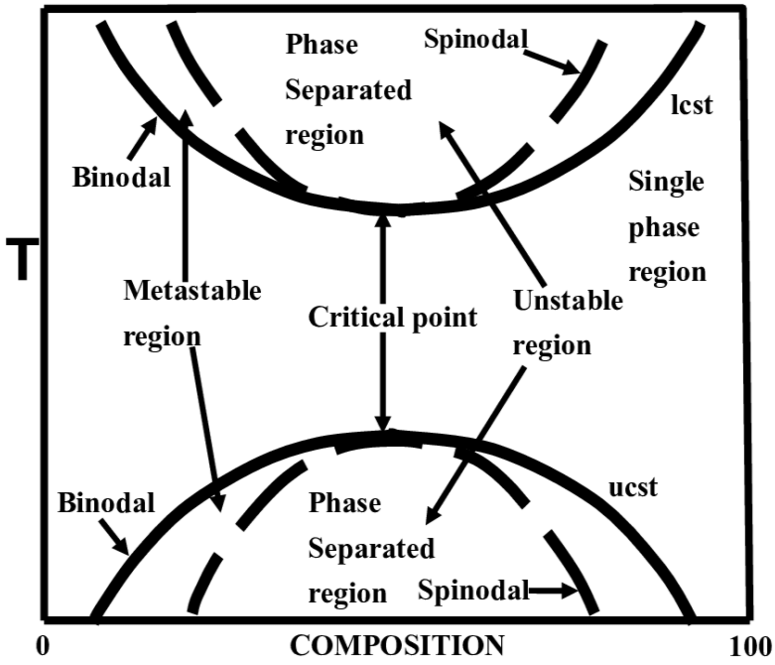

Figure 2.5: Phase diagrams of a regular polymer-diluent mixture represent of the phase behaviour of a mixture as a function of temperature and composition. For a regular polymer-diluent mixture, this includes the region of miscibility and binodal and spinodal curves with upper critical solution temperature (UCST) and lower critical solution temperature (LCST). Figure reproduced with permission (Robeson, 2014)

Flory and Huggins developed a theoretical framework for assessing the miscibility of polymer blends (Flory, 1941, Huggins, 1941). The Flory and Huggins theory considers parameters such as the difference in molecular mass, chemical structure, and interactions between the polymer chains in the blend. The Flory-Huggins equation as noted:

$$\Delta G_{mix} = RT[n_1 \ln \phi_1 + n_2 \ln \phi_2 + n_1 \phi_2 \chi] \quad (2.4)$$

where n_1 and n_2 the moles of solvent and polymer present respectively; χ is the Flory-Huggins interaction parameter; R is the gas constant and T is the absolute temperature. The ϕ_1 and ϕ_2 are the volume fractions of the solvent and the polymer respectively. They are defined as follows:

$$\phi_1 = \frac{V_1 x_1}{V_1 x_1 + V_2 x_2} = \frac{x_1}{x_1 + m x_2} \quad (2.5a)$$

$$\phi_2 = \frac{V_2 x_2}{V_1 x_1 + V_2 x_2} = \frac{m x_2}{x_1 + m x_2} \quad (2.5b)$$

where m is the ratio of the polymer molar volume to that of the solvent:

$$m = V_2/V_1 = (M_2/\rho_2)/(M_1/\rho_1) \quad (2.6)$$

where M_2 is the number average molecular mass of polymer, M_1 is the molecular mass of the solvent and ρ_1 and ρ_2 are the densities of solvent and polymer respectively. Equation (2.4) re-written in terms of moles:

$$\Delta G_{mix} = RT[x_1 \ln \phi_1 + x_2 \ln \phi_2 + x_1 \phi_2 \chi] \quad (2.7)$$

The composition of the polymer solution can be better expressed in terms of volume fraction as follows:

$$\Delta G_{mix} = RT[(1-\phi_2)\ln(1-\phi_2) + (\phi_2/m)\ln\phi_2 + \chi(1-\phi_2)\phi_2] \quad (2.8)$$

where $\phi_1 = 1 - \phi_2$ and m is the ratio of the polymer molar volume to that of the solvent and can be determined by equation (2.6)

The Flory-Huggins theory holds for UCST phase behaviour. The temperature dependent interaction parameter can be simplified by keeping only one temperature term:

$$\chi = A + {}^{B}/_{T} \quad (2.9)$$

The term A and B are constants and T is the absolute temperature. Furthermore, the theory predicts that the critical composition ($\phi_{2,c}$) and the critical interaction parameter (χ_c) can be determined by equation (2.10) & (2.11), respectively. The critical temperature (T_c) can be calculated using equation (2.9) with known values of A and B.

$$\phi_{2,c} = 1/\left(1 + \sqrt{m}\right) \quad (2.10)$$

$$\chi_c = 0.5\left(1 + \sqrt{1/m}\right)^2 \quad (2.11)$$

(McGuire et al., 1994) proposed two equations for locating the tie lines in the liquid coexistence region of UCST phase diagram. The equations relate the tie line compositions with the interaction parameter. These equations present a simple method to extrapolate the binodal curve:

$$\left[\left(\phi_2^{\beta}\right)^2 - (\phi_2^{\alpha})^2\right]\chi = \ln\left[(1-\phi_2^{\alpha})/\left(1-\phi_2^{\beta}\right)\right] + (1-1/m)\left(\phi_2^{\alpha} - \phi_2^{\beta}\right) \quad (2.12)$$

$$m\left[\left(1-\phi_2^{\beta}\right)^2 - (1-\phi_2^{\alpha})^2\right]\chi = \ln\left(\phi_2^{\alpha}/\phi_2^{\beta}\right) + (m-1)\left(\phi_2^{\alpha} - \phi_2^{\beta}\right) \quad (2.13)$$

where ϕ_2^{α} is the polymer's volume fraction in the polymer-poor phase and ϕ_2^{β} is the polymer volume fraction in the polymer-rich phase. The interaction parameter can be determined by simultaneously solving equations (2.12) and (2.13) based on the known ϕ_2^{β} values. Given the experimental determination of the interaction parameter, it is possible to predict the spinodal curve using the following expressions:

$$\phi_2^{\beta} = 1 - 1/\sqrt{2\chi} \quad (2.14)$$

$$1 + m\phi_2^{\alpha}/(1-\phi_2^{\alpha}) - 2m\chi\phi_2^{\alpha} = 0 \quad (2.15)$$

In addition, for semi-crystalline polymer blends, the temperature dependent interaction parameter (χ) can be determined by measuring the melting point depression of the polymer in the presence of the solvent (McGuire et al., 1994). The melting point depression equation is expressed as follows:

$$T_m = \frac{1+(RB/\Delta H_u)(1-\phi_2)^2}{1/T_m^o + (R/\Delta H_u)[(1-1/m)(1-\phi_2) - (ln\,\phi_2)/m - A(1-\phi_2)^2]} \quad (2.16)$$

where T_m^0 and T_m are the equilibrium and apparent melting points of the polymer in its pure state and in the blends; V_1 and V_2 are the molar volume of the solvent and polymer repeating unit; ΔH_2 is the perfect crystal heat of the pure polymer.

Understanding the miscibility state of a polymer blend is important for predicting its properties and performance in various applications. By controlling the mixing state,

researchers can tailor the properties of the blend to meet specific application requirements.

2.9 FACTORS INFLUENCING MISCIBILITY

The extent of miscibility in polymer blends can be influenced by several factors including the molecular mass distribution, chemical composition of the components, composition ratio and temperature of the system. In polyethylene blends it has been found that factors such as differences in molecular structure i.e., degree of branching, and molecular mass are primary contributors towards immiscibility (Zhao and Choi, 2006). With respect to the case of the molecular structure, the wax primarily consists of linear alkanes, which are saturated hydrocarbons without any double bonds. On the other hand, LLDPE contains numerous short branches due to the incorporation of higher alpha-olefins as comonomers (Crist and Hill, 1997). These alpha-olefins introduce branches in the polymer chain, creating a more complex and branched structure compared to the linear structure of wax. Thus, due to the differences in molecular structure, subsequent packing arrangement, and melting behaviour, wax and polyethylene are generally not compatible with each other in the solid state. However, it is worth noting that compatibility in this instance can be influenced by factors such as composition, processing conditions, and type of wax used. Mpanza and Luyt (2006) investigated the influence of three different waxes blended with LLDPE and LDPE on separate studies. The observation also reported that the type of wax blended with polyethylene plays a significant role in determining the levels of interaction, together with the amount of wax mixed with the polymer. Moreover, solid-liquid equilibrium is also observed for wax-polyethylene blends because of the large difference in the melting points. In addition, co-crystallisation of the wax with the polymer was also observed (Hato and Luyt, 2007). It is worth noting that more complicated phase diagrams apply when the solvent used to dissolve the polymer is a binary mixture of two different compounds (Vadalia et al., 1994).

2.10 POLYMER CRYSTALLINITY

Linear low-density polyethylene is a semi-crystalline polymer. Therefore, polyethylene blends include crystallisable chains. The crystallisation process has a significant influence on the ultimate morphology, thermal, optical and mechanical properties. Therefore, it is crucial to understand crystallinity in polyethylene blends for optimizing their properties for given specific applications. This subsection attempts to cover the important topics in polyethylene chain crystallisation which are directly connected to the present research work. It provides a brief overview of the fundamental concepts of crystallisation, factors influencing polymer crystallinity, experimental methods to determine crystallinity and polymer properties affected by crystallinity.

2.10.1 Fundamental concepts of crystallisation

A crystallised polymer unit refers to a single unit or segment within the polymer chain that has undergone crystallisation. The crystallised polymer unit is described as a thin quasi two-dimensional lamella. The term “thin quasi two-dimensional lamella” highlights its morphology, indicating its thinness, two-dimensional nature, and plate-like structure. Figure 2.6 shows a schematic representation of a crystallised polymer unit separated by an amorphous region (Di Lorenzo and Righetti, 2018). In the amorphous molten state, polymer chains exist in a relatively highly entangled form. However, on crystallisation there is simply no possibility to fully disentangle and crystallise in chain-extended formats. Instead, the molecules pack in thin lamellar forms comprising chain folded conformations linked together via tie molecules. The lamellar structure is a consequence of chain folding.

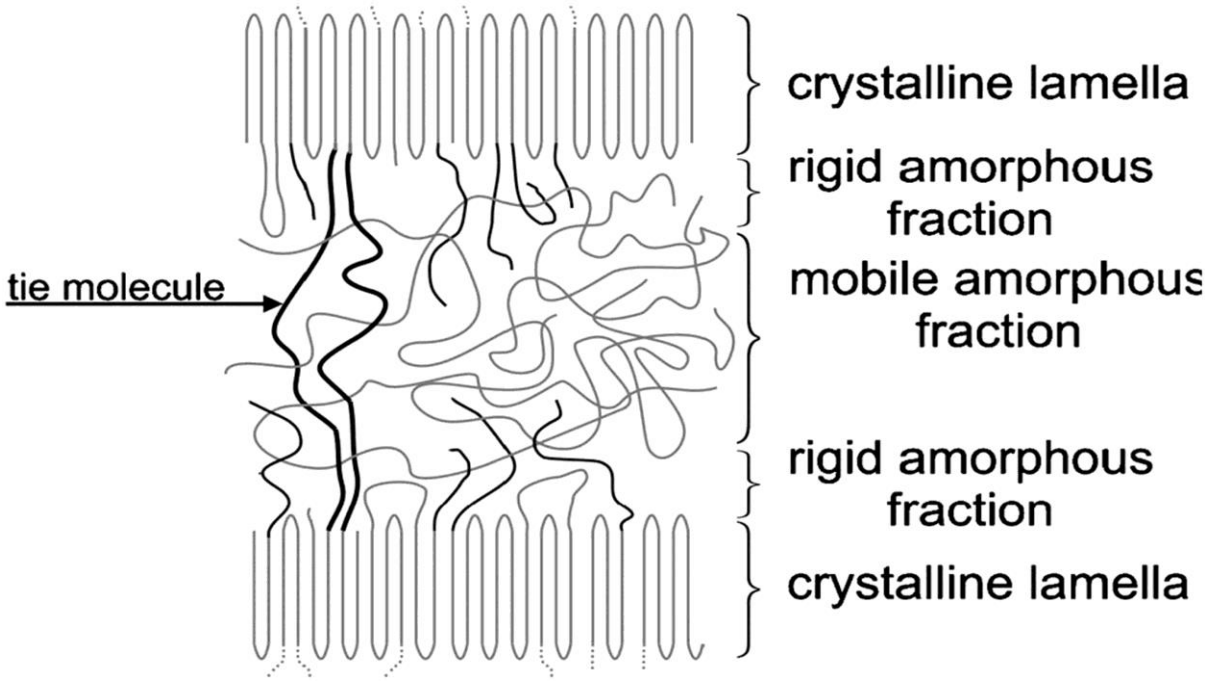

Figure 2.6: Crystalline and amorphous regions. Figure reproduced with permission (Di Lorenzo and Righetti, 2018)

Chain folding is the widely accepted model for polymer crystallisation. The model estimates that a single long polymer chain of a given length is in its most stable state when crystallising into a regular folded-back conformation. The folding of the polymer chains brings segments of the chain into close proximity, promoting strong intermolecular forces such as van der Waals interactions. This leads to the assembling and formation of the lamellar structure. In polymer crystallisation, there are two primary types of chain folding: regular chain folding and irregular chain folding. Figure 2.7(a) shows a schematic of a regular adjacent re-entry chain folded model (Hoffman et al., 1979). In regular chain folding, the polymer chains adopt a repetitive folding pattern with uniform thickness and spacings between the lamellae. This model predicts that upon re-entry, the crystalline chains loops back into the adjacent neighbouring lamella. This type of folding is often associated with polymers that exhibit a high degree of chain rigidity. However, the second model suggests that crystallising polymer chains also tend to assume random orientations and twisting etc. which thwarts regular chain folding. For these occurrences the irregular switchboard model was proposed, refer to Figure 2.7(b) (Flory, 1962). In this model, the

long chain segments which extend into the matrix and are incorporated back into adjacent lamellae are considered. This model predicts that, the same chain that forms the ordered crystalline part, on re-entry can also form and be part of the coiled or entangled disordered region. As a result, the irregular chain folded region consists of a more random arrangement of folded polymer chains leading to a less uniform lamellar structure. This type of folding is often associated with polymers that exhibit more flexible or amorphous chain segments.

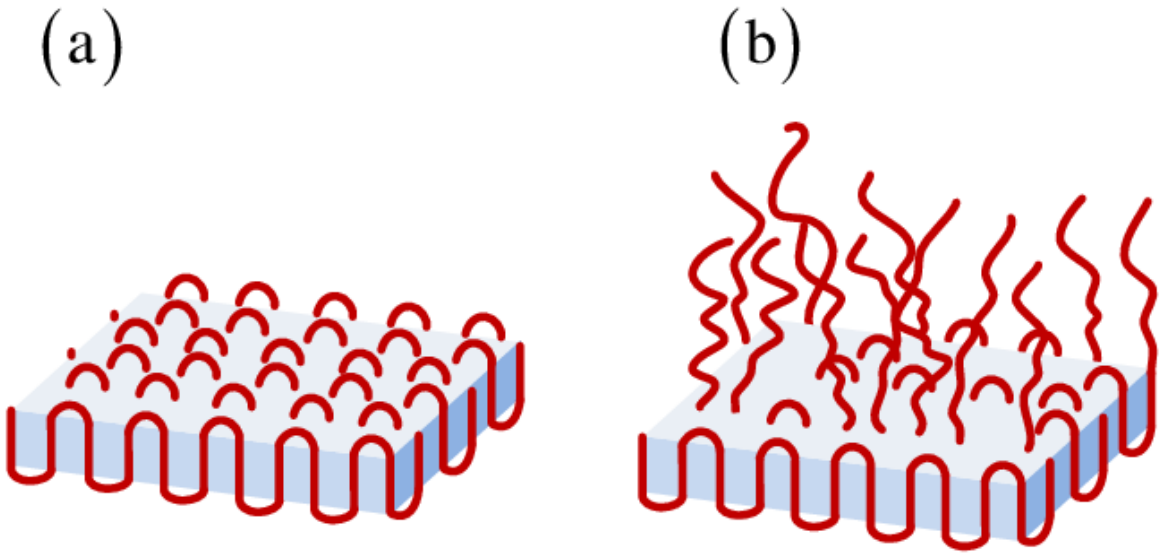

Figure 2.7: Model of crystallites chain folding: (a) regular adjacent re-entry (Hoffman et al., 1979) and (b) irregular Switchboard (Flory, 1962). Figure reproduced with permission (Dargazany et al., 2014)

For many polymers, defects incorporated during crystallisation can cause the lamella to twist and turn to such an extent that the end-result forms a spherulitic structure. The growth of spherulites occurs as more polymer chains fold and stack onto the existing lamellae. Figure 2.8 shows a schematic presentation of a spherical-shaped crystal structure interspersed with amorphous material (Jiang and Xu, 2017). The spherulites are made of the lamellae linked together by tie molecules which can either grow radially or as thread-like fibres (Gránásy et al., 2005). Many polymers including polyethylenes exhibit a characteristic spherulitic crystalline structure upon crystallisation. Polyethylene's

spherulites can be observed under polarised light microscopy. Figure 2.9 shows a typical spherulitic structure of LLDPE. The unique crystalline features in the spherulitic structure can be noted.

Many times it has been shown that the crystallisation temperature has a direct influence on the spherulite structure, and that the size and shapes of spherulites can be interrelated to the cooling rates and selected crystallisation temperatures (Raimo, 2015). It has also been observed that in the growth stage, the fast-growing crystals tend to obstruct and delay the growth of slower growing crystals such that they produce lamellae with a twisted spiral form. Polyethylene spherulites also feature concentric rings referred to as banded or non-banded. Figure 2.9 also shows these typical concentric rings on the polyethylene spherulites. Banded polyethylene spherulites was amongst the first discovered in polymers. Keith and Padden (1996) proposed a model that describes the concentric ring formation as a twist of the lamellae around their growth direction in linear polymers. They revealed that crystal deformation exists as a response to surface stresses.

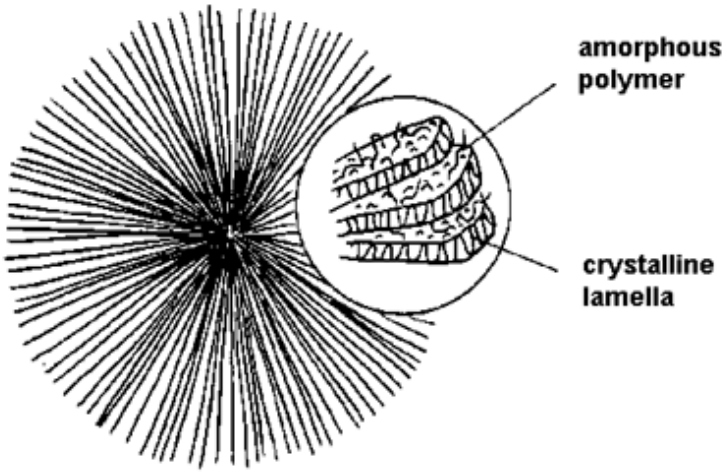

Figure 2.8: Schematic presentation of a spherical-shaped crystal structure interspersed with amorphous material. Figure reproduced with permission (Jiang and Xu, 2017)

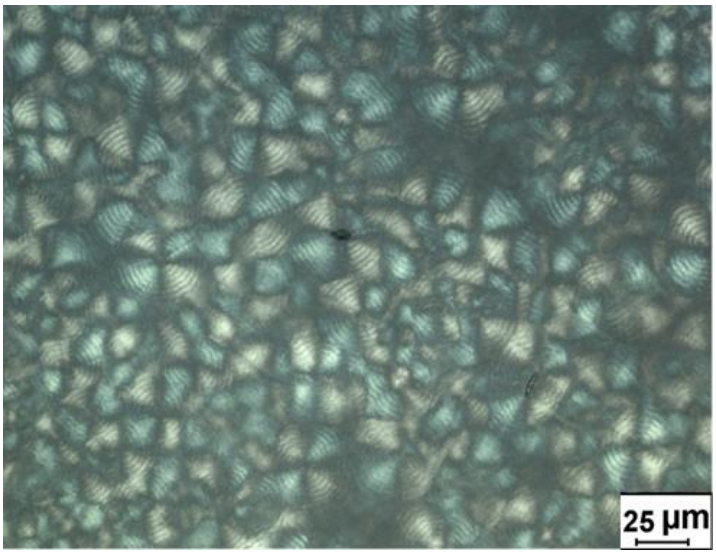

Figure 2.9: Spherulitic structure of polyethylene at 25× µm magnification

According to Höhne and Blankenhorn (1994), *n*-alkane mixtures can be considered to be model systems that assist the understanding of the behaviour of polymers of the polyethylene type. Short chain *n*-alkanes crystallise in a chain extended format building lamellar structures in the solid state. Crystallisation and melting of pure *n*-paraffins of chain lengths up to $C_{60}H_{122}$ can be largely reversible, showing practically no supercooling (Pak and Wunderlich, 2001). The multi-lamellar partial crystallisation behaviour of polyethylene has motivated its thermodynamic modelling in terms of a multi-component *n*-alkane system (Kilian, 1985, Asbach and Kilian, 1991, Höhne and Blankenhorn, 1994). In effect, a low molecular mass polyethylene can be described in terms of a quasi-eutectic system in which the components are mainly chain-folded lamellae organized in spherulites.

The so-called spherulites and tie-molecules play a significant role determining the mechanical integrity and ultimate mechanical properties of the material. Moreover, the consequence of chain folding, and lamellar thickness is that the melting temperature of polyethylene is significantly lower than is theoretically possible. In fact, the melting temperature depends on the lamellar thickness according to the empirical expression (Pak and Wunderlich, 2001, Wunderlich, 2013)

$$L = 0.627 \frac{T_m^o}{T_m^o - T_m} \quad (2.17)$$

where L is the lamellar thickness expressed in nm and $T_m{}^o$ and T_m are the limiting and measured melting temperatures in Kelvin. However, it is worth noting that the overall crystallisation and melting behaviour of polyethylene is a complex interplay of multiple factors, including chain folding, lamellar thickness, molecular mass, and the presence of various molecular species within the material.

2.10.2 Factors influencing crystallisation and polymer properties

In many cases, crystallisation in polymer materials is induced by rapid cooling. However, there are other available processes including cold crystallisation i.e., annealing from the glassy state, re-crystallisation i.e., re-cooling after melting and chain orientation i.e., stretching of long chains to form crystals.

Polymers with linear chains such as HDPE and F-T waxes form a highly crystalline structure when compared to chain molecules with branches or bulky side groups. Consequently, high crystallinity is attributed to the highest order of chain packing in the absence of branches. Cooling rates are known to also influence crystallinity. For instance, faster cooling rates leads to the formation of smaller crystals due to enhanced nucleation. Conversely, slowly cooled crystallisation processes produce crystals that a have broader distribution of crystal size. Likewise, nucleating agents and plasticizers can influence the crystallisation process. In many instances, nucleating agents are added to provide a site or surface for secondary nucleation where, it acts as a pre-existing nucleus for the polymer melt. On the contrary, plasticizers tend to reduce polymer crystallinity. This is because plasticizers are often of relatively smaller size such that they occupy the space between chains. This occurrence obstructs polymer chain packing and crystal growth.

Crystallinity is an inherent property that has direct bearing on the polymer's mechanical, thermal, barrier, optical properties. For example, thermal stability increases with the degree of crystallinity because it requires more heat energy to overcome intermolecular

forces and melt the crystal structure. Hence, semicrystalline polymers such as polyethylene are processed well above their melting temperature. Moreover, a higher degree of crystallinity also increases mechanical strength and modulus. Crystallinity also influences the transparency of polymers, for example the opacity of a polymer increases with crystallinity. Many other physical properties, such as density, ductility, colour, phase transition temperature and yield strength are all highly dependent on the total crystallinity of the polymer.

Normally, the standard analytical techniques utilised for the characterisation of crystallites include (1) optical microscopy which can reveal the nucleation and growth of the crystallites (Crist and Schultz, 2016), (2) electron microscopy which can show the morphology of a folded lamellar structure (Mandelkern, 2011), (3) differential scanning calorimetry (DSC) which measures the crystallisation and melting behaviour of the lamellar structure (Lorenzo et al., 2007), (4) atomic force microscopy which can be used to view the two or three-dimensional crystal structure of macromolecules (McPherson et al., 2000), (5) and wide and small angle x-ray scattering/diffraction of semicrystalline polymer that show sharp and broad peaks corresponding to the crystalline and amorphous regions respectively (Shilpa Kasargod Nagaraj and Siddaramaiah, 2016). However due to limited resources, this work only employed rheometry, DSC and optical microscopy to study the melt and crystalline structure the wax/PE blends. This use of complementary analytical techniques and instrumentation is necessary to deliver property analysis of the wax/polymer blends in greater detail.

2.11 CHARACTERISATION TECHNIQUES AND EQUATIONS

2.11.1 Rheology

2.11.1.1 Brief introduction of rheology

Rheology of polymer melts deals with the study of flow and deformation of polymers under the influence of applied forces or stresses. This technique uses different rheological geometries to test the polymer melt. Commonly used geometries are: (a) parallel plates, or (b) cone-plate, or (c) concentric cylinders, see Figure 2.10. The geometries are different and provide distinct effects on the polymer melt. The parallel plates geometry consists of an inverted in-contact plate with an angle of 0^{o} while the cone-plate consist of an inverted cone in-near contact geometry that can be considered a complex version of the parallel plates as it comes with an angle. In both these tests, the fluid is held in between the upper and lower surfaces, occupying a very narrow gap. The concentric cylinders are generally used for lower-viscosity fluids that will not remain within the parallel plates or a cone-plate. This study employs the cone-plate measurement tools due to the higher level of measurement accuracy obtained due to the uniform velocity (shear) field induced through the angle of the cone.

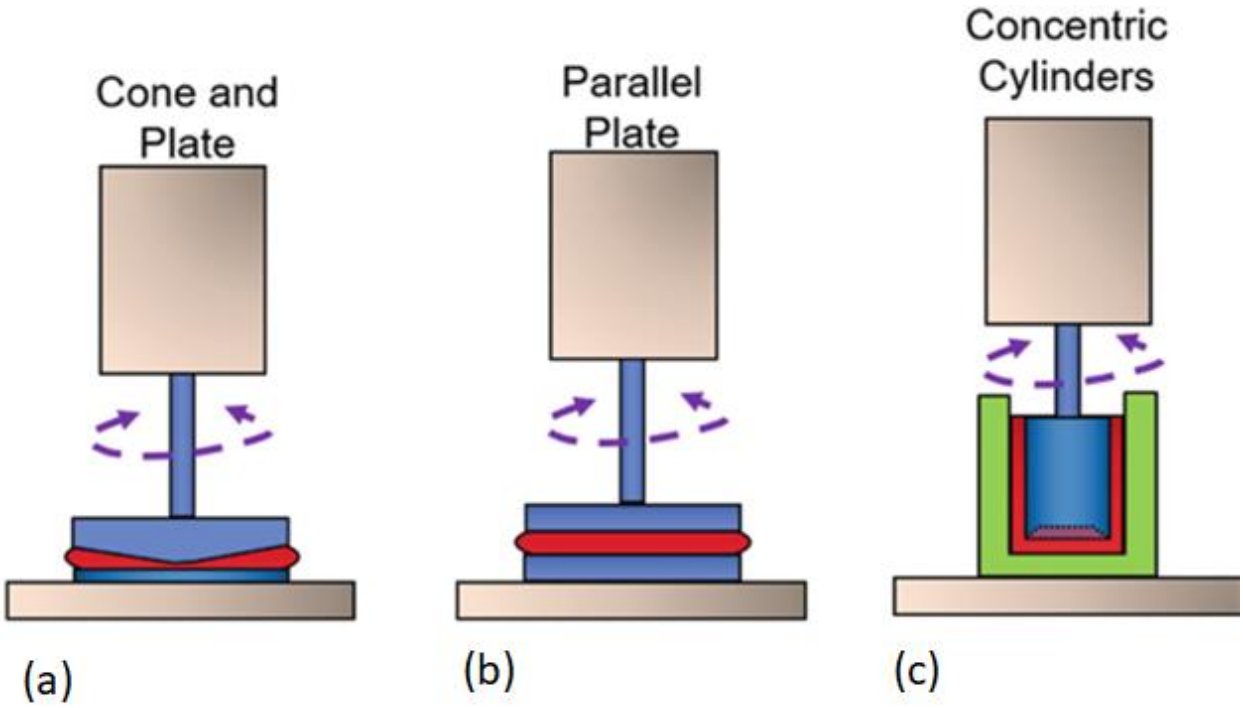

Figure 2.10: Basic geometries for the rotational rheometer: (a) parallel plate, (b) cone and plate, (c) concentric cylinder. Figure reproduced with permission (Fernanda, 2018, Whaley et al., 2019)

For the measurement, a mechanical spindle operates on the polymer melt in a rotational direction, or oscillatory motion. Figure 2.11 shows the schematic demonstration of the two common modes of measurement (a) a continuous rotational test and (b) oscillatory test. During the measurements, the test fluid is continuously sheared between the upper and lower surfaces. Most often in these measurements, the upper surface rotates and the lower is held stationary. The rheological parameters to describe the flow behaviour is commonly illustrated by the two-plate model for shear stress, refer to Figure 2.12. Again, and as shown in the figure, a sample is placed between two plates, upper and lower, separated by distance (*h).* The lower plate is mainly in a fixed position and the upper one is in motion with given velocity (*V*). With applied force on the upper plate, the upper moving plate drags and pulls the sample surface to the right, creating shear stress on the sample between the two plates. Herein, the velocity of the flowing sample increases linearly from the lower plate to maximum velocity at the upper plate.

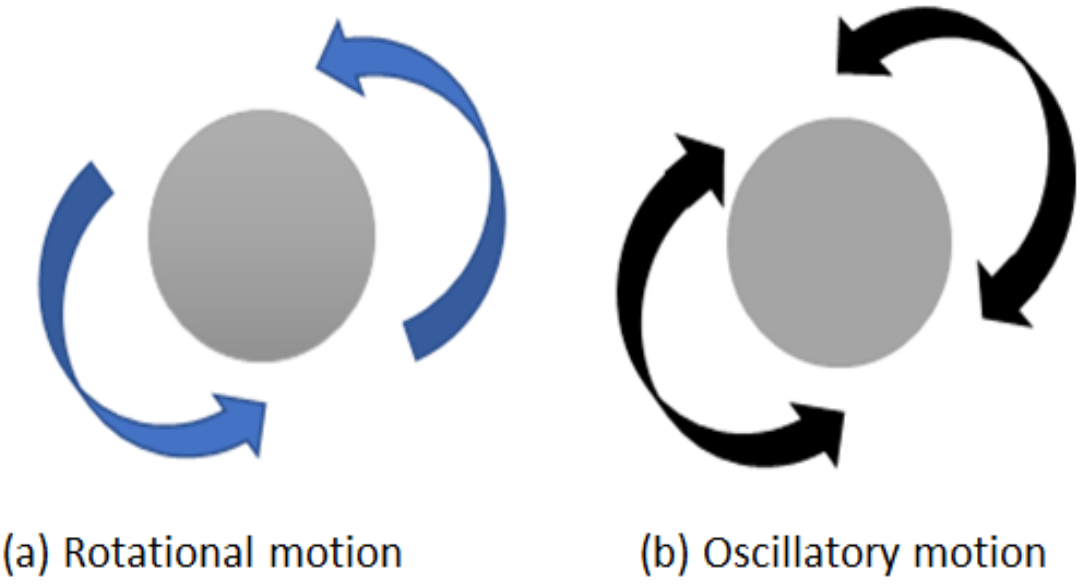

Figure 2.11: Schematic diagram of basic modes of measurement modes (a) a continuous rotational test and (b) oscillatory test for the rotational rheometer

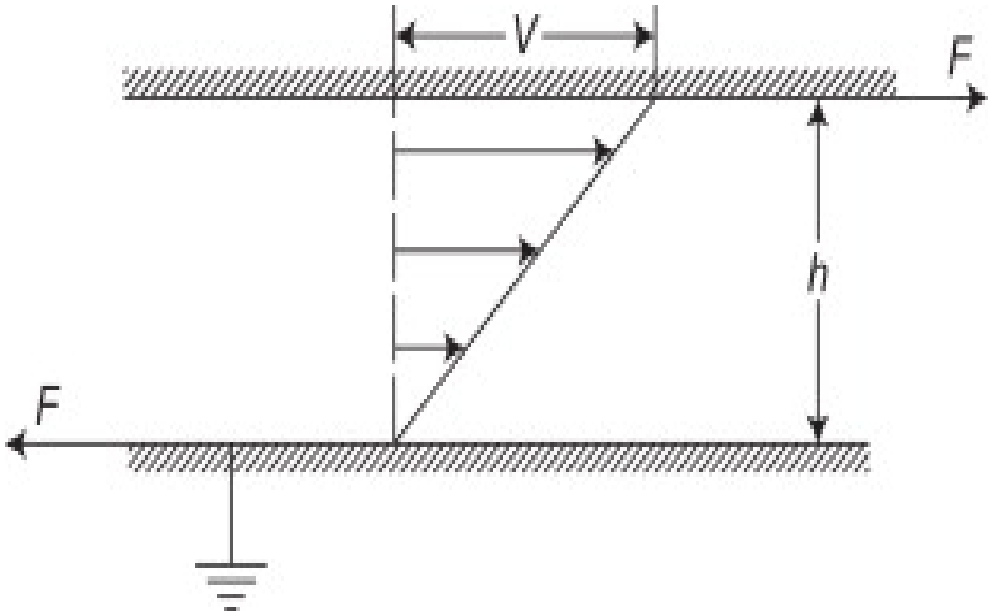

Figure 2.12: Shear flow between parallel plates. Figure reproduced with permission (Houghton et al., 2013)

In these measurements, the shear stress (τ), can be related to the force (F) and area (A) by equation (2.18):

$$\tau = \frac{F}{A} = \eta \frac{dv}{dh} \quad (2.18)$$

where F is the applied force to each plate to maintain the motion and A represents the area of the plates in contact with the fluid, and dV/dh is the velocity gradient representing the shear rate ($\dot{\gamma}$). The unit for shear stress is Pa (pascal) whereas for shear rate is s^{-1}. In shear deformation, shear viscosity (η) is demonstrated by the relationship between the shear rate over the shear stress:

$$\eta = \tau/\dot{\gamma} \quad (2.19)$$

Viscosity is simply the fluid's resistance to flow, and it is expressed in the unit Pa s.

Flow behaviour

Generally, when fluids are subjected to shear stress, their flow tends to show different viscosity behaviour. The behaviour can be classified in terms of Newtonian or non-Newtonian fluid behaviour. Newtonian fluids follow a linear relationship between shear stress and shear rate. A Newtonian fluid behaviour is illustrated in Figure 2.13. The slope of the plot represents the constant viscosity of the fluid. Non-Newtonian fluids exhibit more complex characteristics. Non-Newtonian fluids comprise inelastic non-Newtonian behaviour. Inelastic non-Newtonian fluids are commonly identified by their non-constant viscosity behaviour with respect to shear rate. Inelastic non-Newtonian fluids consists of time-independent and time-dependent fluid properties. In this review work, we only discuss the inelastic time-independent fluid properties.

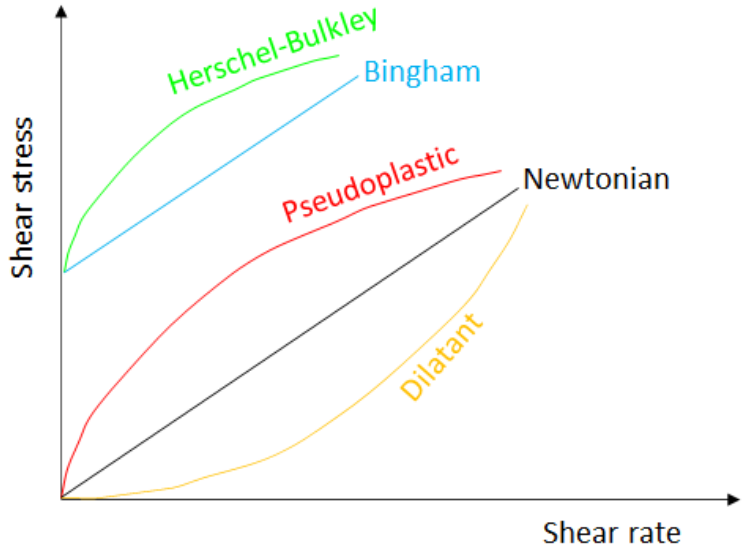

Figure 2.13: Rheology of non-Newtonian fluids. Figure adapted from Berk (2009)

Time-independent characteristics of inelastic non-Newtonian fluid

Figure 2.13 shows the three common models i.e., dilatant, pseudoplastics, Bingham plastic and Herschel Bulkley, demonstrating time-independent characteristics of non-Newtonian fluids. Dilatant and pseudoplastics fluid models describe the non-Newtonian behaviour where the viscosity increases or decreases as the shear rate increases, respectively. This means that dilatant and pseudoplastics fluids have a shear-rate dependent viscosity. Generally, depending on the testing fluid, the decrease in the viscosity displays a phenomenon known as shear-thinning; the opposite is known as shear-thickening. Pseudoplastic fluids tend to undergo the shear-thinning behaviour whereas the dilatant exhibit shear-thickening behaviour. To represent shear-thickening and shear-thinning transition regions, the power-law model also known as the Ostwald-de Waele model is commonly applied. Equation (2.20) shows the model written based on shear stress data:

$$\tau = M(\dot{\gamma})^n \qquad (2.20)$$

In this power law model, τ represents the shear stress, $\dot{y}$ represents the shear rate, M is the consistency coefficient, and n is the flow behaviour index. Depending on the value of n, this model can be used to represent:

- Shear thinning, where $0 < n < 1$,
- Shear thickening, where $1 < n < \infty$
- Newtonian fluids, where $n = 1$

On the other hand, Bingham fluids only follow a linear relationship between stress and shear rate past a yield point. The yield point marks the minimum force needed to induce flow in the fluid. Supplementary to the Bingham fluid model is the Herschel–Bulkley model. The model describes fluids that exhibit both the power law model and a yield point. It is important to note that below the yield point in both Bingham and Herschel-Bulkley fluids, the materials behave like solids. The Herschel–Bulkley model is expressed as follows:

$$\tau = \tau_0 + k\dot{y}^n \qquad (2.21)$$

where τ_0 is the initial flow resistance, k is Herschel–Bulkley consistency index.

Polymer Flow behaviour

Shear-thinning behaviour is typically observed in polymer melts while a minority of the polymer melt follow Newtonian fluid behaviour at very low and infinitely high shear rates. Shear thinning in polymer melts is attributed to polymer chains undergoing stretching and disentanglement as the shear rate increases thereby causing the viscosity to rapidly decrease. Figure 2.14 shows the typical relationship between shear rate and apparent viscosity for polymers melts. The behaviour encompasses the three distinct regions i.e. transition region (power law region), zero- and infinite-shear viscosity regions. The power law region is characterised by a continuous decrease of viscosity in polymers. The polymer melt undergoes major disentanglements as it transitions and enters a shear-rate dependent viscosity zone. The disentanglement is indicative of less resistance to flow

causing the viscosity of the polymer melt to decrease. Herein, the power law model provides a simplified representation to predict the viscosity of the polymer melts at different shear rates.

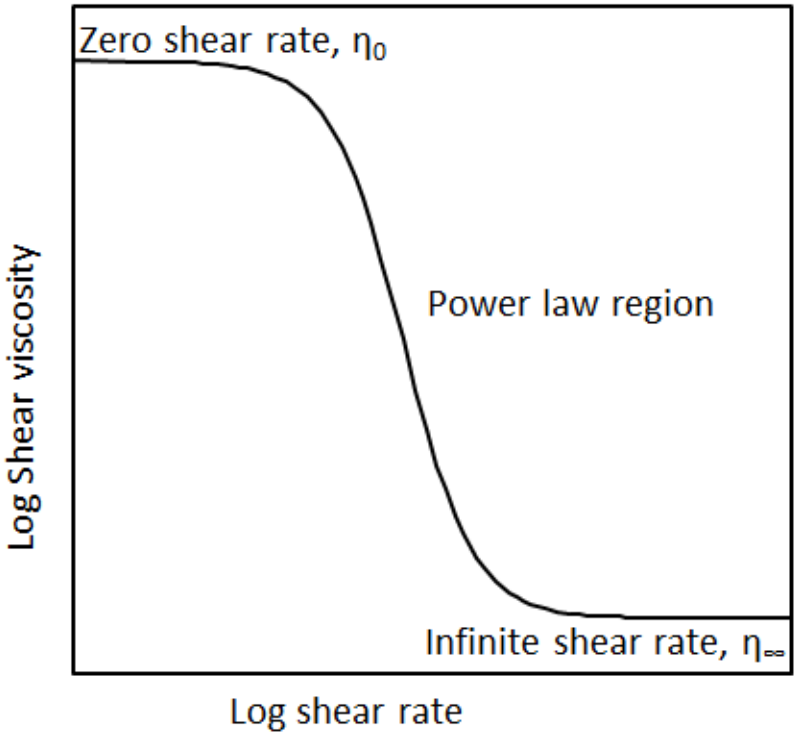

Figure 2.14: Relationship between the shear rate and the apparent viscosity for non-Newtonian fluids demonstrating shear thinning behaviour. Figure adapted from (Amoo and Layi Fagbenle, 2020)

The zero- and infinite-shear viscosity region describes the flow behaviour of the polymer at shear rates approaching zero and infinity, respectively. At both regions, the polymer melt has a constant viscosity and behaves like a Newtonian fluid. At high shear rate, polymer chains move past each other easily. In this region, polymer chains are fully disentangled and aligned, whereas at the low shear-rate regime, the zero-shear viscosity can be determined. To account for all three regions, the Cross model, Carreau-Yasuda model, and Sisko model are frequently applied:

Cross model:

$$\frac{\eta_s-\eta_\infty}{\eta_0-\eta_\infty}=\frac{1}{1+(k\dot{\gamma})^n} \tag{2.22}$$

Carreau-Yasuda model:

$$\frac{\eta_s-\eta_\infty}{\eta_0-\eta_\infty}=\frac{1}{1+((k\dot{\gamma})^a)^{\frac{n-1}{a}}} \tag{2.23}$$

Sisko model:

$$\eta=\eta_\infty+k\dot{\gamma}^{n-1} \tag{2.24}$$

where η_0 is the zero-shear viscosity; η_∞ is the infinite shear viscosity, α is Carreau-Yasuda model transition parameter and k is the consistency index, which is indicative of the onset of shear thinning; The k has the same function for all models.

Viscoelastic fluids

Polymer blends usually display viscoelastic fluid characteristics due to the mixing of two or more different polymers. Viscoelastic fluids are also a type of non-Newtonian fluids which constitutes two different properties. i.e., elastic property (stores energy) and viscous property (dissipates energy). Elastic materials are those that return to their original shape after deformation whereas purely viscous fluids undergo deformation, followed by a long-lasting rearrangement of the fluid molecules. Viscoelastic fluids display intermediate behaviour between these two extreme properties. The viscoelastic behaviour regarding polymer melts is associated with how quickly molecular arrangements occur in response to an applied stress and change in temperature.

When measuring the viscoelastic characteristics of polymer blends, it is important to ensure that the measurements are performed within the material's linear viscoelastic (LVE) region. The LVE region is the range of stress where the material exhibits a linear relationship between stress and strain. In this region the materials response to stress and

strain relationship is proportional. To determine the LVE region experimentally, a strain sweep test is commonly conducted. In this test, the material is subjected to a range of strain amplitudes while measuring its response, such as the storage modulus (G') and loss modulus (G''). The LVE region is identified as the range of strain amplitudes where the storage modulus remains constant, indicating a linear relationship between stress and strain. Beyond the LVE region, the material may exhibit non-linear behaviour, where stress and strain are no longer directly proportional. The breakdown of the linear relationship typically occurs when the stress or strain reaches a certain threshold, causing the material's structure to deform or break down.

Understanding the viscoelastic behaviour of polymer blends is key for various applications, including polymer processing and product design. The viscoelastic behaviour of polymer melts is normally acquired through oscillation tests. There are several types of dynamic oscillation experiments (e.g., temperature sweep, time sweep, stress sweep and a frequency sweep) to provide valuable information about the viscoelastic properties. Viscoelastic behaviour in polymer blends is often frequency dependent. This means that the response of the polymer blend varies depending on the frequency or rate at which the stress is applied. During the dynamic oscillation experiments the materials subjected to sinusoidal deformation or stress, with the amplitude (strain or stress) and frequency of the oscillation. Figure 2.11 showed the motion of the spindle during the oscillation experiment set up. Figure 2.15 shows a sinusoidal function versus time showing phase angle, relative proportion of viscous and elastic behaviour 0 ° and completely elastic 90 °.

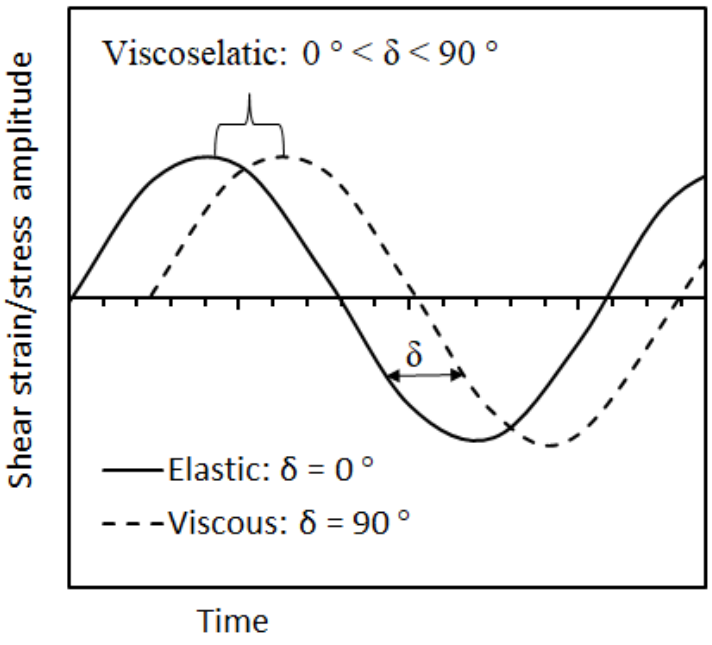

***Figure 2.15*:** A sinusoidal function versus time showing phase angle, relative proportion of viscous and elastic behaviour 0 ° and completely elastic 90 °. Figure adapted from (Dijkstra et al., 2014)

In this test, when the material is subjected to a sinusoidal shear strain, it deforms according to equation (2.25):

$$\gamma = \gamma_0 \sin \omega t \qquad (2.25)$$

Where γ represents the strain amplitude, ω is the frequency and t is time. The applied strain will cause materials to have sinusoidal shear stress, τ, response that lags by a phase angle (δ) as per equation (2.26):

$$\tau = \tau_0 \sin(\omega t + \delta) \qquad (2.26)$$

The phase angle is often expressed in terms of the loss tangent (tan δ). Herein, equation (2.26) can be expressed by the sum of the sine and cosine contributions:

$$\tau = \tau_0 \sin \omega t \cos \delta + \tau_0 \cos \omega t \sin \delta \qquad (2.27)$$

These tests performed measure the phase angle which describes the relative distribution between the elastic (in-phase) and viscous (out-of-phase) components of the overall material's response. It is said to be in-phase when δ = 0° for a perfectly elastic material and out-of-phase when δ = 90° for a purely viscous material. The phase angle strongly depends on temperature and the loading rate. Figure 2.16 shows a vector diagram showing the relationship of complex shear modulus (G^*), storage modulus (G') and loss modulus (G'') and the phase-shift angle δ. The stress response of a linear viscoelastic material to a sinusoidal strain input is given as:

$$\tau = \gamma_0 G' \sin \omega t + \gamma_0 G'' \cos \omega t \qquad (2.28)$$

where,

$$G' = \left({}^{\tau_0}/_{\gamma_0}\right) \cos \delta \quad \& \quad G'' = \left({}^{\tau_0}/_{\gamma_0}\right) \sin \delta \qquad (2.29)$$

Complex modulus, G^*, is a popular dynamic property of viscoelastic materials. It is composed of these two components, storage modulus which represents the storage of energy, and the loss modulus which represents energy loss. The storage modulus and loss modulus are considered the fundamental dynamic properties to describe viscoelastic properties of polymer blends. The structural transitions associated with phase change in polymer melts systems are reflected by the changes in these rheological profiles. The complex modulus as a function of angular frequency (ω) relationship can be expressed in the following form:

$$G^*(\omega) = G'(\omega) + iG''(\omega) \qquad (2.30)$$

&

$$\tan \delta = G''(\omega)/G'(\omega) \qquad (2.31)$$

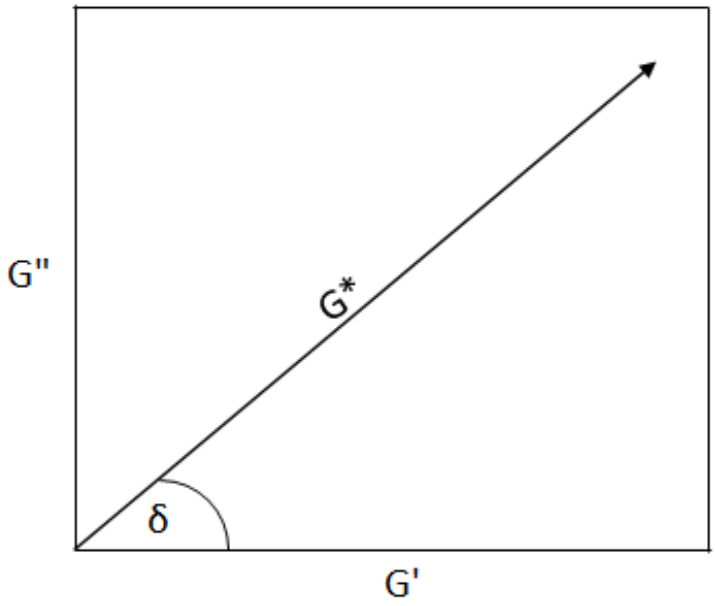

Figure 2.16: Vector diagram showing the relationship of complex shear modulus (G*), storage modulus (G') and loss modulus (G'') and the phase-shift angle (δ). Figure adapted from (Gidde and Pawar, 2017)

Complex viscosity (η*) w is a measure of the total resistance to flow against angular frequency. Complex viscosity is given by the quotient of the maximum stress amplitude and maximum strain rate amplitude as follows:

$$\eta^*(\omega) = G^*(\omega)/\omega = \eta'(\omega) + i\eta''(\omega) \quad (2.32)$$

$$G'(\omega)/\omega = \eta'(\omega) \quad \& \quad G''(\omega)/\omega = \eta''(\omega) \quad (2.33)$$

As can be seen, the complex viscosity combines two limiting cases, that is, the real component and imaginary component, analogous to the complex, loss, and storage modulus.

Figure 2.17 shows a visco-elastic spectrum for an entangled polymer system measured from low to high frequencies. Collectively, the spectrum is composed of a glassy, transitioning, plateau and terminal regions. However, it is important to note that for a given polymer system, depending on the rheometer capabilities and polymer structural

complexity, only a fragment of this spectrum can be observed. The terminal region represents a state where the polymer chains are dominated by viscous behaviour. In this region the polymer is characterised and quantified by the modulus parameters denoting $G'' > G'$. As the frequency increases, a point is reached where $G'' = G'$ denoting the relaxation time (τ_d) also known as the crossover frequency. This relaxation time marks the timescale where the polymer returns to its original state after being stressed. With further increase of the frequency, the polymer enters zones. In the plateau zone, the elastic behaviour of the polymer is the primary dominating parameter quantified by $G' > G''$. At even higher frequencies, the polymer chain enters the glassy region. In the glassy region, the polymer chains appear to be less dependent on the frequency and exhibit low chain mobility.

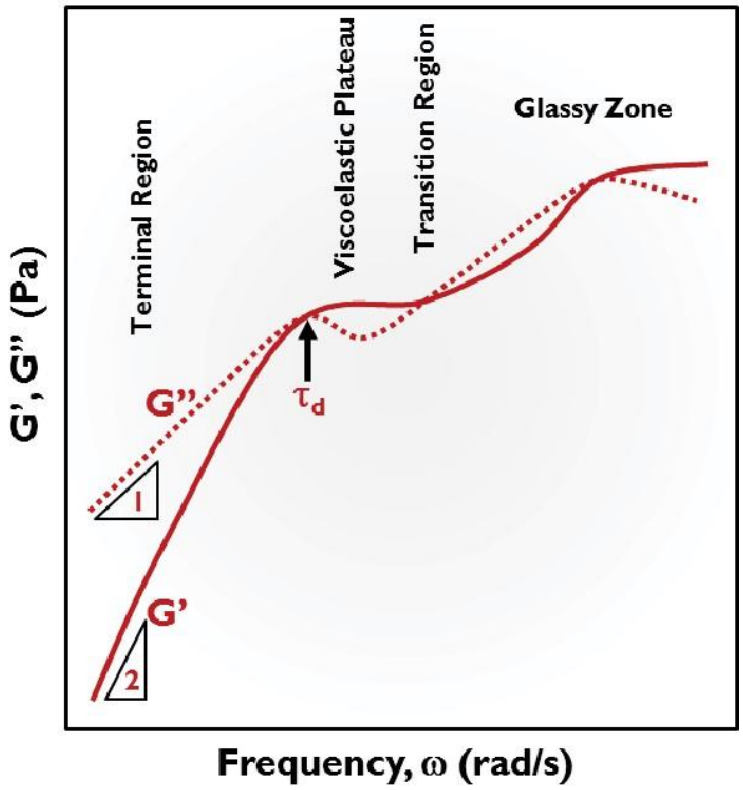

Figure 2.17: Viscoelastic spectrum for an entangled polymer system measured from low to high frequencies. Figure reproduced with permission (Lefebvre and Doublier, 2006)

2.11.1.2 Miscibility using rheology

Miscibility studies employing rheology for polymer/polyethylene blends have been done (Utracki and Schlund, 1987, Müller et al., 1994, Kukaleva et al., 2003). Correlations between rheological functions and molecular mass, composition, temperature etc. have been the subjects of interests. These correlations were used to discover a wide range of phase behaviours that directly influence the properties and ultimate applications of polyethylene blends. Furthermore, to also investigate the degree of miscibility within the polymer blends, many researchers have relied on these correlations (Grunberg and Nissan, 1949, Friedman and Porter, 1975, Utracki and Schlund, 1987). Unfortunately, as a new member in polyethylene blends, there is limited information on the rheological properties and miscibility of F-T waxes and/or F-T wax/PE blends. Although, the associated rheological properties for polyethylene/polyethylene blends display complex behaviours, in general their characteristic responses might give helpful information on the internal structure of F-T wax/PE blends.

Using rheology, the miscibility of blends can be easily established if they exhibit single phase behaviour. For some selected miscible polymer blends, the viscosity follows the popular log-additivity rule (Robeson, 2007, Sotomayor et al., 2014) shown in equation (2.34). It expresses the logarithm of the viscosity (η) as mass fraction (w_i) weighted mean over the logarithm of the viscosity of the pure blend components:

$$\ln \eta = w_1 \ln \eta_1 + w_2 \ln \eta_2 \qquad (2.34)$$

In this equation, the subscripts 1 and 2 correspond to the “diluent” and polymer respectively. This model assumes that the blend components are completely miscible down to the molecular level, i.e., there is no phase separation in the molten state. It is a fully predictable model once the composition and viscosity of the pure components are known. Partially miscible blends, i.e., emulsion-like systems tend to display more complex viscosity behaviour. In these cases, the viscosity will deviate from the log additive rule. Deviations from such systems can arise from many factors including polymer-polymer interaction, molecular mass distribution, chain conformation, chain entanglements, etc.

The viscosity of such mixtures may show either positive or negative deviations from the log additive rule. Positive deviations are likely to arise from strong intermolecular interactions whereas negative deviations can be seen because of weakened interactions or the presence of a dilution factor. Regrettably, deviations from the log additive rule suggests failure to accurately predict the mixing behaviour of these typical polymer mixes. Hence, the development of alternative mixing rules to provide guidance and improve analysis of the phase structure of these blends is key.

To account for the excess viscosity, the log additive rule has been modified to include an excess viscosity term ($\Delta ln\,(\eta)$):

$$\ln \eta = w_1 \ln \eta_1 + w_2 \ln \eta_2 + \Delta \ln(\eta) \qquad (2.35)$$

The addition of an excess viscosity term provides a more accurate estimation of the viscosity behaviour in polymer blends that exhibit more complex viscosity behaviour. The excess viscosity can be determined experimentally and by means of referencing to the predicted viscosity data using the log additive rule. The difference in viscosity from the measured and calculated can be used to predict the magnitude and direction of the excess viscosity term.

On the other hand, for homopolymers, the zero-shear viscosity as a function of molecular mass in polymer melts can be described by an empirical power-law relationship similar to the Mark-Houwink equation:

$$\eta_0 = K M_w^{\alpha}\,, \qquad (2.36)$$

where η_o represents the zero-shear viscosity of the polymer melt, K is a proportionality constant, α is the power-law exponent that relates the viscosity to the molecular mass. M is the mass average molecular mass of the polymer defined by:

$$M_w = \sum w_i M_i \qquad (2.37)$$

The relationship in equation (2.36) is divided into two separate regimens for homopolymers as shown in Figure 2.18.

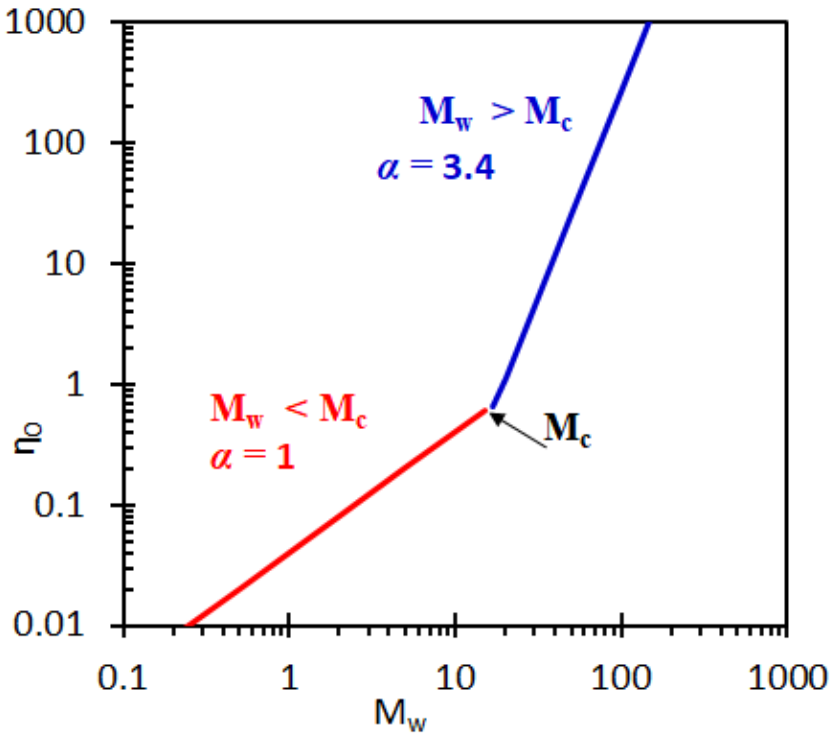

Figure 2.18: Illustration of zero-shear viscosity dependence on molecular mass of polymer melts. Figure adapted from (Padding and Briels, 2002)

Regime (1. red coloured) is below the critical molecular mass for the effect of entanglement on polymer melts (M_c) in a molecular mixture. The zero-shear viscosity generally increases with increasing molecular mass given by:

$$\eta_o = K_1 M_w \tag{2.38}$$

Regime (2. blue colour) is above the critical molecular mass for the effect of entanglement on polymer melt. Herein, the zero-shear viscosity-molecular mass relationship often deviates from the power-law behaviour observed below M_c and the relationship is given by:

$$\eta_o = K_2 M_w^{\alpha} \tag{2.39}$$

The exponent takes on a universal value of α = 3.4. Based on equation (2.39) Friedman and Porter (1975) have proposed that a combination of polymers of a similar chemical structure, but different molecular mass should obey the following mixing rule:

$$\eta_o = \left(w_1\eta_1^{1/\alpha} + w_2\eta_2^{1/\alpha}\right)^{\alpha} \quad (2.40)$$

This model predicts a positive deviation from the log-additive rule for binary miscible molecular blends. It's important to note that the values of K and α are specific to each polymer system and can vary based on factors such as the polymer composition and structure, and experimental conditions. A few other models and theories which consider the interaction parameters have been proposed to model the non-linear dependence of viscosity on composition. The Lederer model can fit both positive and negative deviations from the log-linear blending rule described by equation (2.41) (Lederer, 1931):

$$\ln\eta = (w_1 \ln\eta_1 + \beta w_2 ln\,\eta_2)/(w_1 + \beta w_2) \quad (2.41)$$

Other models that are able to predict deviations from the log-linear relationship include Grunberg and Nissan (1949) and Hind et al. (1960) models.

Grunberg and Nissan (1949):

$$\ln\eta = w_1^2 \ln\eta_1 + 2w_1w_2 \ln\eta_{12} + w_2^2 \ln\eta_2 \quad (2.42)$$

Hind et al. (1960):

$$\eta = w_1^2\eta_1 + 2w_1w_2\eta_{12} + w_2^2\eta_2 \quad (2.43)$$

Other rheological methods to evaluate the presence of morphological changes in polymer blends, associated with miscibility, include the Cole-Cole plots and Han plots (Han and Jhon, 1986, Han, 1988, Mohammadi et al., 2012, Agrawal et al., 2022). These plots have been used to describe the viscoelastic properties of polymer blends having a high degree of relaxation. They are particularly relevant for blends characterised by a two-phase morphology or similar structural complexity. Both these plots are used to explore the presence of different internal structures viz homogenous and heterogenous (co-continuous and dispersed phase) structure. These plots demonstrate relaxation mechanism induced by composition and temperature changes. By analysing these plots for a polymer blend, researchers can gain a better understanding of the blend's rheological behaviour. This enables adjustment to improve processing properties. For the

Cole-Cole plots, the plots are represented by a relationship between the real (η') and the imaginary (η'') parts of the complex viscosity, whereas the Han Plots are plots of log G' versus log G''. A strong linear correlation and a single smooth semi-circular curve in the Han Plots and Cole-Cole plots, respectively, indicates good compatibility. Deviations from the above-mentioned plots suggests heterogeneity of the blend.

In this study, rheology is key to understand the physicochemical nature of the wax/LLDPE blend as a processing aid. Viscosity is an important property to be considered when choosing a processing aid with good mixing properties. For a series of related waxes, the viscosity will increase with the strength of intermolecular forces and molecular mass. Moreover, the rheological properties of waxes are extremely sensitive to changes in the temperature and composition. Importantly, a low melt viscosity can facilitate rapid homogenization of distributed particles without negatively affecting the mechanical properties of the matrix polymer. An extremely low melt viscosity can encourage weak interfacial adhesion and phase separation when mixed with larger polymer molecules in the mixture. Hence it is crucial to understand the overall rheological properties of these blends in their molten state.

2.11.2 Differential scanning calorimetry (DSC)

2.11.2.1 Brief introduction of DSC

Figure 2.19 shows the heat-flux DSC that was utilised in this study. The heat-flux DSC contains a single temperature-controlled oven. In the oven, a sample pan and reference pan (empty) are heated/cooled at the same time. During this process, the DSC computer measures the difference in temperature between the sample and reference at a programmed rate. The difference depends on the nature of the sample pan contents. This difference is presented as a plot of the difference in heat ($\dot{q}$) versus temperature (T). This type of measurements provides qualitative and quantitative information about thermal properties of the sample investigated.

Figure 2.19: Standard heat flux differential scanning calorimeter (DSC)

DSC thermograms are obtainable under conditions of changing temperature or constant temperature throughout the entire process of interest. The former is termed as the non-isothermal process while the latter is an isothermal process. DSC isothermal process is normally employed when studying crystallisation kinetics. This is achievable by using a temperature-controlled heat source system that can maintain a stable temperature.

Figure 2.20 shows a standard non-isothermal dynamic scan of a HDPE polymer. Herein, the DSC was used to study melting and crystallisation behaviour of high-density polyethylene. Upon heating, thermal energy is absorbed to heat the material to higher temperature. The response being proportional to the amount of sample, the heat capacity and the temperature scan rate. Beyond this, additional heat can be absorbed or released when a phase transition occurs. For example, melting of the solid is an endothermic event and the transition is conventionally represented by an upward deviating signal. Crystallisation occurs upon cooling from the melt and the phase transition is shown by a downward exothermic process. The melting and crystallisation processes are represented by a curve. The thermograms tend to show plateaus, i.e., regions where the heat flux remains unchanged corresponding to either liquid or solid phases with constant heat capacities. The highest point on the curve marks the melting point. The change in enthalpy is obtainable from the exothermic or endothermic event as the area of the peak. These measurements can be used to quantify the degree of crystallinity in a blend containing a mass fraction w_p of the polymer by using the following equation:

$$X_c(\%) = \Delta H_m / \left(w_p \Delta H_m^0\right) * 100 \qquad (2.44)$$

where ΔH is the change in enthalpy of the polymer materials and w_p is the mass fraction polymer in the blend. The enthalpy of melting of 100 % crystalline polyethylene is ΔH_m^0 = 293 J/g (Wunderlich and Czornyj, 1977).

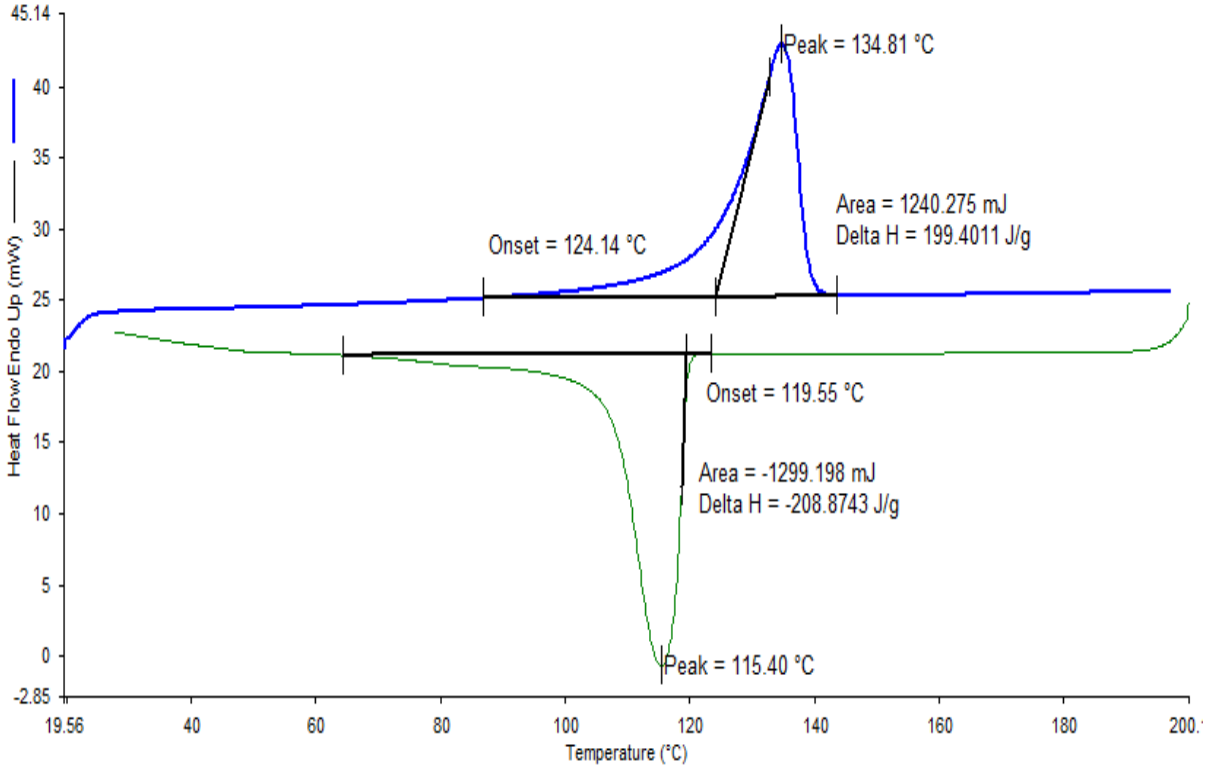

Figure 2.20: Heating and cooling DSC curves, showing crystallisation and melting transitions of HDPE

Melting and crystallisation curves come in different shapes and sizes depending on the polymer phase behaviour. For instance, unlike the HDPE which exhibits a relatively sharp narrower peak, some samples e.g., waxes may exhibit broader melting curves with multiple crystal forms. The DSC scan of a commercial polyethylene wax (Licowax) in Figure 2.21 reveals complex melting behaviour. For the polyethylene wax and other lower molecular mass polyethylene waxes, the first broad peak is commonly referred to as a shoulder peak (Webber, 2009). The shoulder peak represents a solid-solid transition prior to true melting of the crystal (Srivastava et al., 1993). In alkanes, this may take the form of rotator phase transitions (Kuryakov et al., 2020). Handoo et al. (1989) have ascribed solid-solid transitions in petroleum waxes to polymorphism. However, Ungar et al. (1985) attributed the double-peaking in the DSC scan of ultra-long waxes, to the melting of folded chain crystals and extended chain crystal structures. A similar feature of double peaking has been observed in the DSC scan of an F-T wax (refer to Figure 2.22). But, unlike polyolefin waxes, this occurrence was explained to result from the melting of multiple

domains consisting of different molar mass chain lengths (Luyt and Krupa, 2008, Webber, 2009). This reveals that some F-T waxes are comprised of a combination of components with varying chain lengths. Due to their distinct compositions, a blend system featuring F-T waxes, is likely to have formation of multiple domains that melt or crystallise at different temperatures. Therefore, the DSC melting, and crystallisation processes are an important field of study in this project as they provide valuable information about thermal phase transitions and the purity of the materials.

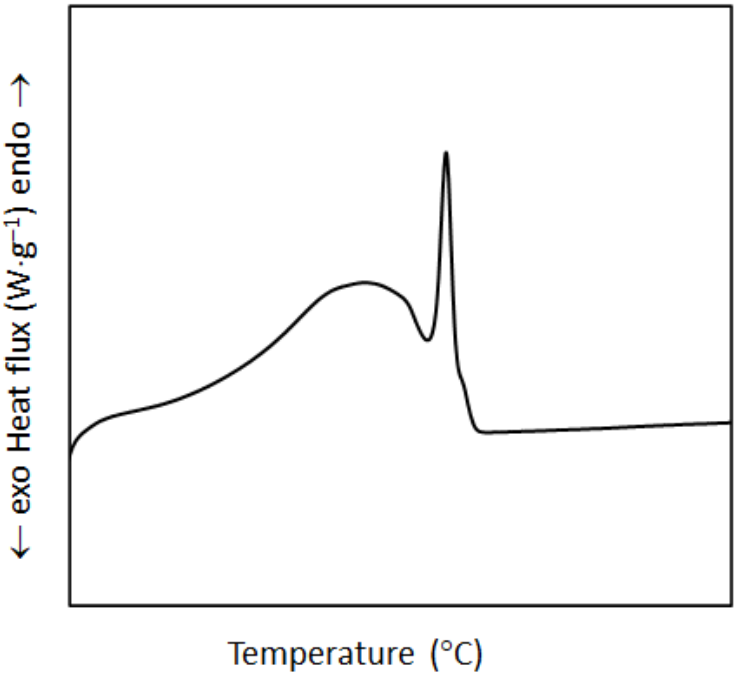

Figure 2.21: DSC scan of polyethylene wax, Licowax

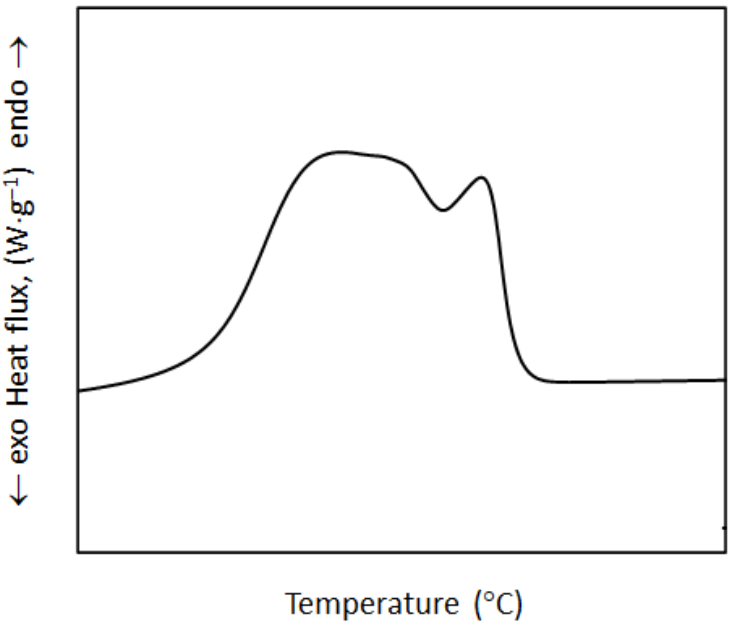

Figure 2.22: DSC scan of an F-T wax

2.11.2.2 Exploring miscibility using DSC

The glass transitioning temperature (T_g) is a parameter used to probe miscibility in polymer blends, whether amorphous or semi-crystalline. The T_g refers to the temperature at which a material transitions from a hard, brittle state to a more rubbery, viscous state. At temperatures below the T_g, the material is typically hard and rigid because its molecular structure is in a more ordered state. As the temperature increases and approaches the T_g, the molecular motion and flexibility of the material increase. Beyond the T_g, the material behaves more like a supercooled liquid, with increased molecular mobility. The T_g can be determined using DSC (Leyva-Porras et al., 2019). In the study of blends, a single T_g, positioned in-between those of the two parent compounds, reflects full miscibility, while the observation of two distinct T_g's (due to their respective components) reflects immiscibility. Similarly, the DSC melting, and crystallisation peak temperatures have been equally applied for semi-crystalline polymer materials. As is the case with the glass transition, a single melting and crystallisation transition suggests the presence of a homogenous crystalline structure whereas two different peaks indicate immiscible crystal

phases. On the other hand, shifts and alterations of the melting/crystalline peak have been associated with co-crystallisation and partial miscibility in the blend system (Gumede et al., 2016).

The DSC is also considered an essential technique for investigating crystallisation kinetics. Crystallisation kinetics provides valuable information about the processes and rates of crystal phase transformations and the growth of pre-existing and new phases. Notably, crystallisation kinetics do not directly predict miscibility in polymer blends. But, the analysis of the phase transformations, where miscibility is a factor, provides significant insights in the structural changes in the solid phase. For example, if two components form an immiscible blend with two distinct solid phases, crystallisation kinetics models can be used to describe the kinetics of the phase transformation of the two solid phases (Avrami, 1939, Avrami, 1940). Accordingly, in the case where changes in the route of the crystallisation process occur, these models can give insight regarding possible chain interaction in the blend (Zachmann and Wutz, 1993).

Isothermal crystallisation is often modelled with the Avrami equation (Avrami, 1939, Avrami, 1940) Other models applicable for isothermal crystallisation include the Lauritzen-Hoffman (L-H) model (Lauritzen and Hoffman, 1960) and the log-logistic distribution, also known as the Hill model (Hill, 1910). In addition, this study also considered a generalized logistic function to represent the overall crystallisation process (Díaz-Díaz et al., 2021). This method considers the possible nucleation and growth processes that may occur for different crystalline forms in the polymer. It does not explicitly identify the nucleation and growth stages nor specify crystalline forms but seeks to minimize experimental errors that can otherwise introduce complicated variables. Like the former models, the generalized logistic function can also represent the DSC curves resulting from isothermal crystallisation experiments.

In this study, DSC was a key technique for understanding the physicochemical nature of the wax/LLDPE blend. The DSC can provide valuable information about the melting & crystallisation behaviour, thermal stability, and miscibility within the blend by examining the thermal transitions. This information is also important for the optimization of the processing conditions.

2.11.3 Polarised optical microscopy (POM)

2.11.3.1 Brief introduction of POM

Figure 2.23 shows the picture of a typical polarised optical microscope used in this study. The optical microscope is a powerful technique that uses visible light and glass lenses to magnify and image micron-sized samples. This technique can provide direct evidence of the evolution of crystallinity in a polymer melt being cooled. It can also reveal the crystalline structure of a solid material. In this study, microscopy was used to observe such crystallisation processes occurring in blends with wax. Optical microscopy has many benefits including a temperature-controllable sample stage which facilitated isothermal crystallisation experiments. It also offers advantages such as high sensitivity and resolution (although inferior to electron microscopes), high speed of data acquisition, qualitative results, and non-invasiveness.

Figure 2.23: Polarised optical microscope (POM)

Sample preparation for microscopic analysis involves sectioning of the polymer solid/pellets and then placing it between two transparent glass slides. The slides are then pressed together to produce a thin film with uniform thickness upon heating. During analysis, the visible light illuminates the specimen eventually allowing the user to acquire a magnified image through the light-sensitive cameras.

Polarised optical microscopes are popular and extensively used to image the crystalline structure of birefringent polymer materials (Raimo, 2019). When the beam of light interacts with an anisotropic or oriented polymer regions, birefringence or double refraction occurs. Birefringence arises due to the asymmetry of the crystalline lattice in the crystal structure. Birefringence is a phenomenon where the light is transmitted and split up into two components, traveling in different directions with different refractive indices. Polarising microscopes work by converting this beam of light to polarised light using polarisers. Polarisers selectively transmit light waves with a specific polarisation orientation in a single direction. By controlling the polarisation of light and studying its interaction with birefringent polymers, polarising microscopes can enhance image contrast and visualize anisotropic structures.

Usually, in the presence of certain alignments of polymer chain orientations, a variety of coloured patterns, including “Maltese cross” pattern can be observed. “Maltese cross” pattern, indicates that the polymer is birefringent therefore has optical property of a refractive index that depends on the polarisation of the light. The "Maltese cross" pattern appears as a dark cross surrounded by bright regions. The crystalline regions appear as bright areas, known as "birefringent regions," while amorphous regions will appear darker (Xu et al., 2018). For example, upon observation of the polyethylene micrograph in Figure 2.9, these unique crystalline features in the structure can be noted and quantified. Birefringence can be quantified by measuring the difference between the refractive indices transmitted and split up into two ray components.

2.11.3.2 Studying miscibility using optical microscopy

Polymer blends may come with distinct phase structures. Polarised optical microscopes can distinguish between such phases due its ability to sense and differentiate crystal sizes, shapes and variations in the uniformity in the crystalline structures. So, in polymer blends, microscopy is useful for revealing the presence of either homogenous or dispersed phases. For example, Chen and Wolcott (2015) used polarised optical microscopy to image the crystalline morphology of paraffin wax/polyethylene blends. Figure 2.24 shows the isothermally crystallised paraffin wax/polyethylene at 70/30 composition ratio at their respective crystallisation temperatures. The study considered different polyethylene grades viz HDPE, LDPE and LLDPE. Although, the general spherulitic morphology of polyethylene was observed, the wax/PE blends consisted of the spherulitic crystallites displaying different degrees of perfection. This means the crystallisation process of the polymer present in the blends was altered. It became more complex compared to the crystallisation behaviour of the two pure components. The differences in crystallisation behaviour results for a variety of reasons including changes in the primary nucleation mechanism, the growth of the crystals and inter-diffusion of crystallisable and non-crystallisable chains to and from the growing crystal (Groeninckx et al., 2014).

Furthermore, optical microscopy is also useful for the determination of cloud points. The cloud point of a homogeneous solution is the temperature at which either a liquid-liquid or a liquid-solid phase separation occurs. In the former case, an emulsion is formed. In the latter case a suspension of crystals is obtained. In both cases, the initially clear solution becomes cloudy in and abrupt fashion. Therefore, cloud point measurements can be used to determine miscibility of systems or the onset of polymer crystallisation. The beginning of cloudiness marks the phase boundary where first crystals appear during cooling from the polymer melt. Optical microscopes, employing a temperature-controlled sample stage, are crucial in controlling the reproducibility of the crystallisation process and cloud point measurements. In both procedures, the microscope can be effectively used to study the effect of temperature and blend ratio on the crystallisation process in polymer blends. The crystallisation temperature has a direct influence on the ultimate crystalline structure.

The sizes and shapes of polyethylene spherulites are determined by the cooling rates or the selected isothermal crystallisation temperature (Raimo, 2015). The crystallisation behaviour of the dispersed phase is also affected by the blending ratio (Mofokeng et al., 2018). Therefore, optical microscopy is a useful technique for studying the crystallisation of blends and their final crystalline structure. This helps to gain better understanding of the corresponding structure-property relationships.

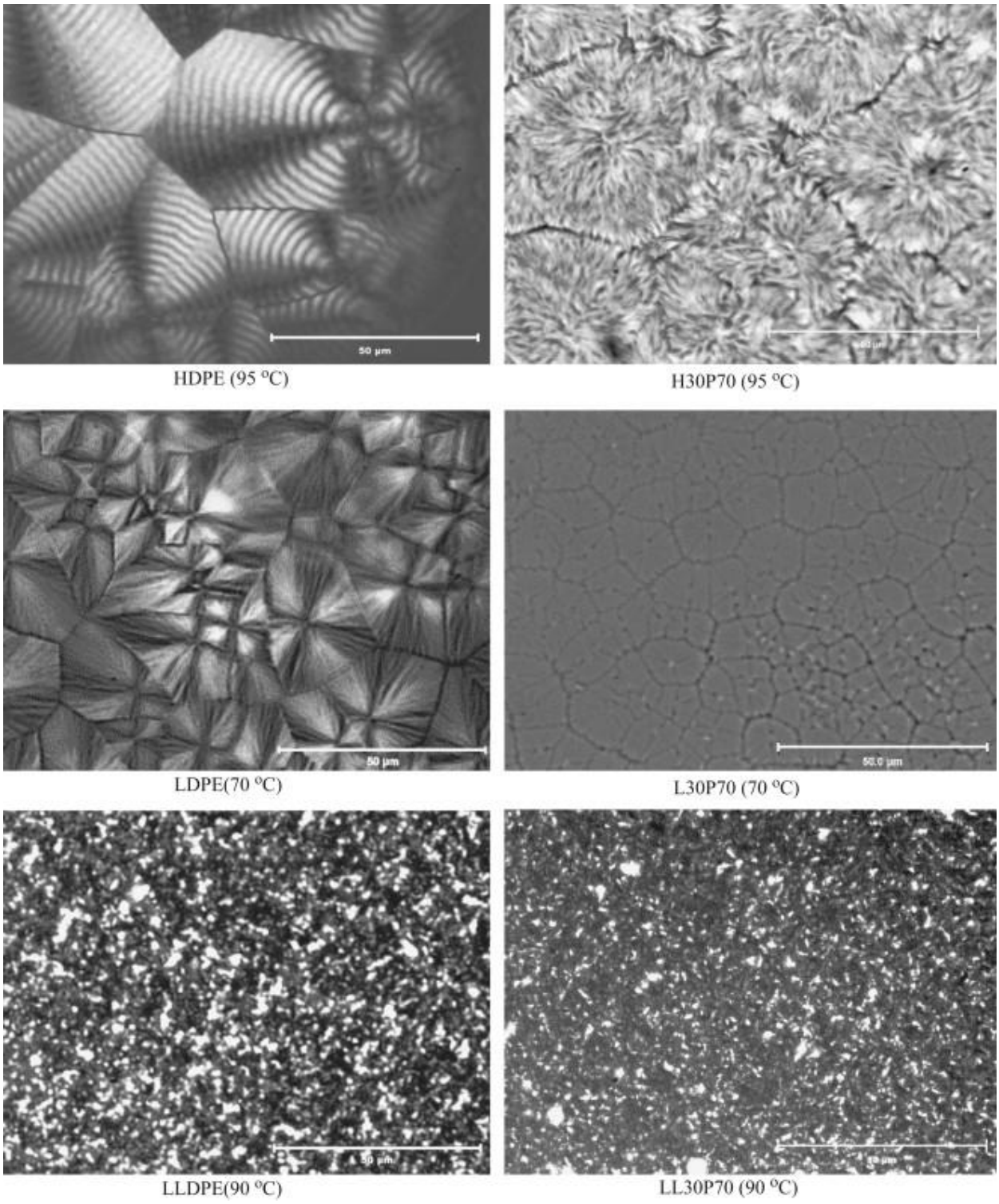

Figure 2.24: POM images of paraffin wax/polyethylene viz HDPE, LDPE, LLDPE crystals isothermally crystallised at specific temperatures a with a formulation of 70 wt-% wax and 30 wt-% polyethylene. Figure reproduced with permission (Chen and Wolcott, 2015)

2.12 MISCIBILITY IN WAX AND POLYETHYLENE BLENDS

The literature reveals that extensive work was done on wax/polyethylene blends. However, many of the blends were prepared for applications other than the one considered presently, i.e., the application as a processing additive. Most studies used comprehensive DSC analysis to determine the extent of compatibility in the wax/polyethylene blends systems. Table 2.2 summarises DSC data for a range of wax-polyethylene blends. It includes the effect of the nature of the components and the blend ratio on the crystallisation peak temperatures and enthalpy of melting. The studies considered both neat and oxidised, paraffin and F-T waxes. Blends of these waxes with HDPE (Luyt and Brüll, 2004, Hato and Luyt, 2007, Molefi et al., 2010, Sotomayor et al., 2014), LDPE (Mtshali et al., 2001, Mtshali et al., 2003a, Krupa et al., 2007) and LLDPE were considered. Some of these studies compared the performance of a single wax with different polyethylene types (Luyt and Brüll, 2004, Hato and Luyt, 2007, Molefi et al., 2010, Mtshali et al., 2003a). Other studies compared the influence of different types of wax blended with one type of polyethylene (Mtshali et al., 2003a, Mpanza and Luyt, 2006a, Hato and Luyt, 2007).

Table 2.2: Wax components used in polyethylene blend studies

PE/Wax	PE/Wax ratio	T_m (°C)	ΔH_m (J g^{-1})	Wax Properties	Reference
LLDPE/EnHance	100/0	127.0	82	Highly crystalline F-T D_m =117 °C; *T_m = 94.2 / 108.1* °C*;* ΔH_m = *215* J g^{-1}	(Mpanza and Luyt, 2006a)
	99/1	127.0	90		
	97/3	125.2	94		
	95/5	120.1	96		
	90/10	119.9	105		
LLDPE/H1	99/1	128	82	F-T paraffin M = 785 Da; D_m =112 °C; ρ = 0.94 g cm^{-3}; C#:C33-C128; *T_m = 102 / 88.3 / 77.1* °C*;* ΔH_m = *205* J g^{-1}	
	97/3	127.2	92		
	95/5	126	86		
	90/10	127	87		
LLDPE/M3	99/1	126.0	85	F-T paraffin *M* = 440 Da; D_m = 73 °C; ρ = 0.90 g cm^{-3}; C#:C15-C78; *T_m = 56.0 / 66.1* °C*;* ΔH_m = *168* J g^{-1}	
	97/3	125.7	81		

	95/5	124.5	80		
	90/10	125	71		
LDPE/Paraffin	100/0	127.7	167.3	Hard, brittle paraffin; T_m = *77.2* °C*;* ΔH_m = *213.1* J g^{-1}	(Krupa and Luyt, 2000)
	98/2	128.4	168.3		
	95/5	128.4	173.45		
	90/10	127.8	172.2		
	80/20	127.2	190.1		
	70/30	127.0	196.1		
	60/40	127.2	175.8		
LDPE/Paraffin	100/0	102.5	83.8	Hard, brittle F-T paraffin M = 785 Da; T_m = 90 °C; ρ = 0.940 g cm^{-3}; C#: C28-C120; T_m = *78.2* °C*;* ΔH_m = *210.4* J g^{-1}	(Mtshali et al., 2001, Luyt and Krupa, 2002)
	90/10	102.6	94.8		
	80/20	102.5	102.4		
	70/30	102.7	102.3		
	60/40	103.1	127.3		

LLDPE/Paraffin	100/0	127.5	161.7	Oxidized F-T paraffin M = 785 Da; ρ = 0.94 g cm^{-3}; T_m = 96 °C; C/O:18.8/1; T_m = *70.5* °C*;* ΔH_m = *174.0* J g^{-1}	(Krupa and Luyt, 2001a, Luyt and Brüll, 2004, Krupa et al., 2007, Luyt and Krupa, 2002)
	95/5	126.7			
	90/10	126.5			
	85/15	126.5			
	80/20	126.1			
	75/25	126.2			
	70/30	126.5			
	60/40	126.2			
	50/0	125.9			
LLDPE/paraffin	100/0	131.2	159.1	Hard F-T paraffin M = 785 Da; T_m = 90°C; T_d = 250 °C; C#: C33-C128; T_m = *77.2* °C*;* ΔH_m = *206.5* J g^{-1}	(Hlangothi et al., 2003)
	95/5	128.9	159.5		
	90/10	128.7	150.0		
	80/20	126.4	160.1		
	70/30	129.2	182.5		

	60/40	128.0	172.4		
LLDPE/wax	-	-	-	Oxidized, hard F-T M = 750 Da; ρ = 0.95 g cm^{-3}	(Mtshali et al., 2003, Djoković et al., 2003)
LDPE/WaxS	100/0	111.5	110	Soft paraffin wax M = 374 Da; C#: C18-C44; T_m = *40.7* °C*;* ΔH_m = *209* J g^{-1}	(Krupa et al., 2007)
	70/30	104.9	138		
	60/40	103.4	150		
	50/50	102.4	161		
	40/60	99.2	174		
LLDPE/H1	100/0	123.7	79.7	F-T Hard paraffin wax M = 813 Da; D =1.25; T_m = 90 °C; ρ = 0.940 g cm^{-3}; C#: C28-C120; T_m = *76.5* °C*;* ΔH_m = *178.8* J g^{-1}	(Hato and Luyt, 2007)
	90/10	125.7	103.7		
	80/20	124.5	95.3		
	70/30	123.7	98.3		
HDPE/H1	100/0	129.9	79.7		
	90/10	131.4	150.6		

	80/20	129.5	166.7	
	70/30	128.7	170.5	
LDPE/H1	100/0	104.2	79.7	
	90/10	104.0	103.7	
	80/20	103.7	95.3	
	70/30	103.4	98.3	
LLDPE/A1	90/10	123.9	71.4	oxidized F-T paraffin wax M = 669 Da; ρ = 0.95 g cm^{-3}; T_m = 96 °C; C/O:18.8/1, T_m = *56.0 / 66.1* °C; ΔH_m = *168* J g^{-1}
	80/20	124.2	67.9	
	70/30	124.2	54.8	
HDPE/A1	90/10	131.2	119.1	
	80/20	129.9	119.8	
	70/30	129.0	122.8	
LDPE/A1	90/10	104.7	71.4	
	80/20	102.0	67.9	

	70/30	101.0	54.8		
LLDPE/M3	0/100	58.4	86.9	Medium-soft F-T paraffin wax M = 440 Da; T_m = 40-60 °C; ρ = 0.90 g cm^{-3}; C#: C15-C78; T_m = *58.4* °C*;* ΔH_m = *86.9* J g^{-1}	(Molefi et al., 2010, Mngomezulu et al., 2010, Mngomezulu et al., 2011, Gumede et al., 2016, Gumede et al., 2017)
	100/0	126.7	172.2		
	70/30	121.8	108.5		
	60/40	119.8	104.9		
	50/50	120.8	130.3		
LDPE/M3	100/0	106.8	75.4		
	70/30	100.4	104.7		
	60/40	96.9	114.0		
	50/50	97.6	111.0		
HDPE/M3	100/0	134.7	149.3		
	70/30	124.6	150.9		
	60/40	124.1	153.2		
	50/50	124.1	148.4		

HDPE/Paraffin	100/0	130.8	178.6	Soft paraffin wax C#: C18-C50	(Sotomayor et al., 2014)
	95/5	129.4	179.8		
	90/10	128.4	180.9		
	80/20	125.4	185.0		
	70/30	124.3	184.1		
	60/40	123.3	205.5		
	50/50	122.4	210.8		

C#: carbon number, D: polydispersity, C/O ratio: Carbon to oxygen ratio, ρ: density, Da: Dalton, M: molecular mass, T_m: melting temperature, D_m: drop melting point, T_c: crystallisation temperature, ΔH: change in enthalpy

All these studies assumed that the presence of a single melting point temperature indicates complete miscibility. Molefi et al. (2010) blended M3 soft paraffin wax with LDPE, LLDPE and HDPE. In the study, they observed two well-separated crystallisation peaks in all the blends with wax contents of 30, 40 and 50 wt-%. This result implied immiscibility of all the polyethylene types with this wax. In mixtures of soft and hard paraffin waxes and LDPE, it was found that only the hard F-T wax co-crystallised with the LDPE (Krupa et al., 2007). Because of the strong distinction of the LDPE peak from the Wax S (the soft wax) peak, the total enthalpy of the mixture exceeded predictions based on the additive rule indicating a higher crystallinity of the polymer than expected (Krupa et al., 2007). However, there was strong peak overlap between the hard F-T wax with the same LDPE (Krupa et al., 2007). Sotomayor et al. (2014) also inferred incompatibility of HDPE with paraffin wax on the basis of dynamic mechanical test results. The HDPE sample featured a unique tan δ peak located at –110 °C. It corresponds to the α-relaxation, i.e., the glass transition temperature (T_g). The blends showed two peaks with one corresponding to the T_g of polyethylene and, another peak centred at –65 °C corresponding to the T_g of the paraffin wax. This proved that the components were not miscible in the solid state.

Some inconsistencies are noted in literature with respect to the miscibility of wax and polyethylenes as far as the composition of the blends is concerned. For instance Hato and Luyt (2007) investigated blends of two paraffin waxes, H1 and A1, with HDPE, LDPE, and LLDPE. Complete solid-state miscibility of HDPE blends with both waxes up to 20 wax-% was found. The LDPE/H1 blend was only partially miscible whereas the LDPE/A1 blends were completely miscible up to 10 wt-% wax. Complete miscibility was observed for all the LLDPE/A1 wax blends. However, in the LLDPE/H1 only partial miscibility was found at all wax contents. Moreover, in blends of cross-linked and uncross-linked low-density polyethylene (LDPE)/F-T wax, a single melting peak, belonging to LDPE phase, was found. This observation strongly suggested complete miscibility considering that the wax has three peaks in its pure state (Mtshali et al., 2001). In other studies, Mtshali et al. (2003a) and Djoković et al. (2003) also observed similar mutual mixing for an oxidised Fischer–Tropsch wax blended with both LDPE and LLDPE.

Luyt and Brüll (2004) performed crystallisation analysis fractionation (CRYSTAF) and size exclusion chromatography coupled to FTIR (SEC-FTIR) on a series of HDPE-wax, LDPE/wax and LLDPE/wax blends. The CRYSTAF analysis shows very little or no co-crystallisation of wax with HDPE and LDPE but provided strong indications of co-crystallisation with LLDPE. Furthermore, the co-elution of wax with LLDPE in SEC-FTIR analyses indicating some chemical interaction between the oxidized wax and LLDPE.

2.13 MISCIBILITY IN WAX/LLDPE BLENDS

Focusing on blends of LLDPE and a variety of waxes, complete miscibility in the crystalline phase has been observed for LLDPE/oxidised Fischer-Tropsch paraffin wax blends (Krupa and Luyt, 2001a, Luyt and Krupa, 2002). This behaviour was indicated by the presence of a single melting and crystallisation peak of an LLDPE-rich phase and the absence of three melting peaks due to the wax in blends containing up to 50 wax-%. When compared to neat Fischer-Tropsch paraffin wax/LLDPE blends only one endothermic peak in blends up to 30 wax-% was seen. Surprisingly, these studies reported that the oxidised wax has virtually no influence on the melting and crystallisation temperature and the corresponding heat of melting. Figure 2.25 & 2.26 shows the heating and cooling DSC scans of the oxidised F-T wax/LLDPE blends. It appeared as if the oxygen-containing groups in oxidised wax caused the wax to interact differently with the LLDPE compared to the neat wax.

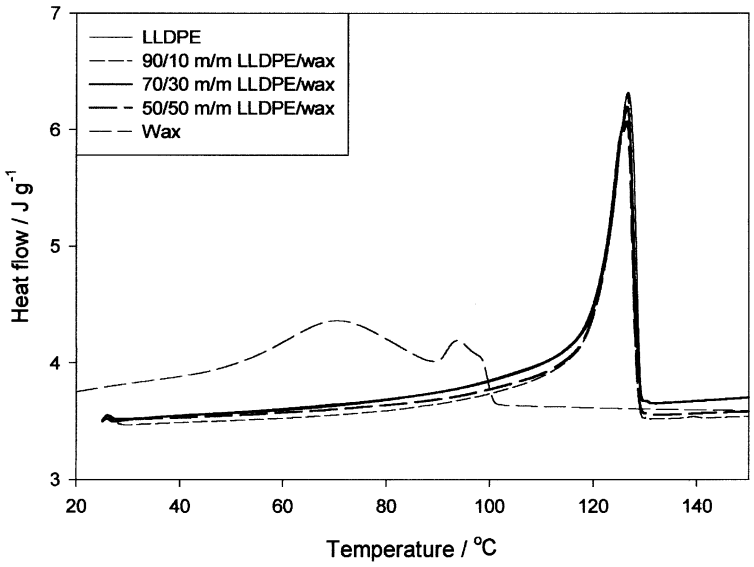

Figure 2.25: DSC heating curves of LLDPE, wax and different LLDPE/wax blends. Figure reproduced with permission (Krupa and Luyt, 2001a)

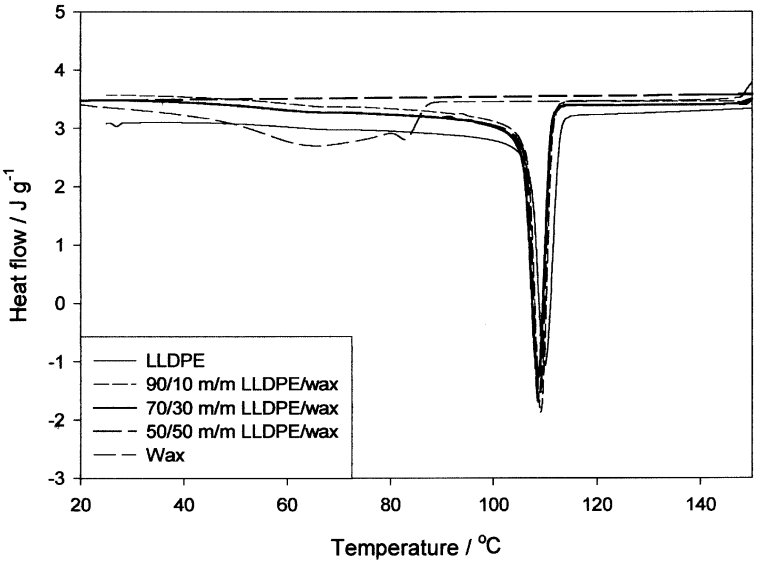

Figure 2.26: DSC cooling curves of LLDPE, wax and different LLDPE/wax blends. Figure reproduced with permission (Krupa and Luyt, 2001a)

Blending LLDPE with oxidised Fischer–Tropsch wax, Mtshali et al. (2003a) also showed that the wax and polyethylene chains do crystallise together, producing a single melting peak for compositions containing up to 30 wt-% wax. However, with increasing wax, a melting peak associated with a wax-rich phase appears at lower temperatures, which shows the presence of crystal phase separation. This result indicated the occurrence of the distinct phase structure belonging to the wax. In

contrast, Mpanza and Luyt (2006a) reported that only trivial amounts of wax can be dissolved in the LLDPE phase. The study compared three different waxes mixed with LLDPE and found partial miscibility up to 5 wt-% wax.

Gumede et al. (2016) investigated the structure and thermal properties of linear low-density polyethylene (LLDPE)/medium soft paraffin wax blends with a range of sophisticated characterisation techniques. Small- and wide-angle X-ray scattering (SAXS) showed that the blends form a single phase in the melt. However, upon cooling from the melt, two crystalline phases, with depressed melting points, develop when more than 10 wt-% wax is present. Gumede et al. (2016) attributed the higher melting point crystalline phase to less-branched LLDPE fractions. Standard DSC results, successive self-nucleation and annealing (SSA) thermal fractionation and the detection of a new SAXS signal were attributed to the lamellar long period of the co-crystals. The results indicate that the lower melting point crystalline phase is a wax-rich phase constituted by co-crystals of extended chain wax and short linear sequences of highly branched LLDPE chains. The implication is that the LLDPE fractions are molecularly segregated as they crystallise upon cooling from the melt to form first the higher melting phase composed of exclusive linear LLDPE chains free of side branches. During this process, the wax molecules are expelled to the amorphous regions. Upon further cooling, the wax chains co-crystallise with the linear portions of highly branched LLDPE chains forming a wax-rich phase. Gumede et al. (2016) attributed this to the wax acting as an effective plasticizer for LLDPE, decreasing both its crystallisation and melting temperature.

2.14 SUMMARY

In summary, the purpose of this work was to investigate the characteristics of F-T waxes blended with high-flow grades of LLDPE for possible use as processing additive in polyethylene masterbatch applications. This study aimed to probed blend compatibility considering the rheology of the melts and the thermal properties and crystalline structure of the solid samples. Briefly, the available literature indicates that, in both crystalline and the melt state, paraffin and F-T waxes are more compatible with LLDPE than with LDPE or HDPE. However, the discussion of the influence of wax composition on the blend compatibility/miscibility and crystallisation behaviour is not

consistent. Moreover, research covering miscibility in F-T wax/LLDPE area is not extensive. On the other hand, experimental studies focusing on rheological properties have been relatively rare. While the influence of composition and temperature have not been fully covered. In conclusion, the versatile role of wax as processing aids, encompassing variety in composition, temperature effect, rheological improvement, and lubrication, underscores their significance in polymer compounding.

CHAPTER 3

3 EXPERIMENTAL

3.1 MATERIALS

Two different polymer materials were used and their molar mass distributions were determined by the Department of Chemistry and Polymer Science, University of Stellenbosch, using size exclusion chromatography (SEC). The high-flow linear low-density polyethylene (LLDPE grade M500026) was supplied by Sabic South Africa (Pty) Ltd. This LLDPE had a melt flow index (MFI) of 50 g/10 min @ 190 °C/2.16 kg and density of 926 kg m^{-3}. The number average molecular mass (M_n) and weight average molecular mass (M) of this grade were 26460 and 92390 Da, respectively. Linear low-density polyethylene (LLDPE grade HM2420) was supplied by Sasol. The density of this grade was 924 kg m^{-3} and the melt Index was 20 g/10 min @ 190 °C/2.16 kg. The number average molecular mass (M_n) and weight average molecular mass (M) of the LLDPE was 23530 and 129100 Da, respectively. Both these materials were milled into a powder (< 400 μm) by Dream Weaver.

Two waxes were used in this study and their molar mass distributions were determined by Cirrebelle (Randburg, South Africa) using a standard gas chromatographic (GC) method. Solid paraffin wax in the form of pellets, code number M3B was sourced from Sasol. The corresponding (M_n) and (M) values were 490 and 493 Da respectively. Sasol also provided an experimental Fischer-Tropsch (F-T) wax 10353 in the form of pellets. The number average (M_n) and weight average (M) molar mass of this wax were 776 and 786 Da, respectively.

Table 3.1: The polymers and waxes are referred as below per their molecular mass in the text, where H- and L- represent high and low molecular mass, respectively:

LLDPE (code: M500026)	L-LLDPE
LLDPE (code: MH2420)	H-LLDPE
Wax (code: 10353)	H-Wax
Wax (code: M3B)	L-Wax

3.2 METHODOLOGY

3.2.1 H-Wax/H-LLDPE and L-Wax/L-LLDPE sample preparation

Both H-Wax/H-LLDPE and L-Wax/L-LLDPE sample blends were prepared by extrusion compounding on a ThermoFischer TSE 24 co-rotating twin-screw compounder (24 mm Φ, 30 L/D). The die had a single exit hole with a diameter of 5.5 mm. The screw speed was set at 50 rpm. The temperature profile, from hopper to die, was set as follows, 60/110/140/170/170/170/170 °C. Wax/LLDPE blends were prepared by mixing predetermined quantities of the wax and the polyethylene powders in increments of 10 wt-%. The blend containing 90 wt-% wax was not prepared using the extrusion method because of the low melt viscosity posed processing problems. The blend containing 90 wt-% wax was prepared differently. The mixture was placed in aluminium pans and covered with aluminium foil before heating to 170 °C in an oven. After 30 min, the liquid mixture was vigorously stirred, then left in the oven for an additional 30 min. This was done to facilitate melting and the homogenisation of the materials via molecular diffusion.

3.3 MATERIAL CHARACTERISATION

3.3.1 Rheometry

The samples were subjected to rheological characterisation on an Anton Paar MCR301 rheometer fitted with a cone and plate configuration. Shear experiments were conducted isothermally at temperatures of 160, 170 and 180 °C. After heating to the measurement temperature, the sample was squeezed down to a gap setting of 0.051 mm. The sample was pre-sheared for 1 minute at a shear rate of 5 s^{-1} followed by 1 min of rest. The viscosity data were collected at applied shear rates varying from 0.01 s^{-1} to 100 s^{-1}. The complex viscosity, loss modulus and storage modulus were determined using frequency sweeps in the oscillatory mode. The applied frequency was scanned from 100 rad s^{-1} to 1 rad s^{-1} at selected isothermal temperature and fixed strain of 0.05 %. The complex viscosity was also determined using temperature sweeps in the oscillatory mode. In these experiments, the temperature was scanned from 180 to 120 °C at a fixed strain of 0.05 % and an angular frequency of 10 rad s^{-1}.

3.3.2 Differential Scanning Calorimetry

Thermal analysis was performed on a Perkin Elmer DSC 4000 analyser. The samples (15 ± 1 mg) were crimped in 50 µL aluminium pans with lids. Nitrogen gas, flowing at a rate of 20 mL min^{-1}, ensured that an inert atmosphere was maintained. The thermal history of each sample was erased by holding it for 5 min at 170 °C.

Non-isothermal crystallisation was studied by cycling the temperature between 0 °C to 170 °C at a scan rate of 10 °C min^{-1}. The data obtained during the second heating and cooling scans were used to determine the peak melting temperature, the peak crystallisation temperature and the enthalpies associated with the melting and crystallisation phase transitions.

Only L-Wax/L-LLDPE samples were explored concerning crystallisation kinetics. It's important to note that the reasons for focusing on this specific sample was based on materials uniqueness in terms of its crystallisation peaks. This L-Wax/L-LLDPE mixture displayed well separated crystallisation peaks while H-Wax/H-LLDPE consisted of overlapping peaks. Analysing crystallisation kinetics can be a complex

process and studying blends with overlapping peaks may introduce additional complexities. The isothermal crystallisation behaviour of the polymer was investigated in the temperature range 98 - 106 °C. The chosen temperature range represented optimal conditions for observing and analysing the crystallisation kinetics of L-Wax/L-LLDPE. This range provided a balance between achieving measurable crystallisation rates and maintaining experimental control. The experiments commenced by cooling the molten sample at 60 °C min^{-1} down to the desired crystallisation temperature. The measured response included an artefact due to the dynamic response of the instrument. This was removed by subtracting the measured response obtained using a run according to the same protocol with the poly(D-lactic acid) as the sample material. This amorphous polymer was chosen as it had no thermal transitions in the temperature range of interest.

3.3.3 Hot Stage Polarised Optical Microscope

The solidification of L-Wax/L-LLDPE melts was studied with a Leica DM2500M optical microscope fitted with a Linkam Scientific CSS450 heating stage. Images were recorded with a Leica DFC420 digital camera. The optical micrographs were obtained under polarised light with a 1 λ retarder plate. Samples were placed on the heating stage and covered with a glass slide to ensure that a thin molten film was obtained. The thin sample was heated from room temperature to 170 °C at a rate of 10 °C min^{-1}, then held there for 5 minutes. Thereafter, the sample was cooled to a selected isothermal crystallisation temperature, 65 °C for pure wax and 100 °C for the LLDPE and the blends. During this time, micrographs of the crystalline structure were captured at one-minute intervals at 2.5×, 10× and 20× magnification.

The equilibrium melting temperature T_m^o of the polymer-rich phase was determined according to the procedure described by Martínez-Salazar et al., (1991). An initial programme temperature of 170 °C and subsequent holding for 5 minutes were chosen to ensure complete melting of the crystals and removal of any residual crystal nuclei. Next, the sample was cooled to the selected isothermal crystallisation temperature, T_c, at a rate of 30 °C min^{-1}. Four crystallisation temperatures in the range of 105 - 120 °C were selected. Crystal growth was observed, after five-minute intervals at the isothermal crystallisation temperature, sample was reheated at a rate of 10 °C min^{-1}.

The melting temperature, $T_{m,}$ was taken to correspond to the temperature where the last crystal disappeared, i.e., melted.

In conclusion, the chosen characterization techniques are considered standard and relevant in this field of study. The resolution and precision required for this study guided the choice of the techniques. Furthermore, these characterization techniques have proven successful in similar studies on polymer blends to produce consistent and comparable of results.

CHAPTER 4

4 RESULTS AND DISCUSSIONS

4 BRIEF INTRODUCTION

The high molecular mass wax (H-Wax) and the low (L-Wax) molecular mass commercial Fischer-Tropsch (F-T) wax were melt-blended with the high-flow H-LLDPE and L-LLDPE grade, respectively. Differential scanning calorimetry (DSC), hot-stage polarised optical microscopy (POM) and dynamic rheological measurements in the melt-state and solid-state were performed covering a wide range of compositions. The aim was to understand how the thermophysical properties and rheological behaviour of the neat and blend samples varied with different polymer blend ratios and temperatures. The objective was to gain a comprehensive understanding of how the components interacted and influenced each other's properties in the molten- and solid states. These data are important for optimizing processing conditions, predicting material behaviour, and designing applications for these blends.

The results of the experiments are discussed in two parts. The first part presents characterisation of F-T H-Wax/H-LLDPE blends and the second part discusses the L-Wax/L-LLDPE blends, respectively. Notably, in the case of the former blend system, the focus was primarily on investigating the rheological properties. In contrast, for the latter blend system, greater emphasis was placed on studying thermophysical properties. However, the structural changes that occur in the blends and the relationship between these structural changes and the properties of the blends are discussed in all the sections.

4.1 CHARACTERISATION OF F-T H-WAX/H-LLDPE BLENDS

4.1.1 Rheology

4.1.1.1 Shear flow

Flow curves, for the different compositions of H-Wax/H-LLDPE, were obtained at temperatures of 160 °C, 170 °C and 180 °C in the rotational shear mode. Figure 4.1(a-c) shows the viscosity (η) versus applied shear rate ($\dot{\gamma}$) results obtained for selected blends at their respective temperatures. As expected, the apparent viscosity increases in magnitude with increase in LLDPE content. At low shear rates the blends behave like Newtonian fluids. Newtonian behaviour is observed up to applied shear rates of 250 s^{-1}. The zero-shear viscosities (η_0) correspond to the plateau values observed at low shear rates, and they are plotted in Figure 4.2. The flow curves for the LLDPE-rich blends showed shear-thinning behaviour at higher shear rates. This apparent decrease in the melt viscosity is caused by progressive disentanglement of the random-coil polymer chains with increase in the applied shear rate. This explains the observations that shear-thinning behaviour becomes more pronounced with increase in the LLDPE content. While the wax enhances molecular chain mobility (Sotomayor et al., 2014), the viscosity of the blends was dominated by the amount of LLDPE present.

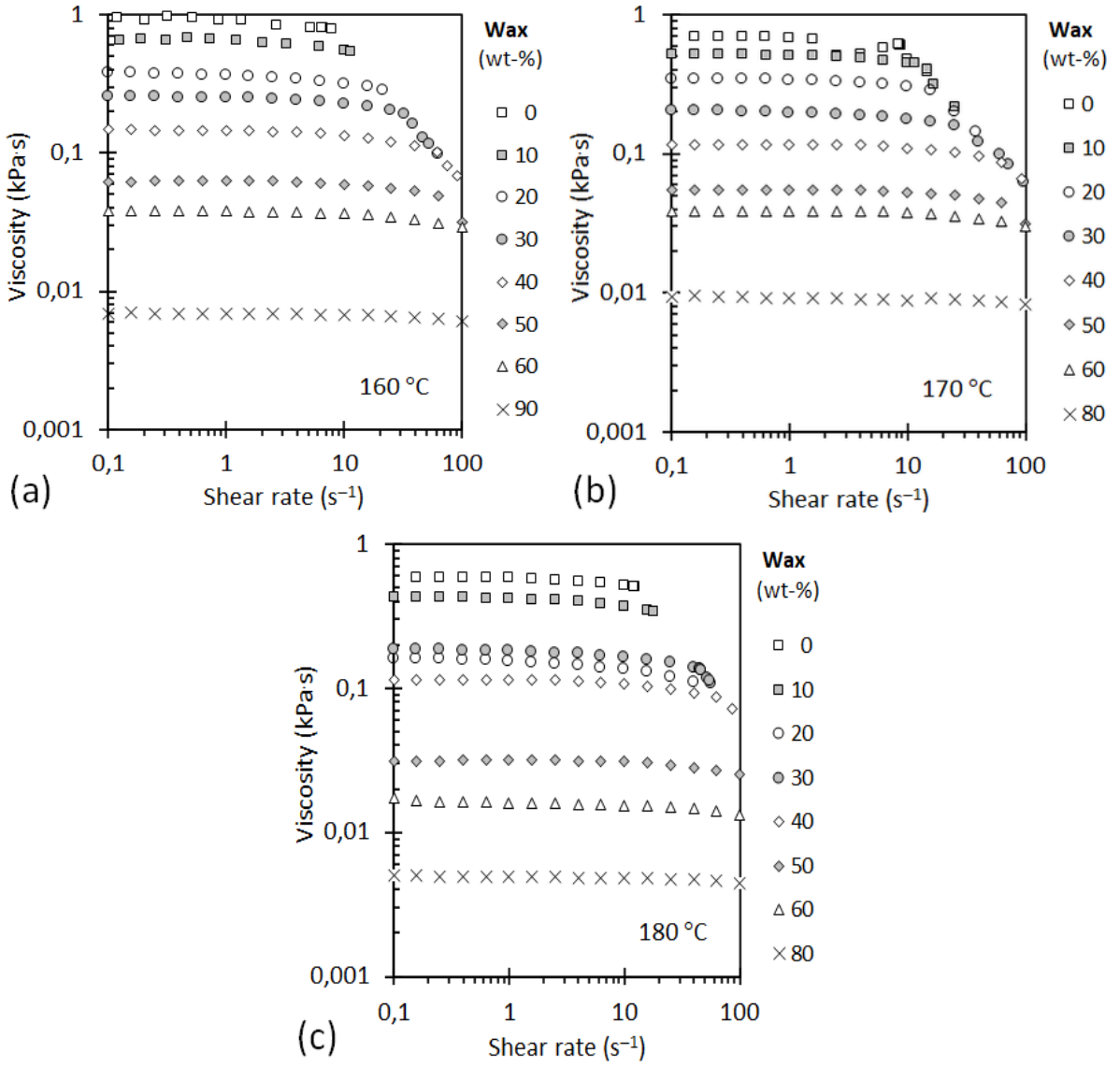

Figure 4.1: Flow curves of the H-Wax/H-LLDPE melt blends at (a) 160 °C, (b) 170 °C and (c) 180 °C

Numerous mixing rules exist which link the variation of Newtonian liquid viscosity to the composition of the fluid. These mixing rules are used to estimate the viscosity of a mixture based on the individual viscosities and volume fractions of its components. They include the Lederer (1931) model, equation (2.41), Grunberg and Nissan model Grunberg and Nissan (1949), equation (2.42) and the Hind et al. (1960) model, equation (2.43). The adjustable parameter η_{12} in the Hind et al. (1960) and Grunberg and Nissan (1949) models represents an interaction viscosity while the constant β in the Lederer model introduces a shift in the composition variable. The utility of these correlative expressions was tested using least squares regression on the zero shear

melt viscosity data. The results are shown in Figure 4.2. The Hind model overestimates the mixture viscosity whereas the other two models underestimate it. Even so, the Lederer model predictions are closest to the actual data.

Sotomayor et al. (2014) studied blends of high-density polyethylene with a soft paraffin wax. In effect, they assumed that the Grunberg and Nissan model applies with the following combining rule for the logarithm of the interaction viscosity:

$$\ln \eta_{12} = \left(\ln \eta_2 + \ln \eta_1\right)/2 \qquad (4.1)$$

where w represents mass fraction, and subscript 1 & 2 represents component 1, wax, and component 2, LLDPE This assumption reduces the mixing rule to a logarithmic additivity rule, equation (2.34). This expression is the expected composition dependence for the “ideal molten liquid mixture”. Note that that equation (2.34) corresponds to a mass fraction-weighted geometric mixing rule for the viscosity:

$$\eta = \eta_2^{w_2}\ \eta_1^{w_1} \qquad (4.2)$$

Equation (2.34) can be cast in a form that more clearly shows the linear dependence of the logarithm of the blend viscosity on the wax content:

$$\ln \eta = \ln \eta_2 + w_1 \ln\left(\eta_1/\eta_2\right) \qquad (4.3)$$

In equation (4.3), $\ln \eta_2$ is the intercept at $w_1 = 0$ and $\ln\left(\eta_1/\eta_2\right)$ represents the slope of the straight line on the semi-logarithmic plot of the zero-shear viscosity against mass fraction wax present in the blend. Sotomayor et al. (2014) did indeed notice that their data fell more-or-less on a straight line in their plot. However, they only considered samples with a wax content up to 50 wt-%. The plots shown in Figure 4.2 admit a similar linear approximation in this composition range. However, the zero-shear viscosity deviates precipitously from this linear trend at higher wax concentrations. Therefore, equation (2.34), or equation (4.3), cannot be used to estimate the viscosity of the wax by way of extrapolation to 100 wt-% wax in the blend when the only data available contains less than 50 wt-% wax.

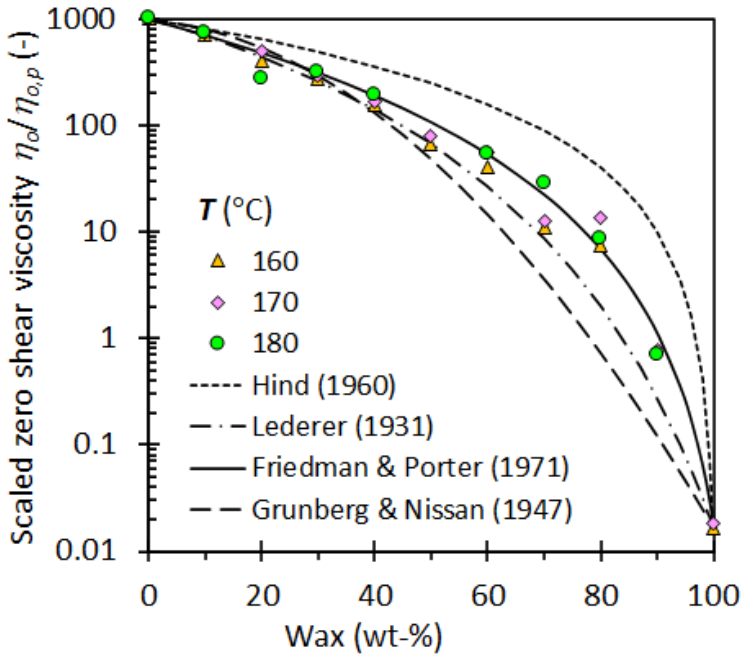

Figure 4.2: Variation of the scaled zero-shear viscosity with wax content. Testing different predictive viscosity mixture rules

The Fischer-Tropsch wax and the LLDPE share a similar chemical structure. Although the LLDPE also features short branches along the chain, the main difference is in the length of the molecules involved. The melt viscosity of short-chain oligomers increases linearly with molar mass. This applies to the wax and therefore equation (2.38) holds. Beyond a critical molar mass (M_c), the zero-shear melt viscosity increases with the 3.4th power of weight-average molar mass due to the onset of chain entanglement (Fetters et al., 2007, Friedman and Porter, 1975). This situation applies to the LLDPE and therefore equation (2.39) holds. The weight average molar mass of a wax/LLDPE blend was given by equation (2.37), where w_1 and w_2 represent the weight fractions of wax and polymer, respectively, in the binary blend and $w_1 + w_2 = 1$. If a blend of two low molar mass compounds are considered, combination of equation (2.37) with equation (2.38) leads to the following mixing rule, which should apply if one mixes two waxes:

$$\eta = w_2 \eta_2 + w_1 \eta_1 \qquad (4.5)$$

If, instead a blend of two polymers are considered, combining equation (2.37) and (2.39) leads to the Friedman and Porter (1975) mixing rule equation (2.40). Note that equation (2.40) is equivalent to a weighted power-mean mixing rule of order $p = 1/\alpha$.

At the critical molar mass (M_c), equation (2.42) and equation (2.43) predict the same zero-shear viscosity. This condition links the values of the two viscosity constants:

$$K_1 = K_2 M_c^{\alpha-1} \qquad (4.6)$$

It is usually assumed that the critical molar mass is a fixed quantity. If that is indeed the case, it implies that the ratio K_1/K_2 is temperature independent. In other words, apart from a proportionality constant, the temperature dependence of the constants is the same. Therefore, due to their similar molecular structure, the temperature dependence of the zero-shear viscosity, as applied to wax/polymer blends, is removed if scaling with the viscosity of the neat polymer is done.

Note that the theoretical values for the critical molar mass of polyethylene is M_c = 2900 Dalton (Stadler et al., 2006). The molar mass of the present LLDPE (M_2 = 129100 Dalton) is much higher than that of the wax (M_1 = 786 Dalton). This means that the critical molar mass of the blend was exceeded when as little as 1.6 wt-% LLDPE was present in the blend. This is much lower than the lowest LLDPE content (10 wt-%) considered presently. Therefore, equation (2.40) is likely to provide good data representation for blends forming thermodynamic solutions even though the exponent applicable to the neat wax is unity instead of α = 3.4. Figure 4.3 shows that this was indeed the case. The fully predictive Friedman and Porter, equation (2.40), provided much better data fits. It outperformed the conventional viscosity mixture models even though every single one of the latter models featured an adjustable parameter.

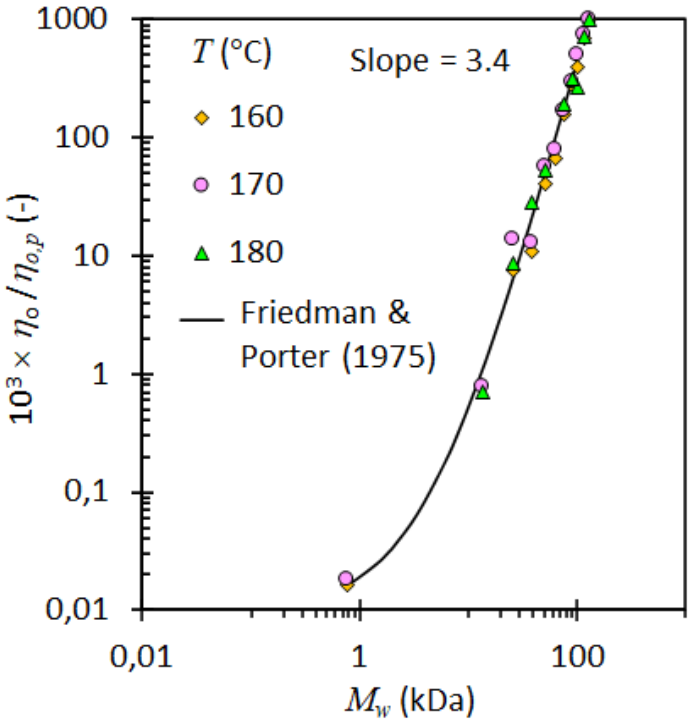

Figure 4.3: Zero-shear viscosity versus the calculated average molecular mass of the blends at various testing temperatures

4.1.1.2 Oscillatory rheology

Figure 4.4 shows representative plots of the complex viscosity (η^*) measured at 160 °C, 170 °C and 180 °C for selected H-Wax/H-LLDPE blends. The complex viscosity refers to the viscosity of a material when subjected to oscillatory shear forces. The complex viscosity was strongly altered by the wax content. This implied that as the wax content increased, the complex viscosity of the wax/LLDPE blend decreased. The frequency dependence was weak but showed a slight decline on increasing the angular frequency. This indicated that at higher frequencies, the material exhibited slightly lower complex viscosity. All measurements made at different temperatures gave similar results.

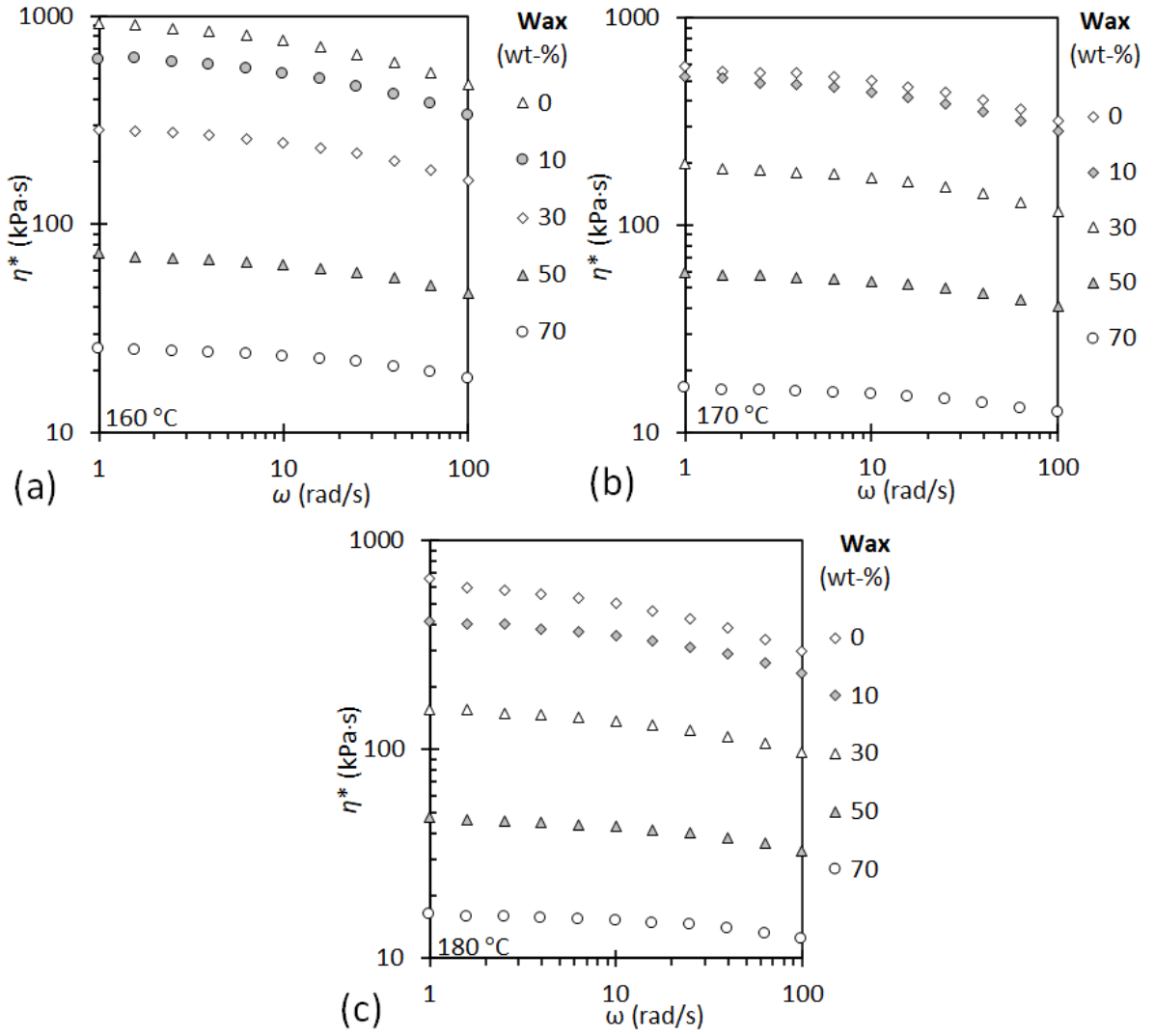

Figure 4.4: Effect of varying the angular frequency and the wax content on the complex viscosity measured at 160 °C, 170 °C and 180 °C

Figure 4.5 shows the effect of blend composition on the complex viscosity at a fixed angular frequency of 10 rad s^{-1}. Again, a very strong dependence on wax content is observed. The plots against the inverse of the absolute temperature are straight lines indicating an Arrhenius-like temperature dependence (Eyring and Hirschfelder, 1937):

$$\eta^* = A\exp\left(E_\eta/RT\right) \qquad (4.7)$$

The activation energy was the same for all the compositions and equalled 27.5 ± 1.3 kJ·mol^{-1}. It was not possible to measure the complex viscosity of the neat wax due to a lack of measurable elastic behaviour. Therefore, it was estimated by an extrapolation technique. First it was assumed that the same activation energy applied, and that the

composition dependence of the complex viscosity also follows the Friedman and Porter mixture rule as defined by equation (2.40). The mixture rule exponent and the pre-exponential constant for the wax were fixed by least-squares data regression using the full set shown in Figure 4.5. This resulted in $\alpha = 4.81$ and $A = 2.45 \times 10^{-4}$ for the two adjustable parameters. From this, the viscosity of the neat wax was calculated as a function of temperature and plotted as a line in Figure 4.5.

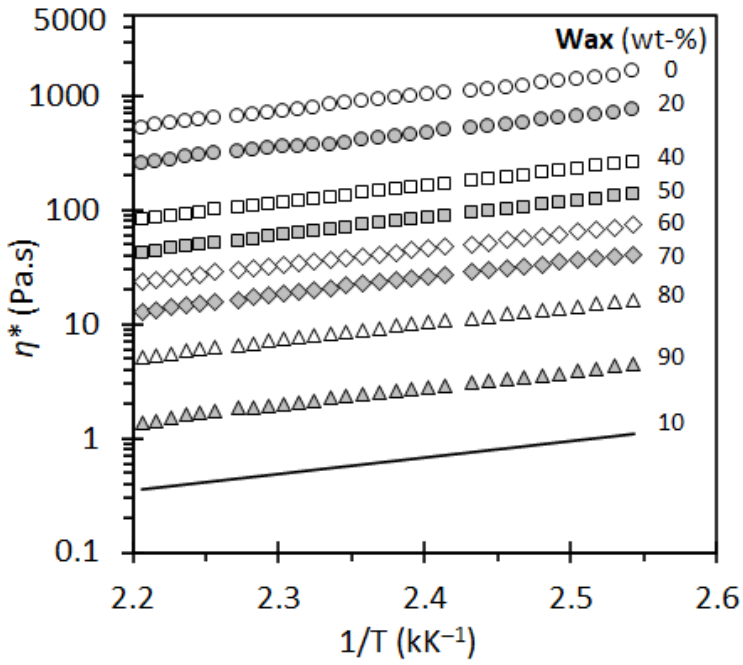

Figure 4.5: Temperature dependence of the complex viscosity measured from 180 °C to 120 °C at a fixed strain of 0.05 % and an angular frequency of 10 rad s^{-1}. Note that the values shown for the neat wax represent extrapolated values

An excess complex viscosity can be defined as the difference relative to the complex viscosity of the "ideal molten liquid mixture". The expected value for the latter is defined by equation (4.2). From this, the excess complex viscosity can be calculated from the experimentally measured values using:

$$\Delta\eta^* = \eta^* - \eta_1^{w_1}\eta_2^{w_2} \qquad (4.8)$$

where w represents mass fraction, and the subscripts 1 & 2 represents component 1, wax, and component 2, LLDPE, respectively. The theoretical expectation, for a system that obeys the Friedman and Porter mixing rule, is given by:

$$\Delta\eta^* = \left[w_1(\eta_1^*)^{1/\alpha} + w_2(\eta_2^*)^{1/\alpha}\right]^{\alpha} - \eta_1^{w_1}\eta_1^{w_2} \qquad (4.9)$$

Figure 4.6 compares selected experimental data for $\Delta\eta^*$ with the predictions of equation (4.9). Reasonable agreement between the experimental values and predictions based on the viscosity values of the neat components, is evident. In fact, the standard deviation between experimental and predicted complex viscosity values is 8.1 % and the maximum deviation between measured and predicted viscosity was 16 %.

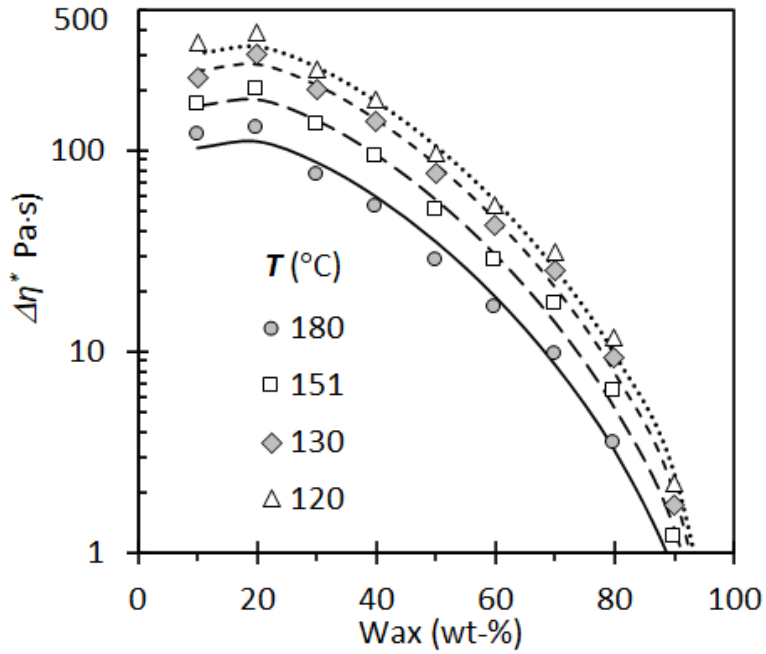

Figure 4.6: Experimental excess complex viscosity data (symbols) calculated using Equation (4.8) compared to predictions (lines) based on the Friedman and Porter mixture model (with α = 4.81) as presented by Equation (4.9)

The viscoelastic properties of polymer melts are best characterised by the storage and loss moduli. These are linked to the components of the complex viscosity via the following relationships based on equation (2.32) and (2.33) (Ferry, 1961).

Figure 4.7 shows representative log-log plots of the storage and loss moduli as a function of the angular frequency. At the respective measurement temperatures, all the blends indicate a more viscous behaviour as is indicated by the larger loss modulus. In the case of both moduli, a logarithmic-linear dependence on the angular frequency is indicated. The slope of the lines of loss modulus are lower than those of the storage modulus. The slope of the logarithm of the storage modulus with respect

to the logarithm of the angular frequency is approximately equal to 5/4. It increases with wax content reaching a value of approximately 3/2 at a wax content of 70 wt-%. The corresponding slopes of the logarithm of the loss modulus with respect to the logarithm of the angular frequency is less affected by composition. It is about 0.85 for the neat LLDPE and increases to about 0.94 for the blend with 70 wt-% wax.

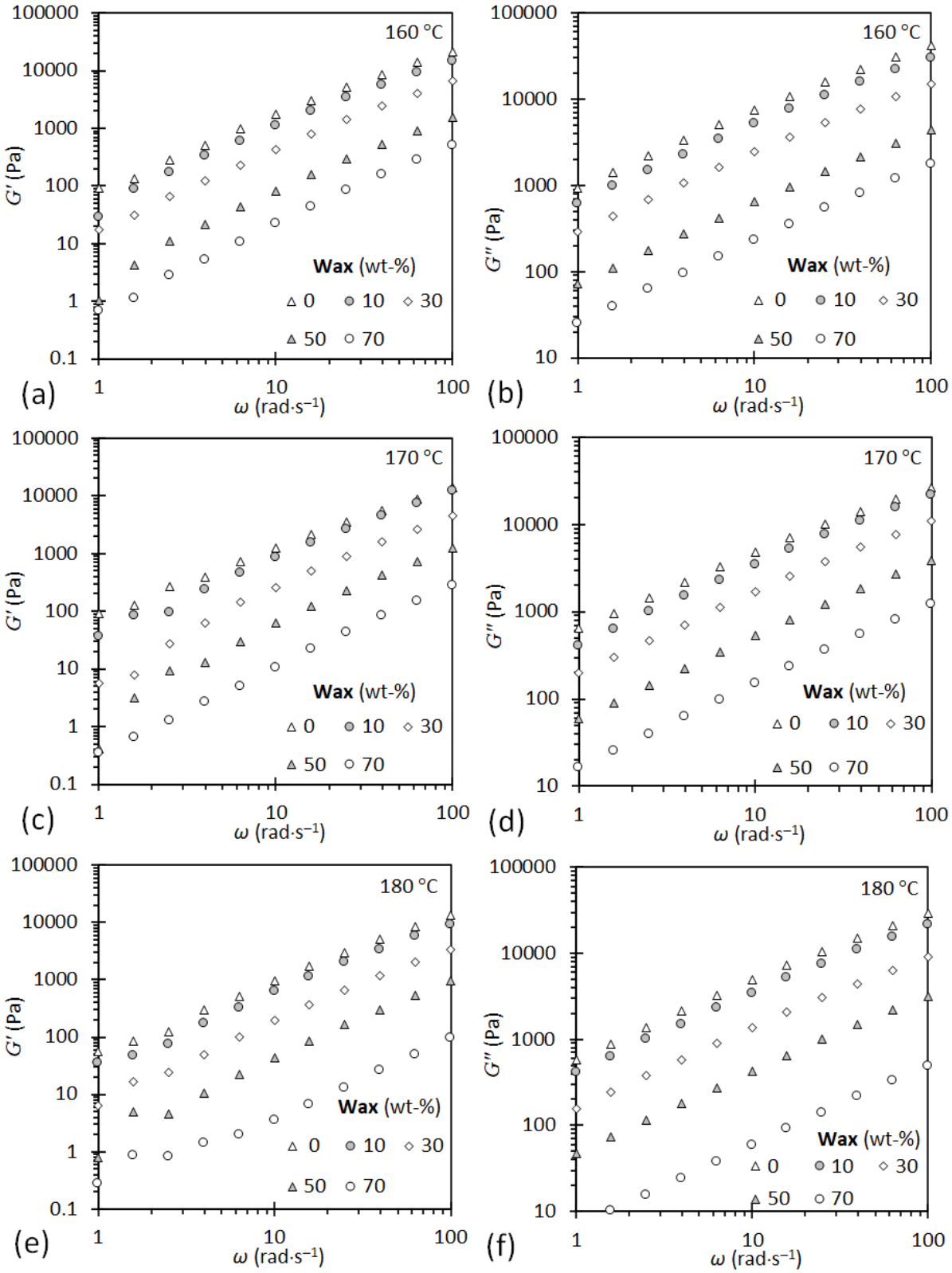

Figure 4.7: Plots of G' and G'' versus ω for selected H-Wax/H-LLDPE blends measured at 160 °C, 170 °C and 180 °C

Rheological investigation of oscillatory shear flow behaviour, obtained on melts, can provide information on the nature of the liquid phase (Han and Chuang, 1985, Han and Jhon, 1986, Sotomayor et al., 2014). A Han plot of log G' versus log G'' can be used to detect liquid-liquid phase separation in thermoplastic polymer blends. In general, linear temperature-independent and composition-independent Han plots are indicative of homogenous single-phase behaviour of liquid melts (Han and Chuang, 1985). Figure 4.8 shows such plots for the current H-Wax/H-LLDPE blends. The indicated data trends confirm the thermodynamic compatibility of the present wax/LLDPE blends in the molten liquid state at temperatures as low as 120 °C.

Cole-Cole plots also provide information on the miscibility of blends in the molten state (Agrawal et al., 2022, Bai et al., 2010, Cho et al., 1998). Semi-circular shapes of plots of the imaginary viscosity (η'') against the real viscosity (η') imply miscibility. Figure 4.9 shows that this was indeed the case for the for all the blends analysed for the present wax/LLDPE system. This provides additional evidence for the miscibility of wax and LLDPE in the fully molten state (Cho et al., 1998).

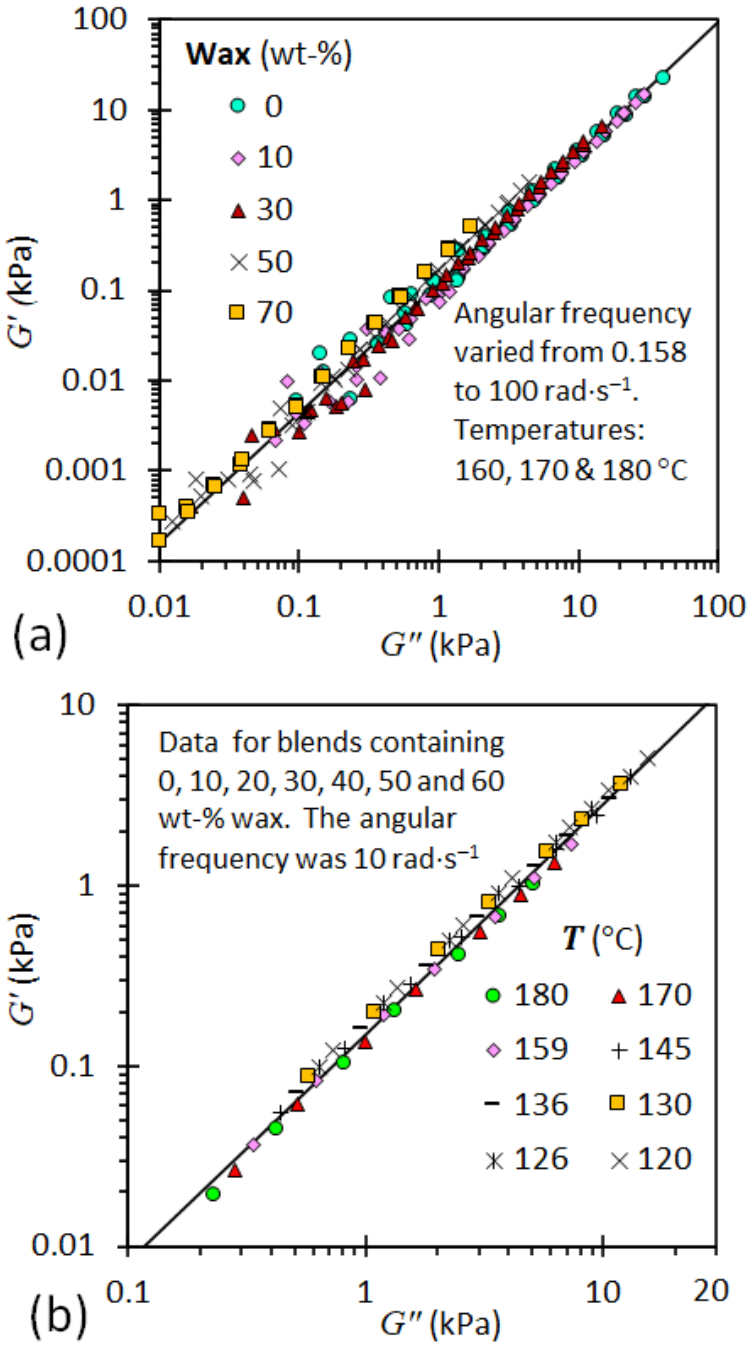

Figure 4.8: Han and Chuang (1987) plots of G' versus G'' for H-Wax/H-LLDPE blends. (a) Emphasizing the effect of blend composition at three different temperatures and five wax content levels. (b) Emphasizing the effect of temperature at seven different wax content levels at a fixed angular frequency of 10 rad s^{-1}

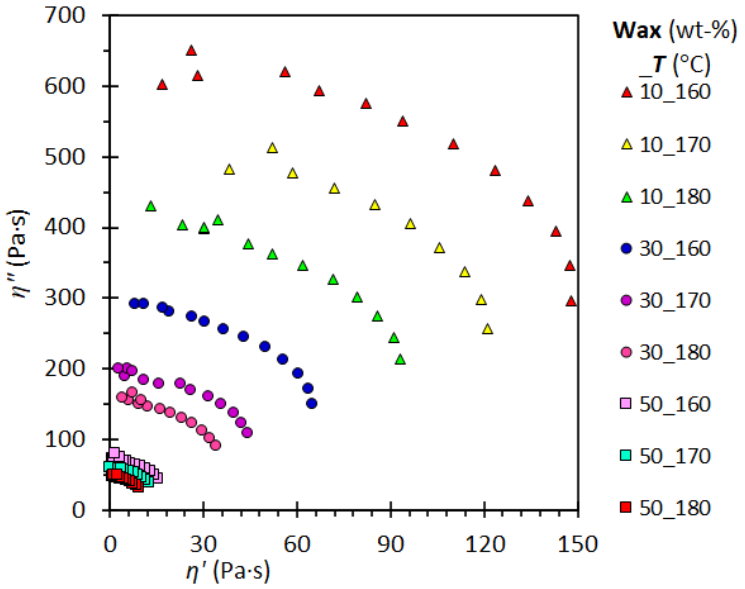

Figure 4.9: Cole–Cole plots of η'' against η' for H-Wax/H-LLDPE blends

4.1.2 Differential scanning calorimetry

4.1.2.1 Non-isothermal melting and crystallisation

Figure 4.10 presents typical DSC melting and crystallisation curves obtained for the H-Wax/H-LLDPE blends. The curves are plots of the normalized heat flux versus temperature with the orientation of the curves such that endothermic processes appeared up and exothermic processes appeared down. Table 4.1 presents the derived melting & crystallisation onset- and peak temperatures obtained for the H-Wax/H-LLDPE blends. These results represent the melting and crystallisation processes of the blends obtained from the second and third scans for the purpose of comparisons. In the pure state, the wax displays a broad melting curve with a doublet peak while the LLDPE featured a single, narrower melting peak. Due to the broad nature and the poor resolution between the two peaks due to the wax, it was rather difficult to analyse the melting peaks with increasing LLDPE concentration. However, it is clear that the original two wax peaks tend to merge into one single wax peak as the LLDPE content of the blend is increased.

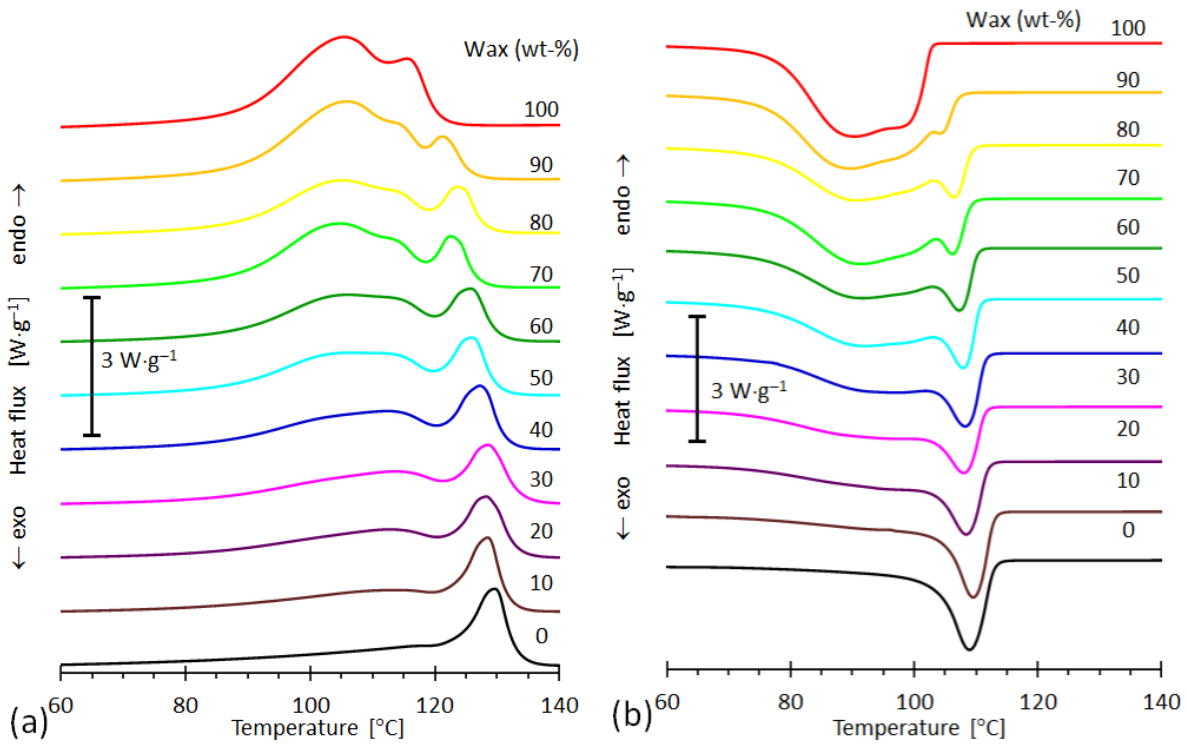

Figure 4.10: Typical DSC curves for the F-T H-Wax/H-LLDPE blends. (a) melting during heating scans and (b) crystallisation during cooling scans

Table 4.1: DSC results for F-T H-Wax/H-LLDPE

Wax (wt-%)	T_o Blend (°C)	$T_{p1,m}$ Wax(°C)	$T_{p2,m}$ Wax (°C)	$T_{o,c}$ Wax(°C)	$T_{p,m}$ PE(°C)	$T_{p,c}$ PE(°C)
100	-	105.5	115.8	90.42	-	-
90	105.1	105.7	113.2	89.9	121.4	104.4
80	107.9	105.3	112.9	90.5	122.5	105.8
70	108.8	104.3	112.6	91.9	122.5	106.3
60	109.4	106.4	53.5	91.4	125.7	106.8
50	111.3	106.8	56.1	91.5	126.6	107.5
40	113.2	-	113.5	96.8	127.5	107.9
30	111.9	-	113.4	98.7	128.1	108.4
20	115.9	-	112.9	-	128.2	108.8
10	114.7	-	-	-	128.4	109.8
0	116.5	-	-	-	129.3	109.3

*T – temperature, o – onset, p – Peak, m – melting, c - crystallisation

In order to assess the extent of compatibility, the melting and crystallisation curves are reproduced in Figure 4.11. The experimental DSC results are compared to the predictions based on mass fraction-weighted combinations of the DSC traces obtained for the neat wax and LLDPE. Figure 4.11(a) shows the results for the blend containing 10 wt-% LLDPE. The melting peak, at the highest temperature, is associated with the LLDPE-rich phase. It is noteworthy that this peak has shifted to a significantly lower temperature and that its intensity has increased. The latter observation indicates that portion of the wax must have co-crystallised with the LLDPE. Furthermore, this means that this part of the wax now has a higher melting point than what it had when present in the neat wax. This portion probably derived from that part of the wax responsible for the second wax melting peak. This is indicated by the fact that the heat flux in in this region was disproportionally reduced when compared to that of the lower melting peak of the wax.

In Figure 4.11(b) the difference between the melting curves, measured and calculated for the blend containing 30 wt-% LLDPE, is particularly striking. The peak attributed to the LLDPE-rich phase has shifted to even lower temperatures but now the intensity is about the same as would be expected for the neat polymer. However, the heat flux in the wax-rich regions has increased significantly. This suggests that a portion of the LLDPE, which would normally remain amorphous, co-crystalized with the wax. This increase in the specific enthalpy is also reflected in the crystallisation exotherms.

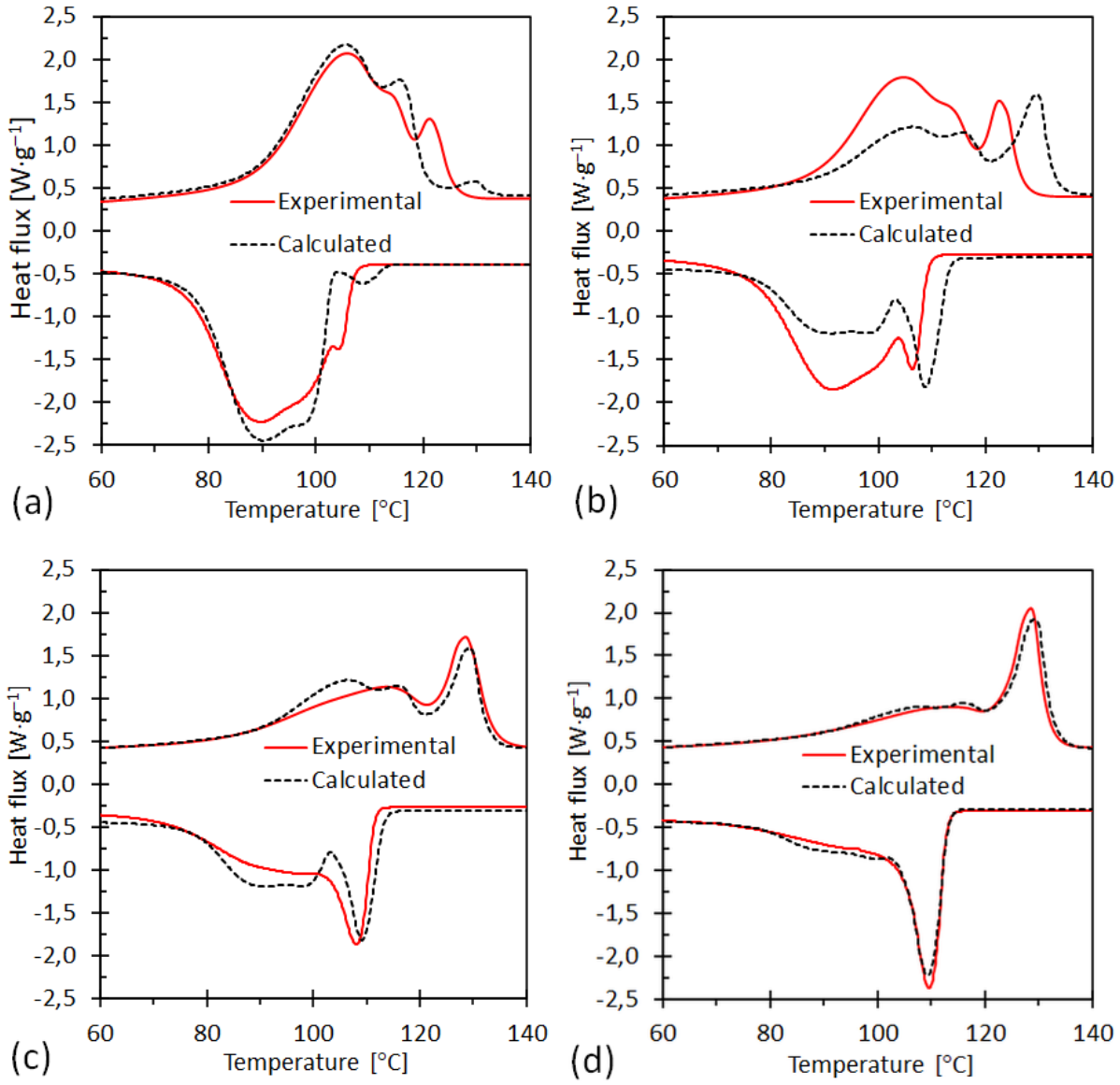

Figure 4.11: Comparing measured and predicted melting and crystallisation curves for (a) 90/10, (b) 70/30, (c) 30/70, and (d) 10/90 H-Wax/H-LLDPE blends

Figure 4.11(c) and Figure 4.11(d) show the results obtained at higher LLDPE content. The changes in both of the two melting endotherms and the two crystallisation exotherms curves are striking. They are consistent with the notion of co-crystallisation having happened in both the wax-rich phase and the LLDPE-rich phases.

Figure 4.12 plots the peak temperatures for the wax-rich phases and the LLDPE-rich phase as they evolve with changes in the blend composition. These results reveal significant melting point depression of the LLDPE-rich phase with increasing wax concentration. The melting peaks of the wax-rich phase tends to overlap and ultimately form a relatively high-melting single temperature peak with decreasing wax

concentration. Similar miscibility studies in the crystalline phase were previously reported for other wax types (Chen and Wolcott, 2015, Chen and Wolcott, 2014, Gumede et al., 2016). Chen et al. (2014, 2015) used DSC to investigate the phase morphology of a wide range of paraffin wax/LLDPE blends whereas Gumede et al. (2016) studied a 30/70 wax/LLDPE composite. Both groups observed two distinct crystallisation endotherms, two distinct crystallisation exotherms and significant melting point depression of polyethylene. The latter is indicative of miscibility in the molten state while the elevation of the melting temperature of the wax-rich phase is consistent with co-crystallisation with the LLDPE (Gumede et al., 2016). Therefore, the present results confirm previous results that indicate LLDPE is soluble in molten wax and that it co-crystallises with the wax.

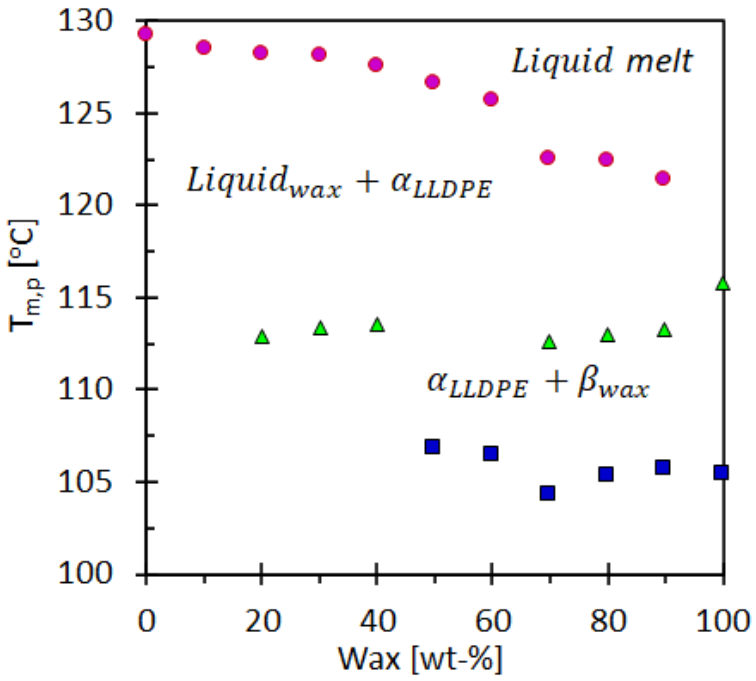

Figure 4.12: Phase diagram based on the loci of the melting peaks associated with the wax-rich β-phases and the LLDPE-rich α-phase driven by composition changes

4.2 CHARACTERISATION OF F-T L-WAX/L-LLDPE BLENDS

4.2.1 Rheology

4.2.1.1 Shear flow

Figure 4.13 shows the effects of wax content on the melt viscosity measured at different shear rates and a temperature of 170 °C of neat L-LLDPE and L-Wax/L-LLDPE at various blend composition. As expected, the apparent viscosity decreased with increasing wax content of the blends. This suggests that the presence, of the low melting wax, increases the overall mobility of the polymer chain molecules in the blend.

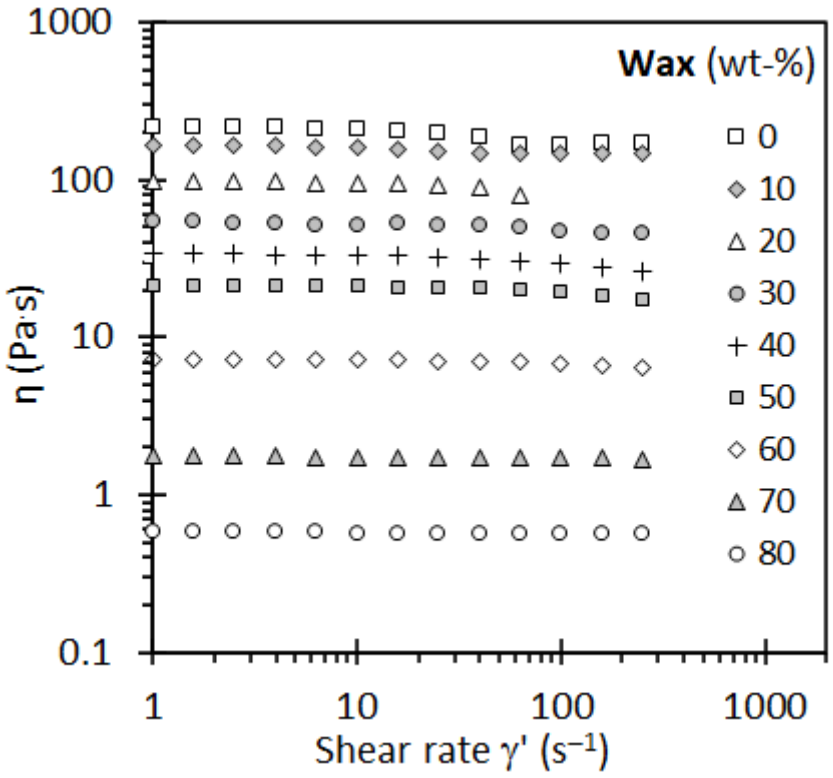

Figure 4. 13: Viscosity flow curves of neat L-LLDPE and L-Wax/L-LLDPE at various blend compositions

Figure 4.14 plots the zero-shear viscosity vs. the fraction wax of the L-Wax/L-LLDPE blends. In the context of this study, the wax can be considered to be a low-molecular mass oligomer of the linear low-density polyethylene. Below a critical shear rate, the melt viscosity of polymers shows Newtonian behaviour characterised by the zero-shear viscosity, as is shown in Figure 4.14. The Rouse model predicts that this zero-shear viscosity should be proportional to the molecular mass (Dealy and Larson,

2006). It is expected that shorter chain molecules, below the critical molecular mass of entanglement, will display Newtonian behaviour, i.e., as is the case for the wax. However, long-chain molecules are in a state of entanglement in the melt. This leads to significantly higher viscosities as only cooperative molecular motion is required (Fox and Flory, 1951). The study by Friedman and Porter (1975) confirmed that the zero-shear viscosity of such a series of oligomers, polymers, and even their blends, depends uniquely on the weight average molecular mass. Therefore, the molecular mass dependence of the zero-shear viscosity can be summarised as per equation (2.38) and (2.39) (Fox and Flory, 1951, Nichetti and Manas-Zloczower, 1998), where K_1 and K_2 are constants which are dependent on the temperature and the polymer system under investigation. Again, the exponent α takes on the universal value of 3.4 for linear polymers. The breakpoint is defined by M_c, the critical molecular mass above which chain entanglement ensues. The critical molecular mass of polyethylene is approximately 3800 Da (Fetters et al., 2007). Consequently, for the viscosity of polymer blends, with the weight-average molecular mass exceeding M_c, the following mixing rule applies (Friedman and Porter, 1975) equation (2.40). This curve is plotted in Figure 4.14 with the value of K_2 = 9.91x10^{-17} established from the measured zero-shear viscosity for the polymer melt and its weight-average molecular mass of 245.7 kDa. This is a fully predictive model for a blend of the Fischer-Tropsch L-Wax with L-LLDPE featuring a relatively high molecular mass. The agreement with the experimental results is reasonably good. Empirical correlations were also considered including the Lederer-Roegiers model (Lederer, 1931, Roegiers and Roegiers, 1947) which is recommended for predicting the viscosity of lubricant blends (Zhmud, 2014) equation (2.41). Least-squares data regression yielded an excellent data fit with the adjustable parameter taking the value β = 3.375. A less satisfactory fit was achieved using a modified version of the Grunberg and Nissan (Grunberg and Nissan, 1949) model equation (2.42), i.e., red curve. In this case the least squares regression yielded, for the interaction viscosity, a value equal to η_{12} = 191.8 Pa·s. The curves predicted by both these models are also shown in Figure 4.14. Another empirical model is one due to (Hind et al., 1960), equation (2.43). However, this model was incapable of reproducing the experimental data trends.

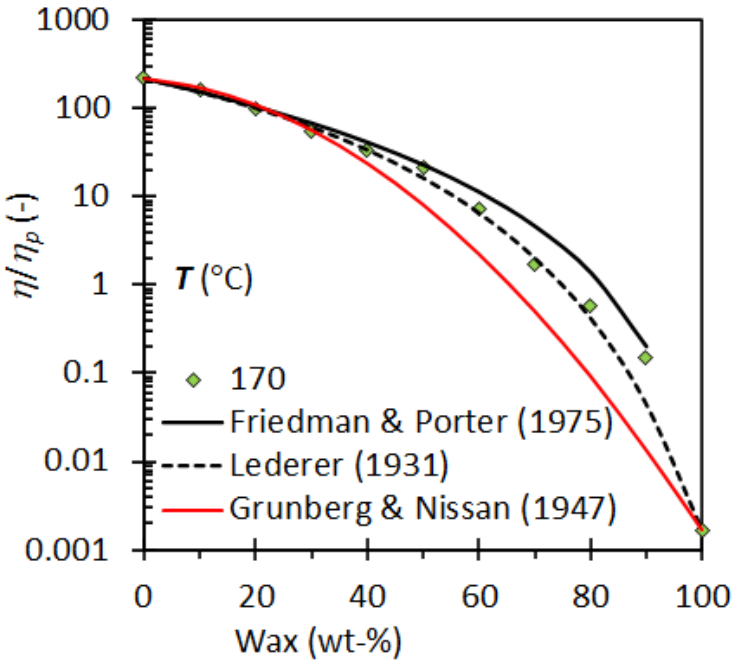

Figure 4.14: Experimental zero-shear viscosity (measured at 170 °C) as a function of L-Wax/L-LLDPE in comparison to few empirical viscosity blending models at various blend compositions

4.2.2 Differential scanning calorimetry

4.2.2.1 Non-isothermal melting and crystallisation

The non-isothermal DSC thermograms in Figure 4.15 & Table 4.2 show the melting and crystallisation behaviour of the neat components as well as the blends of L-Wax/L-LLDPE. The melting and crystallisation peak temperatures of the wax were 60.4 °C and 47.0 °C respectively. The corresponding values for the LLDPE were 125.6 °C and 103.0 °C respectively. The blend containing 10 wt-% wax did not feature melting or crystallisation peaks that could be attributed to a wax phase. This is indicative of miscibility.

Furthermore, one can observe significant variations in the melting and crystallisation curves of the experimental data, Figure 4.16, in comparison to mass-based linear blending calculated data for four selected blends. The melting peak temperatures of the wax-rich phase remains constant, while the crystallisation peak temperature slightly increases, but both these peaks are also observed to broaden in the direction of increasing temperature. In addition, a developing shoulder-peak during crystallisation of wax was observed in both Figure 4.15 & 4.16. This may be indicative of a slower relaxation due to interaction with polymer chains. On the other hand, both the melting and crystallisation peak temperatures of the LLDPE-rich phase decrease considerably with increasing wax concentration. Similar results were previously reported (Krupa and Luyt, 2001a, Mtshali et al., 2003a, Mpanza and Luyt, 2006). They were attributed to partial miscibility in the solid state, i.e., incorporation of the wax in LLDPE crystallites. Furthermore, the LLDPE melting peak splits into two low and high melting peaks, forming a bimodal peak. This is consistent with a portion of the polymer co-crystallising with the wax.

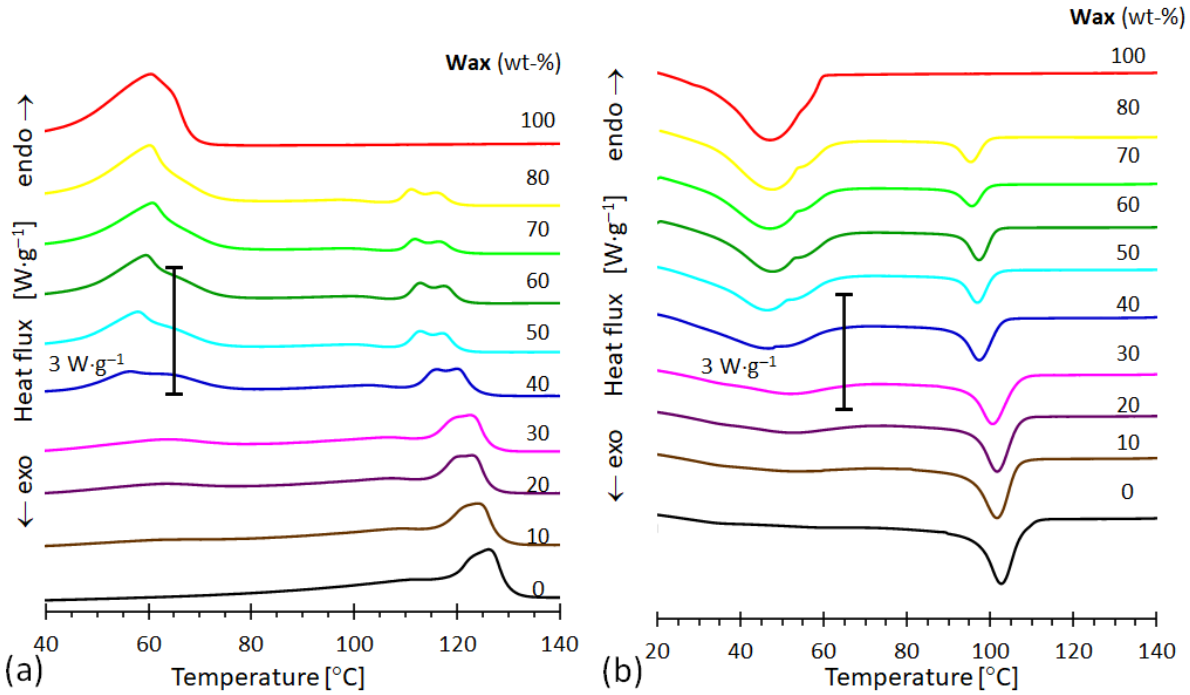

Figure 4.15: Plot of (a) melting and (b) crystallisation curves of L-Wax/L-LLDPE at various blend compositions

Table 4.2: DSC results for L-Wax/L-LLDPE

Wax (wt-%)	$T_{o,m}$ Wax (°C)	$T_{p,m}$ Wax (°C)	$T_{p,c}$ Wax (°C)	$T_{o,m}$ PE (°C)	$T_{p2,m}$ PE (°C)	$T_{p1,m}$ PE (°C)	$T_{p,c}$ PE (°C)	ΔH_m Wax (J g^{-1})	ΔH_m PE (J g^{-1})	X_c Wax (%)	X_c PE (%)
100	41.39	60.4	47.06		-	-	-	193.51	-	80.63	-
90	43.37	60.64	48.93	105.2	110.3	114.2	94.9	137.4	14.59	51.66	49.44
80	43.8	60.2	47.4	107.9	111.2	115.1	95.6	130.80	18.55	43.55	31.50
70	45.1	60.8	47.4	108.8	111.9	115.9	96.8	116.54	20.45	33.94	23.19
60	45.5	59.5	47.8	109.4	113.0	116.9	97.4	102.89	28.36	25.70	24.17
50	47.0	57.9	46.9	111.3	114.1	120.3	97.9	65.54	43.18	13.65	28.34
40	45.8	56.5	49.0	113.2	116.9	122.9	98.4	43.81	56.75	7.31	32.31
30	46.5	63.2	50.0	111.9	-	122.9	100.4	28.76	70.69	3.60	34.64
20	42.1	62.7	25.7	115.9	-	123.7	102.0	19.38	90.45	1.62	38.60
10	-	-	-	114.7	-	124.9	101.9	-	101.28	-	38.47
0	-	-	-	116.5	-	125.6	103.7	-	111.9	-	38.20

*T- Temperature, o – onset, p – Peak, m – melting, c – crystallisation, ΔH – change enthalpy, X_c - total crystallinity

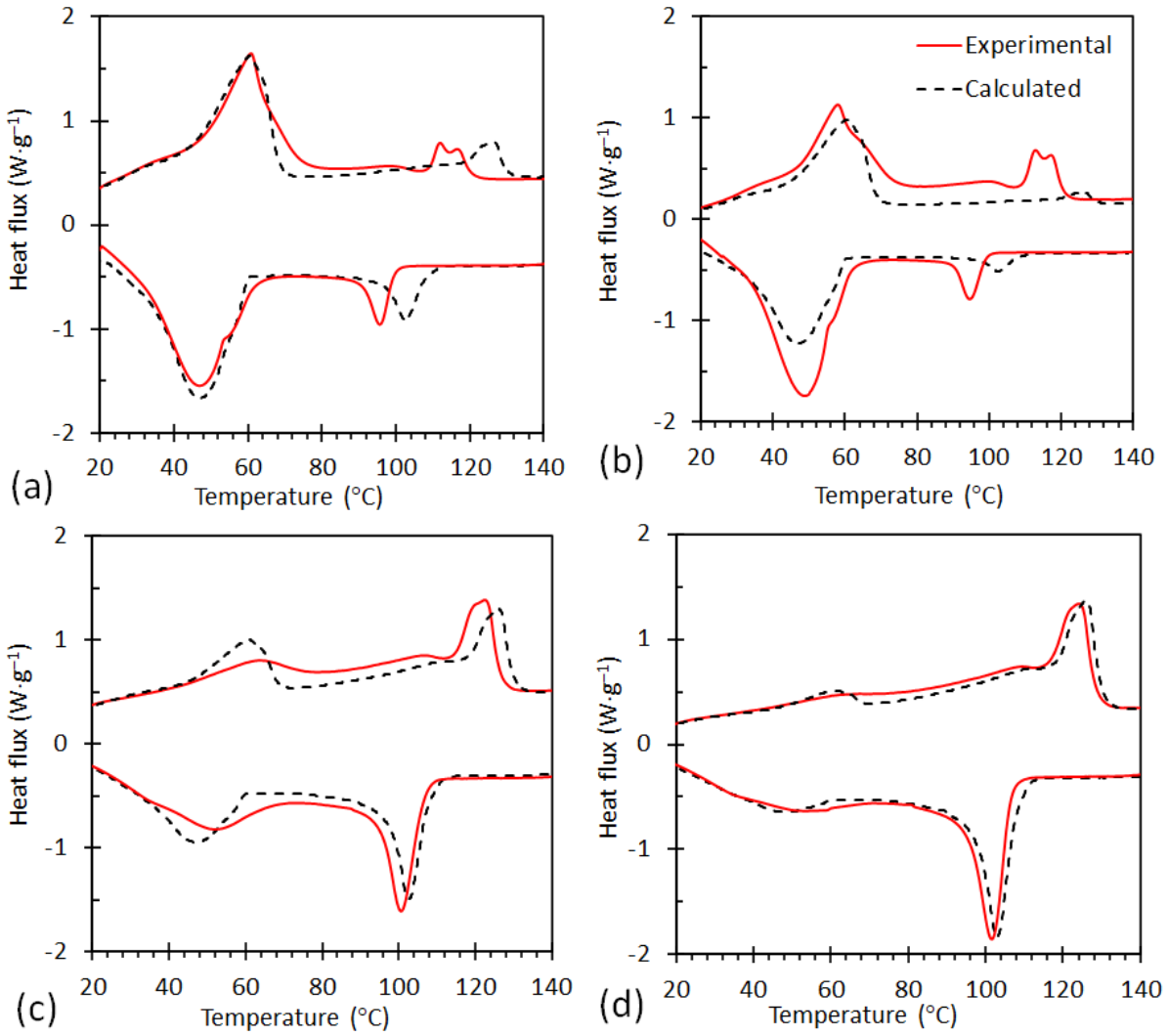

Figure 4.16: Plot of experimental and predicted melting and crystallisation curves for L-Wax/L-LLDPE blends. The compositions are (a) 70/30, (b) 50/50, (c) 30/70 and (d) 10/90

Plots of the melting peak temperatures of the wax and LLDPE are shown in Figure 4.17 for the blends of different compositions. Significant melting-point depression of the LLDPE-rich phase is evident while the melting-point of the wax-rich phase appears to be largely unaffected. Above the melting temperature of the wax, the molten wax coexists with solid LLDPE until the liquidus temperature is reached.

The depression of the melting temperature of the LLDPE phase is an indicator of miscibility or partial miscibility of the wax and the LLDPE in the melt. The depression of the melting temperature is likely determined by entropy of mixing effects. Moreover, taking into consideration the occurrence of the bimodal curve distribution, these results suggest that there is a portion of the LLDPE that crystallises at a lower temperature,

while a portion of the wax crystallises at a higher temperature. This tendency of the wax to act as a plasticizer in the wax/LLDPE binary mixture was previously reported (Gumede et al., 2016). Moreover, it is well known that, although LLPDE consists predominately of high temperature melting linear chain molecules, it may have relatively lower melting segments due to the random nature of copolymerization. As a result, the chain segments with a lower melting temperature are more compatible with the shorter chain molecules constituting the wax. Further work is necessary to confirm this speculation. However, it does provide a rational explanation for the observed degree of compatibility indicated by the apparent co-crystallisation of the two components.

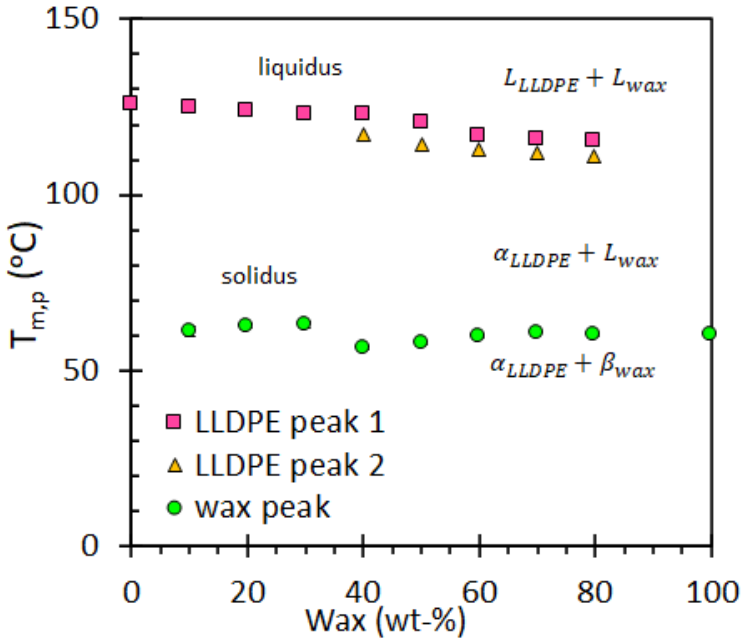

Figure 4.17: Plot of peak melting temperature as a function of L-Wax/L-LLDPE at various blend compositions

The effect of wax content on the melting enthalpy, ΔH, corresponding to the wax-rich phase and LLDPE-rich phase are shown in Figure 4.18(a). The normalized melting enthalpy was determined by the integration of the area under the melting peak and was compared to the theorical melting enthalpy according to equation (4.10):

$$\Delta H = w_1 \Delta H_2 + w_2 \Delta H_2 \qquad (4.10)$$

where w represents mass fraction and 1 & 2 represents component 1, wax, and component 2, LLDPE. A strong deviation from the mass-based linear blending rule with the composition was observed. This occurrence was more evident with the wax than the LLDPE. This indicates a strong molecular chain interference in the crystallisation process of both components. Consequently, the degree of crystallinity, X_c, of the blends was calculated from the obtained melting enthalpies using equation (2.44). The standard heat of fusion of the pure LLDPE and wax were taken as 293 J g^{-1} (Wunderlich and Czornyj, 1977) and 240 J g^{-1}, respectively (Chen and Wolcott, 2014). The results are presented in Figure 4. 18(b). The total crystallinity based on the wax-rich phase increased nearly-linearly with increasing wax fraction. The total crystallinity due to the LLDPE-rich phase is relatively constant up to 20 wt-% wax. However, with increasing wax fractions, a gradual reduction that reaches a minimum at 70 wt-% wax and then starts to increase reaching the highest degree of crystallisation at 80 wt-% wax compositions is observed. The DSC cooling scan from Figure 4.15(b) showed that, at the crystallisation temperature of the LLDPE phase, the wax-rich phase is in the molten state. This can affect the overall crystallisation process of the LLDPE phase. These results indicate that crystallisation of a fraction of LLDPE-rich phase is not favoured with increasing wax fractions. The presence of the low molecular mass wax increases the free volume in the system, thereby reducing the viscosity of the molten liquid. It was anticipated that this would enhance the mobility of the polymer chains facilitating reorganisation and their incorporation into crystallites. Clearly, this was not the case at low- and intermediate- wax fractions. However, it was observed for the 80 wt-% wax composition. At this point it was not clear why the LLDPE crystallisation was inhibited at intermediate-wax content.

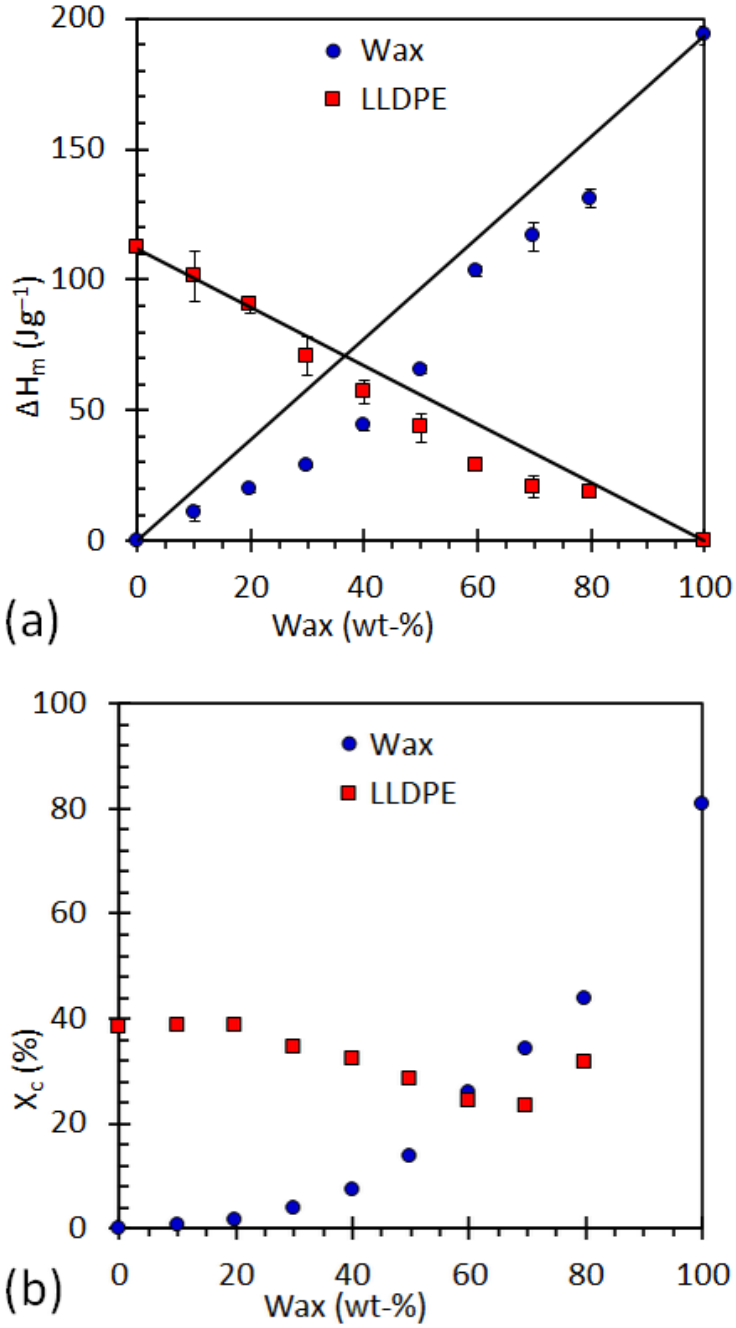

Figure 4.18: Plot of (a) melting enthalpies, and (b) degree of crystallinity as a function of L-Wax/L-LLDPE at various blend compositions

4.2.2.2 Isothermal crystallisation kinetics

Figure 4.19 displays a typical DSC trace obtained from a representative wax/LLDPE blend. The figure shows that the crystallisation exotherm labelled as specific heat flow (HF) partially overlaps with an artefact resulting from the change from cooling to isotherm. It is clear that the conveniently scaled artefact perfectly matches the left part of the specific HF curve. It is also observed that there's little change on the baseline that results from the crystallisation as the heat capacity of the crystal is lower than that of the amorphous phase. A vertical line marks the beginning of the isothermal condition. It can be observed in the temperature curve that a tiny overheating is produced as a consequence of the exothermic process. Thus, before doing any kinetic analysis, the artefact was removed from the bulk DSC data as follows: taking as a reference Figure 4.19, the "a"-labelled part of the specific HF curve clearly corresponds to the aforementioned artefact and is well separated from the crystallisation peak. Thus, we can assume that this part practically corresponds to the artefact. This part of the specific HF curve is vertically shifted for baseline matching and fitted by the artefact multiplied by a scale factor (sf). It can be observed that the matching of both curves is nearly perfect until a divergence appears in region "b", where the effect of crystallisation begins to be evident. The neat exotherm curve region "c''obtained by the removal of the scaled artefact is also displayed in the same figure.

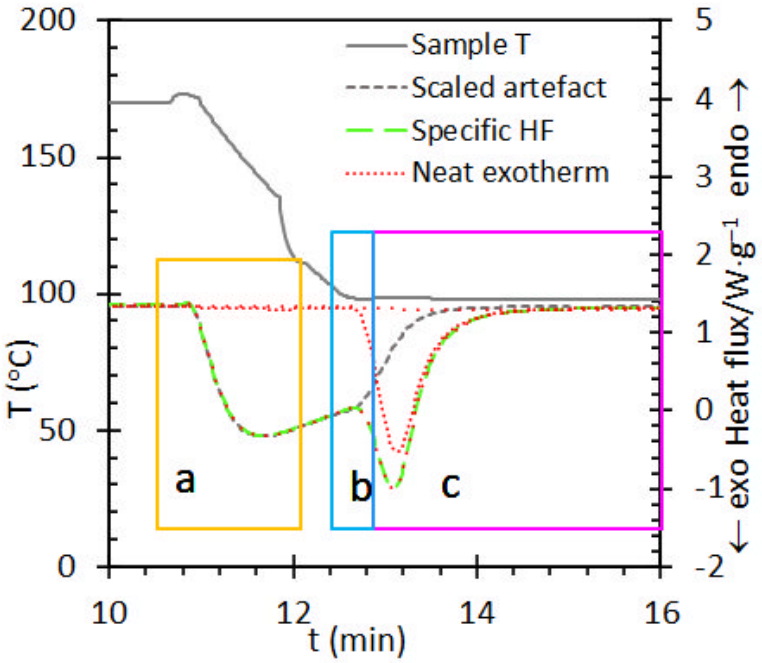

Figure 4.19: Illustration of the areas of the curves considered for the different fitting steps

Figure 4.20(a) displays neat DSC traces, resulting from the removal of the artefact, showing the selected isothermal crystallisation temperature for a blend containing 30wax/70LLDPE (wt-%). Figure 4.20(b) shows corresponding plots at an isothermal temperature of 100 °C but for different blend compositions. The shape of the crystallisation exotherms were determined by the mode of the nucleation process, the subsequent crystal growth kinetics and finally also by the effect of spherulites impinging on each other. Figure 4.20(a) indicates that the exotherm peaks shifted to later times with increasing crystallisation temperature. Therefore, complete crystallisation of the LLDPE phase in the 30/70 wax/LLDPE blend composition is achieved within shorter times as the crystallisation temperature is reduced. Similarly, at a fixed temperature shown in Figure 4.20(b), increasing the wax content lowers the rate of crystallisation of the LLDPE-phase.

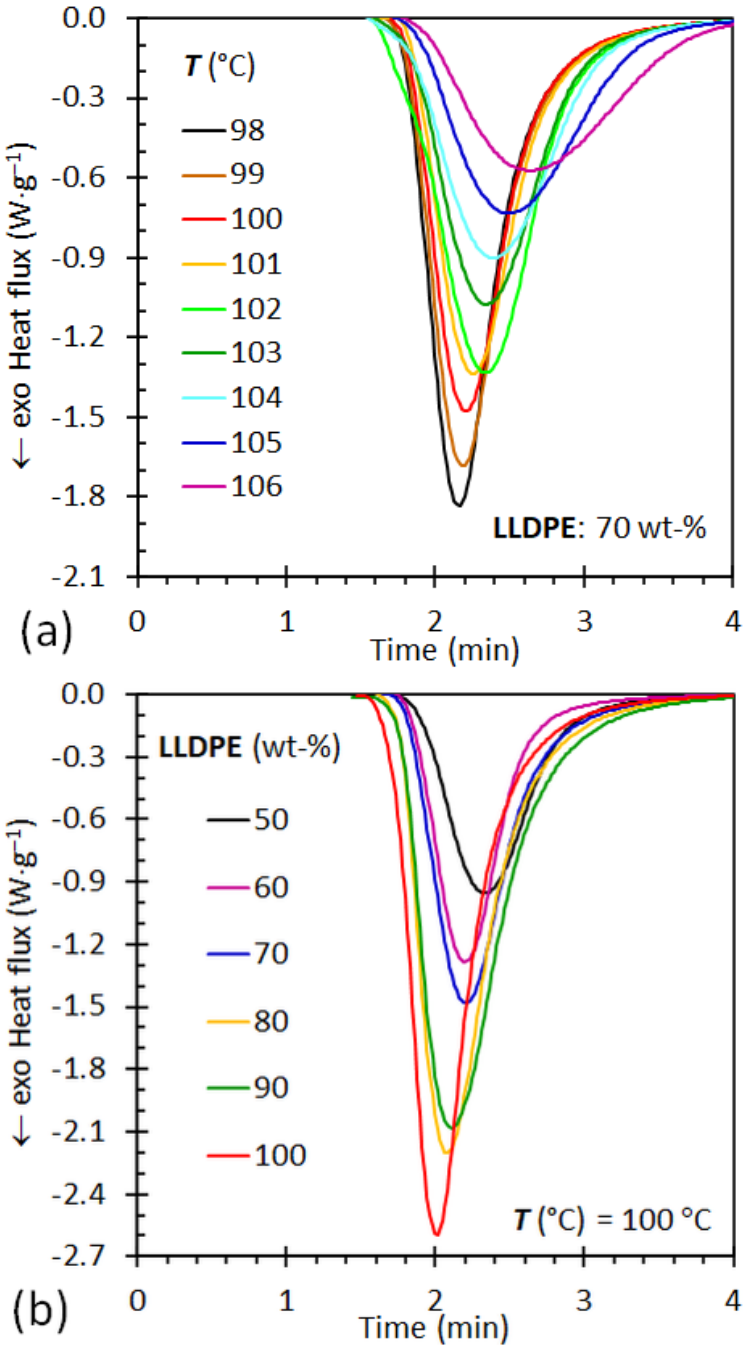

Figure 4.20: Isothermal crystallisation curves of (a) wax/LLDPE 30/70 blend composition at different values of T_c, and (b) various wax/LDPE blend compositions at T_c = 100 °C

Clearly, the temperature significantly affected the crystallisation kinetics of the LLDPE polymer. The log-logistic distribution provides an alternative expression to represent the crystallisation process (Focke et al., 2017). In addition, there is a method based on generalized logistics which allows for very good fittings of polymer crystallisations in different contexts (Díaz-Díaz et al., 2021).

The method applied here consisted of fitting each individual crystallisation isothermal DSC curves by a mixture of a time-derivative generalized logistic function (DGL), which accounts for the crystallisation exotherm, and a generalized logistic function (GL) multiplied by a scale factor, which accounts for the change of heat flow along the process:

$$y_{fit}(t) = y_2(t) + sf \cdot y_1(t) \tag{4.11}$$

where $y_1(t)$ and $y_2(t)$ represents GL and DGL respectively. GL and DGL share the rate and the symmetry parameters and the time location of the maximum. Thus, GL and DGL are synchronized as both enthalpy and heat capacity (C_p), changes that come from the same crystallisation process:

$$y_1(t) = \frac{1}{\left(1+\tau\cdot\exp\left(-b\cdot(t_{apm}-t)\right)\right)^{1/\tau}} \tag{4.12}$$

$$y_2(t) = \frac{c\cdot b\cdot\exp\left(-b\cdot(t_{apm}-t)\right)}{\left(1+\tau\cdot\exp\left(-b\cdot(t_{apm}-t)\right)\right)^{(1+\tau)/\tau}} \tag{4.13}$$

where t_{apm} is the time at the peak maximum, c represents the area of the peak, τ is the symmetry factor, where $\tau = 1$ means perfect symmetry and b is a rate factor which depends on temperature. The baseline-change along the transition, which comes from the change of C_p along the crystallisation process, is represented by the product of y_1 by a scale factor, ΔHF, which is the difference of heat flow as measured from t = 10 minutes to t = 16 minutes. After several trials it was found that the shape of the artefact curve in the “b”-region of Figure 4.19 is not very reproducible. A small anticipation or delay with respect to the specific HF drop in that area may lead to important distortions of the calculated specific HF curve. Consequently, the data contained in the “b”-region was disregarded and only the specific HF exotherm data contained at the “c”-region were used for the fitting through equation (4.13) by minimizing the average squared

error (ASE). For this fitting we used the ΔHF scale factor as a fixed parameter. The fitting parameters were t_{apm}, c, b, and τ. Figure 4.21 plots how the fitting parameters depend on the crystallisation temperature. It is observed that the area of the peak, represented by c, slightly decreases as the crystallisation temperature increases. This suggests that perhaps some of the lowest molecular mass fractions fail to crystalize when the crystallisation temperature is increased. On the other hand, parameters b and τ follow a shape that looks like half a bell, generally decreasing as the temperature increases above 100 ºC. According to Equation (4.11), τ = 1 represents a perfect symmetry of the crystallisation rate around the central temperature (in this case about 103 °C). On the other hand, Equation (4.15) shows that the apparent reaction order is τ+1. In this case, it means a reaction order of 2. The fact that b and τ follows similar trends with temperature suggests that a higher b value is obtained with a higher reaction order, that is, when a higher number of "species" are contributing to the crystallisation process. It is well known that the crystallisation rate follows a bell-shaped trend decreasing both sides towards the glass transition temperature and to the melting temperature (Hill, 1910, Avrami, 1939). Thus, following a similar approach than in a previous work, the *b* values were fitted to a Gaussian function (Díaz-Díaz et al., 2021):

$$b(T) = \frac{1}{t_{cryst}} \cdot \exp\left(-ln(2) \cdot \left(\frac{T - T_{cent}}{T_{hwhm}}\right)^2\right) \qquad (4.14)$$

where t_{cryst} represents a crystallisation time, T_{cent} the temperature at which the maximum rate is obtained, and T_{hwhm} the half width at height maximum, which is related to how b decreases as T diverges from T_{cent}. According to this expression, the rate parameter is dependent on a characteristic temperature and characteristic crystallisation time, which are specific for a given crystal structure. The values resulting from the fit are displayed on Table 4.3. Accordingly, the temperature at which the LLDPE can crystallise at its highest crystallisation rate is about 97.8 ºC. The crystallisation rate of this form was found to be 355.9 s which decreases to half of its maximum when moving 5.6 ºC up or down from the central value.

Figure 4.22(a &b) shows how the experimental data fit into a Gaussian distribution of the crystallisation rate versus crystallisation temperature. The equivalent crystallisation times are also plotted. It is observed that the longer the distance to the central temperature, the stronger the effect of a change in temperature on the time to crystallise. On the other hand, τ, which represents the symmetry of the peak, can be simulated to a reaction order since equation (4.13) can be re-written as a function of the conversion:

$$d\alpha/_{dt} = c \cdot b \cdot exp\left[-b \cdot \left(t_{apm} - t\right)\right] \cdot [(1-\alpha)]^{1+\tau} \qquad (4.15)$$

where α is the conversion. The idea that crystallisation from the melt can be simulated using a reaction order process would not be meaningless given that it is at intermediate temperatures, of maximum crystallisation rate, where a greater number of interactions of nucleation and crystal growth phenomena are expected to occur.

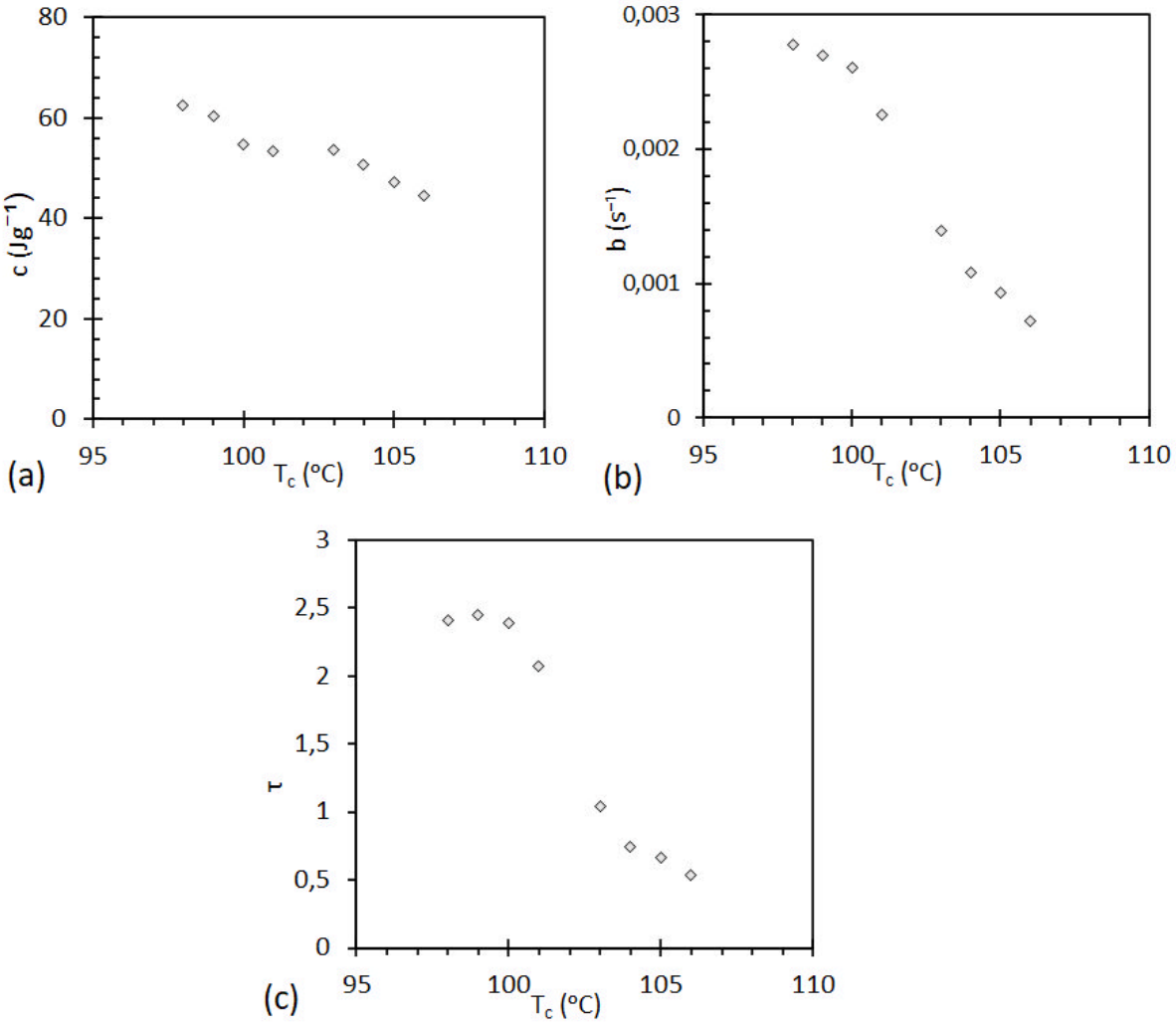

Figure 4.21: Plots of the logistic fitting parameters (a) crystallisation enthalpy vs the crystallisation temperature, (b) b parameter vs. the crystallisation temperature and (c) τ vs. the crystallisation temperature at 105 °C and 98 °C respectively for a blend containing 70 wt-% LLDPE

Table 4.3: Parameter values of the fitting of the b parameter values by equation (4.14)

	***b* parameters**	
t_{cryst} **(s)**	T_{cent} **(ºC)**	T_{hwhm} **(ºC)**
355.9	97.8	5.6

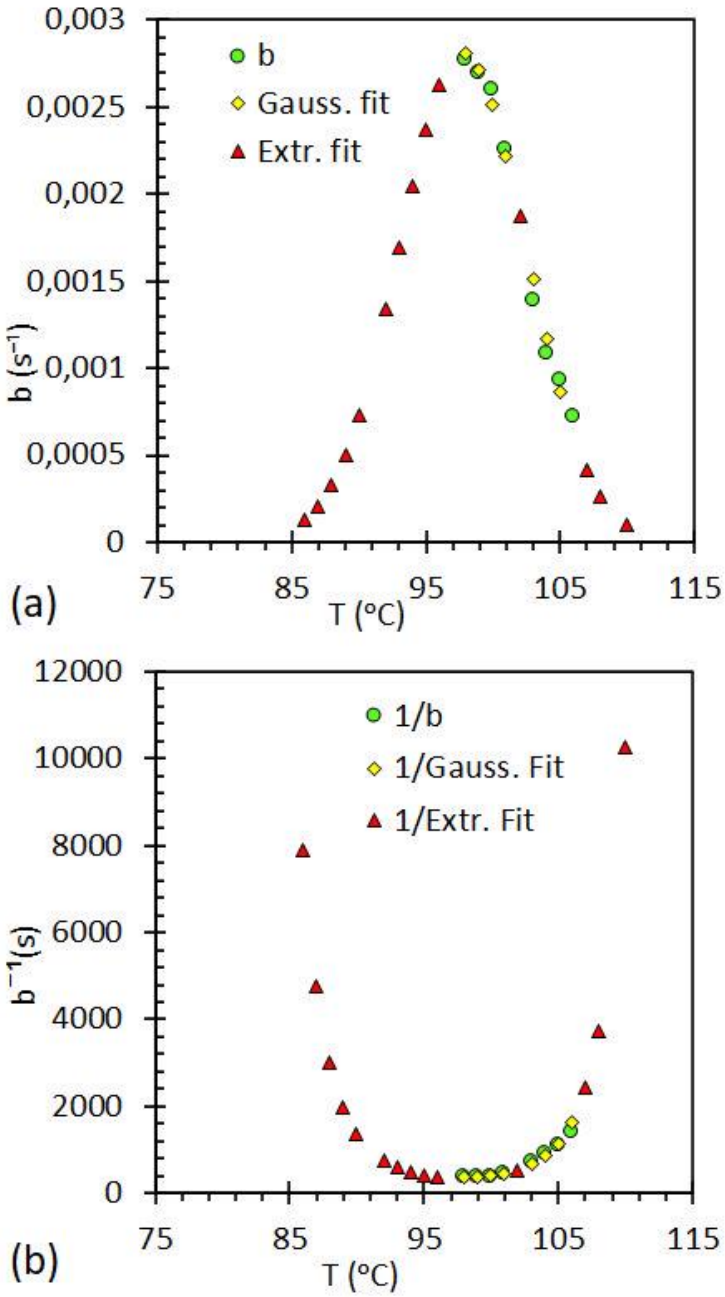

Figure 4.22: Fit of the b parameters versus the crystallisation temperature by (a) a Gaussian function and the (b) equivalent crystallisation times

Other attempts were made to model the phase transformation kinetics of the LLDPE-rich phase in the blends with the Johnson-Mehl-Avrami equation (Marotta et al., 1982, Avrami, 1939):

$$X_c(t) = 1 - exp[-(t/\tau)^n] \quad (4.16)$$

where X_c is the normalized crystallinity at time t, τ is a characteristic time constant for the overall crystallisation rate and n is the Avrami exponent. The DSC crystallisation exotherms are proportional to the rate of change in the crystallinity, i.e.:

$$\dot{q} = A\frac{dX_c}{dt} \quad (4.17)$$

where $\dot{q}$ is the heat flux in W g^{-1}, and A is a proportionality factor with units J g^{-1}. For the Avrami model, presented as equation (4.17), the rate is given by:

$$\dot{q} = A\frac{n}{\tau}\left(\frac{t}{\tau}\right)^{n-1} exp\left[-\left(\frac{t}{\tau}\right)^n\right] \quad (4.18)$$

The expression reaches a peak value at $t_{peak} = \tau$,

$$t_{peak} = \tau[n/(n-1)]^{1/n} \quad (4.19)$$

An induction time is observed before crystallisation commences in both Figure 4.20 (a) and (b). The induction time (t_{ind}) is almost identical irrespective of the composition or temperature of crystallisation. The log-logistic distribution, also known as the Hill model (Hill, 1910), provides an alternative expression that could be used to represent the crystallisation process (Focke et al., 2017):

$$X_c(t) = (t/\tau)^n/[1 + (t/\tau)^n] \quad (4.20)$$

The corresponding rate equation is:

$$\dot{q} = A\,(t/\tau)^{n-1}/[1 + (t/\tau)^n] \quad (4.21)$$

This rate equation reaches a maximum at:

$$t_{peak} = \tau[(n+1)/(n-1)]^{1/n} \quad (4.22)$$

Note that it is assumed that the crystallisation process is characterised by a characteristic induction time t_{ind} during which no crystallisation takes place. The time

(t) used in the rate equations listed above, is defined as the experimental time minus this induction time:

$$t = t_{exp} - t_{ind} \tag{4.23}$$

The adjustable parameters in the Avrami and Hill models and the induction time (t_{ind}) were determined by least-squares regression of the full set of isothermal crystallisation data. For each model it was assumed that the exponent n took a universal value valid for all data. This means that the same exponent n was the same constant irrespective of the blend composition and the crystallisation temperature. Patel (2012) previously noted a constant value for the exponent when studying the crystallisation of LLDPE in a similar temperature range. The characteristic time constant τ was not obtained by independent regression. Instead, it was calculated using either equation (4.20) or (4.22) for the Avrami and Hill models respectively. This ensured that the predicted and experimental exotherms reached their peak values at the same time. Table 4.4 lists the parameter values obtained as a function of the blend composition and the crystallisation temperature. Figure 4.23 shows representative model fits. It also indicates the range of experimental values used for the least-squares regression.

Perusal of the results presented in Table 4.4 revealed the following when the crystallisation temperature was varied for the blend containing 70 wt-% LLDPE. Both the enthalpy of crystallisation and the induction time initially increased with the lowering of the crystallisation temperature. However, it seems that plateau values of ca. ΔH_c = 61 J g^{-1} and t_{ind} = 1.57 min were reached for temperatures at and below 100 °C. The characteristic time constants (τ) decreased and the proportionality factor (A) increased as the temperature was lowered. This just reflects the fact that the crystallisation exotherms were sharper at the lower crystallisation temperatures as seen in Figure 4.20.

The following observation was made with respect to the effect of increasing the LLDPE content of the blend. As expected, the enthalpy of crystallisation increased with polymer content. Surprisingly though, the highest value was observed for the blend containing 10 wt-% wax. The presence of the lower molar mass component increases the free volume in the system, reduces the viscosity of the molten liquid and thereby enhances the mobility of the polymer chains. Perhaps, this can explain the increased

crystallinity of the 90 wt-% LLDPE blend as the chain are better able to reorganise and incorporate into crystallites. The induction time increased slightly with decrease in polymer content. The characteristic time constants increased, and the proportionality factor decreased with increasing wax content. This agrees with the broadening of the crystallisation exotherm, with increase in wax content, seen in Figure 4.20.

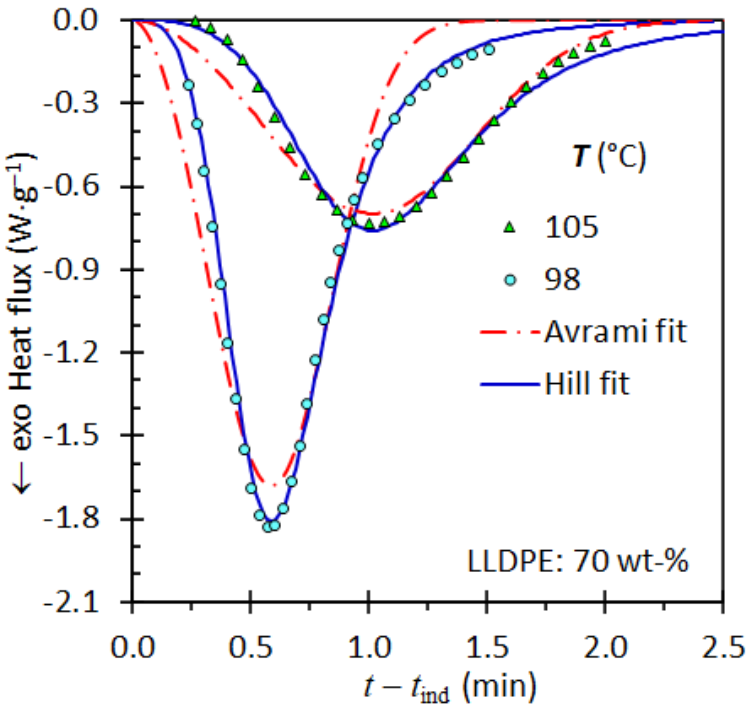

Figure 4.23: Representative model fits. The symbols show experimental data values obtained

Table 4.4: Effect of blend composition and temperature on the enthalpy of crystallisation and the parameters quantifying the kinetics of the process

LLDPE	T	ΔH_c	t_{ind}	t_{max}	Avrami (n = 2.88)			Hill (n = 4.30)		
(wt-%)	(°C)	(J g^{-1})	(min)	(min)	τ (min)	A (J g^{-1})	R*	τ (min)	A (J g^{-1})	R*
70	**98**	63	1.57	0.59	0.68	1.01	0.9742	0.66	1.59	0.9974
70	**99**	61	1.57	0.61	0.71	0.97	0.9692	0.68	1.48	0.9994
70	**100**	61	1.58	0.63	0.73	0.89	0.9767	0.71	1.30	0.9955
70	**101**	52	1.59	0.66	0.76	0.84	0.9673	0.74	1.19	0.9989
70	**102**	63	1.50	0.85	0.98	1.06	0.9892	0.95	1.15	0.9627
70	**103**	50	1.52	0.83	0.96	0.85	0.9833	0.92	0.96	0.9890
70	**104**	48	1.44	0.96	1.11	0.82	0.9883	1.07	0.80	0.9912
70	**105**	42	1.48	1.02	1.18	0.72	0.9717	1.13	0.67	0.9946
70	**106**	39	1.42	1.22	1.41	0.68	0.9552	1.36	0.52	0.9951
50	**100**	38	1.65	0.68	0.79	0.63	0.9837	0.76	0.85	0.9942
60	**100**	41	1.66	0.53	0.62	0.66	0.9882	0.59	1.14	0.9943
70	**100**	55	1.58	0.63	0.73	0.89	0.9795	0.71	1.30	0.9956
80	**100**	53	1.50	0.58	0.67	1.21	0.9362	0.65	1.97	0.9931
90	**100**	84	1.47	0.65	0.75	1.29	0.9161	0.72	1.89	0.9899
100	**100**	81	1.50	0.52	0.60	1.24	0.9719	0.58	2.24	0.9983

*The data regression was done over the time interval $0.25 \leq t \leq 1.5$. The correlation coefficient R was calculated for the values in this same interval

The value presently found for the Avrami kinetic exponent is 2.88 which falls in the range of 2.5 – 3.0 reported for the crystallisation of LLDPE in blends with a paraffin wax (Gumede et al., 2017). This value is also close to 3, the one theoretically expected for volume nucleation and 2D growth (Matsushita and Sakka, 1981). However, considering the values obtained for the correlation coefficients presented in Table 4.4, it is clear that compared to the Avrami analysis, the empirical Hill model was most often significantly better at representing the experimental data.

4.2.3 Polarised optical microscopy

4.2.3.1 Crystalline morphology from hot-stage microscopy

Figure 4.24 shows the crystalline morphology of the wax/LLDPE blends at selected temperatures as revealed by hot stage polarised optical microscopy. The image in Figure 4.24(a) represents the neat wax at a temperature of 65 °C. It reveals a crystalline morphology featuring fine, needle-like structures. Figure 4.24(b) to 22(f) show the crystalline morphologies observed at 100 °C for selected blends. The dark coloured background represents a molten liquid region in which vibrantly coloured crystalline regions are observable. Adding even small amounts of LLDPE to the wax, results in a transition away from the wax needle-like texture towards that of a fine "mosaic"-like texture. This is likely caused by higher nucleation rates which lead to rapid impingement of the growing crystal domains. LLDPE-rich samples feature the distinctive "Maltese cross" pattern found for the spherulitic crystallisation of PE (Saville, 1989). Closer inspection also revealed the presence of banded structures typically observed for polyethylene (Keith and Padden, 1996). These observations agree with the phase images reported by Chen and Wolcott (2015) for paraffin wax/LLDPE blends. The slight colourisation found in the amorphous fraction, which is prominent in the 30/70 blend, may be indicative of crystalline regions that are at a depth beyond the focal length.

As the wax fraction increased to 50 wt-%, the LLDPE spherulitic domains decreased in size. Eventually a point, observable in Figure 4.24(c-d), is reached where they could not be distinguished at the magnification employed. Table 4.5 lists estimates for the

observed spherulite diameters. The decrease in size, at higher wax fractions, appears to be caused by enhanced nucleation.

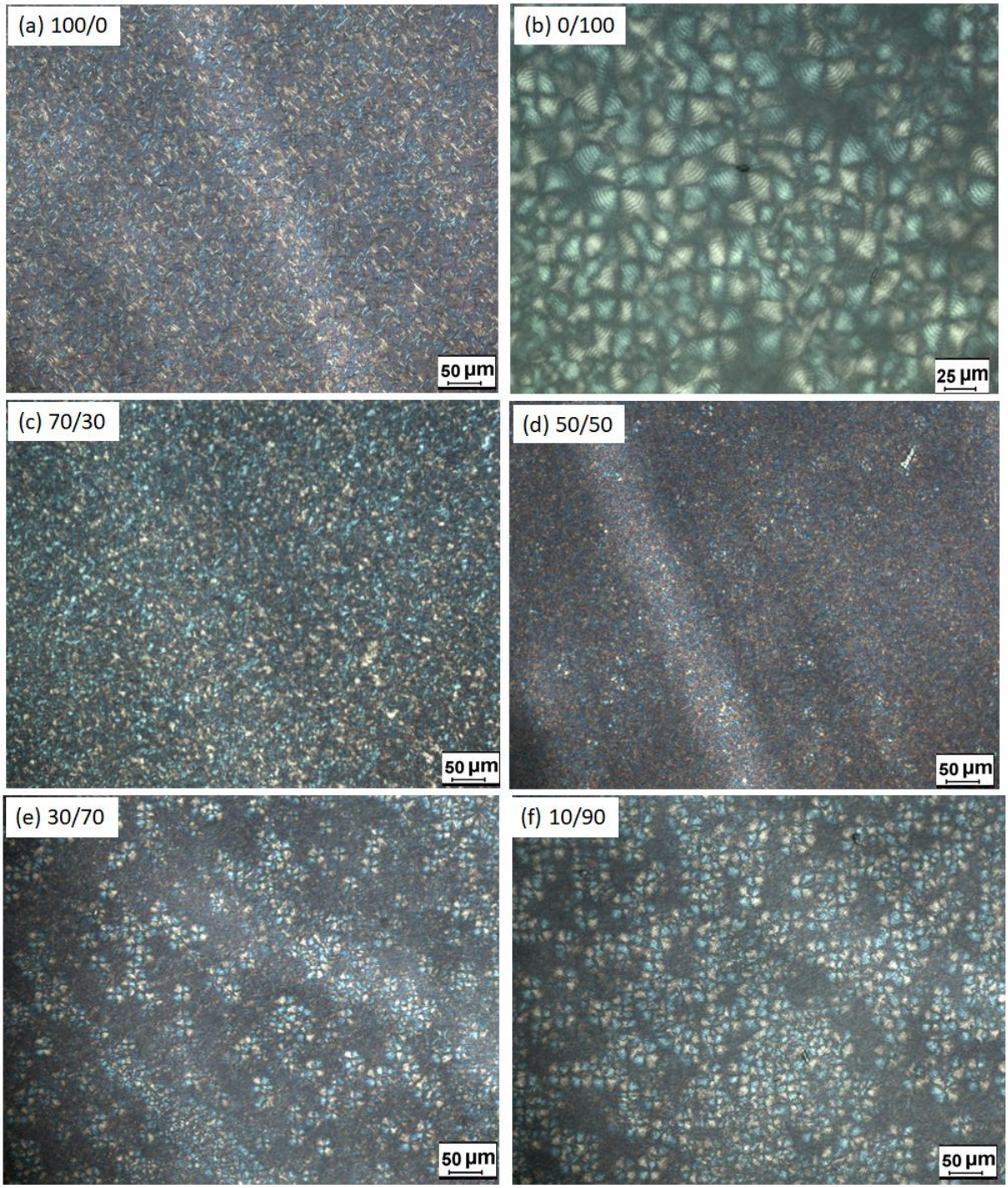

Figure 4.24: Polarised optical microscopy images of (a) pure wax at 65 °C, (b) pure LLDPE at 100 °C, and (c-f) blends micro-graphed at a temperature of 100 °C at different L-Wax/L-LLDPE mass ratios

4.2.3.2 H-LLDPE equilibrium temperature-isothermal process

The Hoffmann-Weeks equation (Hoffman et al., 1975, Weeks, 1963) for the lamellar thickness was used to estimate the ultimate equilibrium melting temperature of the LLDPE:

$$T_m = T_c/\beta + (1 - 1/\beta)T_m^o \quad (4.24)$$

where the parameter β represents the lamellar thickening ratio which links the experimentally determined isothermal crystallisation temperature, $T_{c,}$ to the melting temperature, T_m, and the equilibrium melting point, T_m^o. According to this equation, a plot of T_m against T_c should yield a straight line with slope $1/\beta$ and intercept $(1 - 1/\beta)T_m^o$. The ultimate equilibrium melting temperature is obtained as the intersection of the straight-line plot of T_m against T_c with the line defined by $T_m^o = T_c$. It is important to note that, the Hoffmann-Weeks equation is based on the assumption that the difference between the isothermal crystallisation temperature and observed melting temperature only depends on the thickness of the lameller formed during isothermal crystallisation. In effect, equation (4.24) defines the relationship between T_m^o in response to the crystallisation temperature of a given system (Mohammadi et al., 2018). Figure 4.25 shows this relationship in a form of linear plots generated from the data obtained from the hot stage optical microscopy studies. The estimated equilibrium melting temperatures, with the corresponding lamellar thickening ratio's, are listed in Table 4.5. Increasing the wax fraction in the blends significantly depressed the equilibrium melting temperature of the LLDPE. Interestingly, the thickening ratio was essentially the same for all the blends studied. This suggests that the dynamics of the lamellar thickening ratio of crystal structure was preserved while the equilibrium melting temperature varied with the blend composition as expected for a colligative property, i.e., the melting point depression.

Table 4.5: Mean spherulite diameters (d), equilibrium melting temperature (T_m^o) and lamellar thickness ratio (β) found in isothermal LLDPE crystallisation of L-Wax/L-LLDPE blends

Wax	***d***		***β***
wt-%	**µm**	**°C**	**-**
80	-	125.3	1.08
60	-	128.6	1.11
50	10.08±0.03	126.8	1.09
30	15.83±0.10	127.7	1.17
20	19.54±0.07	131.9	1.1
10	23.17±0.09	135.4	1.1
0	33.21±0.20	136.9	1.12

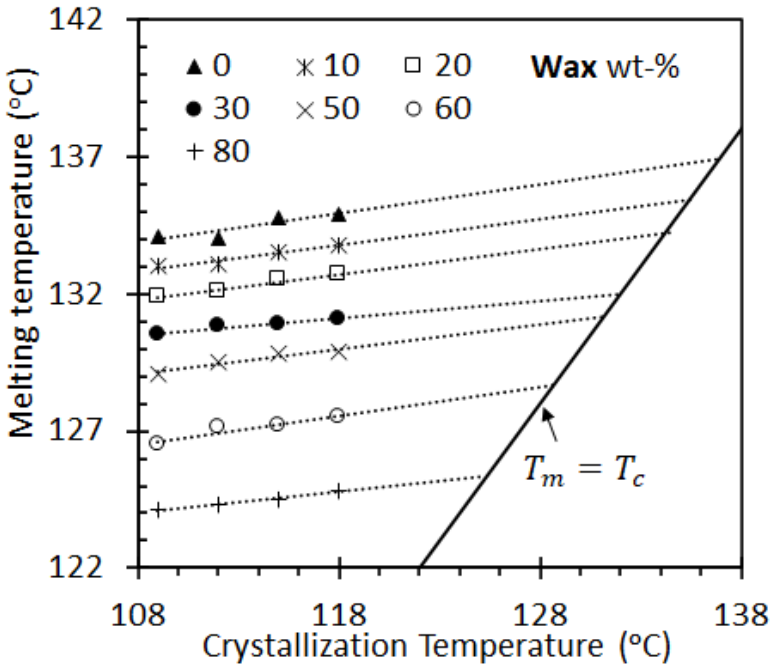

Figure 4.25: Ultimate equilibrium melting temperature of L-LLDPE spherulites formed at various L-Wax/L-LLDPE blend compositions as determined from the hot stage optical microscopy data

CHAPTER 5

5 CONCLUSIONS AND RECOMMENDATIONS

The purpose of this work was to investigate the characteristics of F-T waxes blended with high-flow grades of LLDPE for possible use as processing additive in polyethylene masterbatch applications. This study probed blend compatibility considering the rheological of melts and the thermal properties and crystalline structure of solid samples. The composition ratio, temperature and shear rates/stresses were the variables of interest. The samples were prepared by melt blending using extrusion. F-T Wax/LLDPE samples were prepared in predetermined quantities of the wax and polyethylene in increments of 10 wt-%. This study provides a survey of characterisation methods and principles using rheology, differential scanning calorimetry (DSC), and hot stage polarised optical microscopy (POM). Both sample preparation and characterisation work were conducted in a temperature range of 120 – 180 °C.

The phase behaviour of F-T waxes and LLDPEs blend were explored using DSC. The results showed a significant LLDPE melting point depression indicating solubility of the polymer in the molten wax. Furthermore, the DSC traces for the blends differed substantially from linear combinations of the parent materials. This supports partial crystallisation of the polymer with the wax and also of the wax with the polymer. However, the overall enthalpy of crystallisation was less than expected from the linear blending rule. The reduction in the degree of crystallisation achieved was more pronounced for the LLDPE portion indicating that the presence of the wax interfered.

Optical microscopic monitoring of isothermal crystallisation, of the LLDPE phase, showed that adding wax decreased the size of the spherulites. Beyond 50 wt-% wax, it was not possible to distinguish the spherulites at the magnification applied (25×). Moreover, the ultimate melting temperature of the LLDPE phase was 137 °C. It decreased progressively with increase in wax content reaching 125 °C at 80 wt-% wax. However, the Hoffman–Weeks parameter was independent of blend composition. This indicated that the dynamics of the lamellar thickening process, for the LLDPE crystallites, was not affected by the presence of the wax.

Isothermal crystallisation kinetics, obtained in DSC studies, were modelled using a generalized logistic equation for the blend containing 70 wt-% LLDPE. The crystallisation rate versus temperature approached a Gaussian distribution. The characteristic temperature where the crystallisation rate reached a maximum was 97.8 °C. The isothermal crystallisation kinetics for LLDPE were also modelled using the Avrami and Hill equations. The overall crystallisation rate of LLDPE increased with decreasing temperature and increasing LLDPE content. The maximum crystallisation rate was observed at 98 °C and 10 wax-% respectively. The Avrami exponent was n = 2.88 for all the blend samples confirming the three-dimensional athermal and instantaneous nucleation of spherulites. However, the Hill exponent was n = 4.30 and surprisingly a better fit compared to the Avrami model.

The composition dependence of the zero-shear viscosity agreed with the predictions of the Friedman and Porter model for molten mixtures controlled by polymer chain entanglements. This implied complete compatibility of the components in the molten state from 160 to 180 °C. In addition, a slightly better data fit was also possible with the Lederer–Roegiers empirical mixture model. The composition dependence of the complex viscosity also followed the Friedman and Porter mixture rule except that the exponent differed from the one applicable to the zero-shear viscosity, that is, α = 4.81 instead of α = 3.4. The complex viscosity of all the blends obeyed an Arrhenius-like temperature dependence with an activation energy of 27.5 ± 1.3 kJ mol^{-1}. Plots of log G' versus G'' (so-called Han plots) were linear and essentially independent of composition, temperature and the applied angular frequency. The Cole–Cole plots also indicated that the wax-LDPE blends are miscible in the melt state. Together, these confirmed the miscibility of the wax and the LLDPE down to temperatures as low as 120 °C.

Overall, the results indicate full miscibility of the wax and the LLDPE in the melt and partial co-crystallisation in the solid state. Moreover, in the dynamic DSC scan, the near complete absence of a wax-like melting peak for the blend containing 10 wt-% wax suggests complete miscibility at that concentration.

The rheological methods employed in this thesis, viz shear rate rheometry, has provided valuable insights into the rheological behaviour of the wax/LLDPE blend. However, there are additional rheological methods that can complement this existing

knowledge and enlarged the scope of the blend's rheological properties. For example, further studies can incorporate methods such as controlled shear stress rheometry, creep test and stress relaxation etc to gain more comprehensive understanding about the internal molecular rearrangements and time-dependent behaviour of the blends.

In DSC analysis of both blends, the LLDPE appeared as dissimilar phase to the wax phase however its melting point depression was seen. Therefore, it is unclear whether the polyethylene insoluble fraction was the short, branched chains due to the incorporation of higher alpha-olefins as comonomers or an entirely different fraction present in small quantities. Therefore, further work to study the structural and molecular mass distribution of the blend would be needed to identify this fraction, also accompanied by extra studies to elucidate the blends thermal degradation with time. On the other hand, the use of multifunctional nanofillers represent a new trend in polyolefin blends for various applications for the purpose of enhancing primary properties and/or create new functionalities. Perhaps the F-T wax/PE blends coupled with such nanofillers could exploit these properties adding value to existing applications.

REFERENCES

AGRAWAL, P., SILVA, M. H. A., CAVALCANTI, S. N., FREITAS, D. M. G., ARAÚJO, J. P., OLIVEIRA, A. D. B. & MÉLO, T. J. A. 2022. Rheological properties of high-density polyethylene/linear low-density polyethylene and high-density polyethylene/low-density polyethylene blends. *Polymer Bulletin,* 79**,** 2321-2343.

AMOO, L. M. & LAYI FAGBENLE, R. 2020. 14 - Overview of non-Newtonian boundary layer flows and heat transfer. *In:* FAGBENLE, R. O., AMOO, O. M., ALIU, S. & FALANA, A. (eds.) *Applications of Heat, Mass and Fluid Boundary Layers.* Woodhead Publishing.

ASBACH, G. I. & KILIAN, H. G. 1991. Investigation of equilibrium crystallisation processes of n-alkane multicomponent systems. *Polymer,* 32**,** 3006-3012.

AVRAMI, M. 1939. Kinetics of phase change I: General theory. *The Journal of Chemical Physics,* 7**,** 1103-1112.

AVRAMI, M. 1940. Kinetics of phase change II: Transformation-time relations for random distribution of nuclei. *Journal of Chemical Physics,* 8**,** 212-224.

BAI, L., LI, Y. M., YANG, W. & YANG, M.-B. 2010. Rheological behaviour and mechanical properties of high-density polyethylene blends with different molecular weights. *Journal of Applied Polymer Science,* 118**,** 1356-1363.

BAKSHI, A. K. & GHOSH, A. K. 2022. Processability and physico-mechanical properties of ultrahigh-molecular-weight polyethylene using low-molecular-weight olefin wax. *Polymer Engineering & Science,* 62**,** 2335-2350.

BAYAT, M. H., ABDOUSS, M. & JAVANBAKHT, M. 2013. Quantification of polyethylene wax in semibatch laboratory reactor and a study of different

parameters on wax production as a by-product in the slurry ethylene polymerization. *Journal of Applied Polymer Science,* 127**,** 1027-1031.

BENNETT, H. 1944. *Commercial waxes, natural and synthetic, including properties, uses, methods of handling and formulas for making commercial wax compositions,* Brooklyn, N. Y, Chemical publishing co., inc.

BERK, Z. 2009. Chapter 2 - Fluid flow. *In:* BERK, Z. (ed.) *Food Process Engineering and Technology.* San Diego: Academic Press.

BERNARD, D. A. & NOOLANDI, J. 1982. Zero-shear viscosity exponent and polydispersity effects. *Macromolecules,* 15**,** 1553-1559.

BOYRON, O., TAAM, M. & BOISSON, C. 2019. Chemical composition of hexene-based linear low-density polyethylene by infrared spectroscopy and chemometrics. *Macromolecular Chemistry and Physics,* 220**,** 1900376.

CHALOUPKOVÁ, K. & ZATLOUKAL, M. 2009. Effect of die design on die drool phenomenon for metallocene based LLDPE: Theoretical and experimental investigation. *Journal of Applied Polymer Science,* 111**,** 1728-1737.

CHEN, F. & WOLCOTT, M. 2015. Polyethylene/paraffin binary composites for phase change material energy storage in building: A morphology, thermal properties, and paraffin leakage study. *Solar Energy Materials and Solar Cells,* 137**,** 79-85.

CHEN, F. & WOLCOTT, M. P. 2014. Miscibility studies of paraffin/polyethylene blends as form-stable phase change materials. *European Polymer Journal,* 52**,** 44-52.

CHO, K., LEE, B. H., HWANG, K.-M., LEE, H. & CHOE, S. 1998. Rheological and mechanical properties in polyethylene blends. *Polymer Engineering & Science,* 38**,** 1969-1975.

CIESIŃSKA, W., LISZYŃSKA, B. & ZIELIŃSKI, J. 2016. Selected thermal properties of polyethylene waxes. *Journal of Thermal Analysis and Calorimetry,* 125**,** 1439-1443.

CORAN, A. Y. & ANAGNOSTOPOULOS, C. E. 1962. Polymer–diluent interactions. III. Polyethylene—diluent interactions. *Journal of Polymer Science,* 57**,** 13-23.

CRIST, B. & HILL, M. J. 1997. Recent developments in phase separation of polyolefin melt blends. *Journal of Polymer Science Part B: Polymer Physics,* 35**,** 2329-2353.

CRIST, B. & SCHULTZ, J. M. 2016. Polymer spherulites: A critical review. *Progress in Polymer Science,* 56**,** 1-63.

DANGTUNGEE, R., YUN, J. & SUPAPHOL, P. 2005. Melt rheology and extrudate swell of calcium carbonate nanoparticle-filled isotactic polypropylene. *Polymer Testing,* 24**,** 2–11.

DARGAZANY, R., KHIÊM, V., POSHTAN, E. & ITSKOV, M. 2014. Constitutive modeling of strain-induced crystallisation in filled rubbers. *Physical Review E,* 89**,** 022604.

DEALY, J. & LARSON, R. 2006. *Structure and rheology of molten polymers: From structure to flow behaviour and back again,* Chiron media (United Kingdom), Carl Hanser Verlag GmbH & Co

DEALY, J. M. 1991. Rheology of molten polymers. *MRS Bulletin,* 16**,** 24-26.

DESHMUKH, S. P., PARMAR, M. B., RAO, A. C. & WADHWA, V. 2010. Polymer- and wax-based monoconcentrate predispersed pigments in the colouring of plastics. *Coloration Technology,* 126**,** 189-193.

DI LORENZO, M. L. & RIGHETTI, M. C. 2018. Crystallisation-induced formation of rigid amorphous fraction. *Polymer crystallisation,* 1**,** e10023.

DÍAZ-DÍAZ, A. M., LÓPEZ-BECEIRO, J., LI, Y., CHENG, Y. & ARTIAGA, R. 2021. Crystallisation kinetics of a commercial poly(lactic acid) based on characteristic crystallisation time and optimal crystallisation temperature. *Journal of Thermal Analysis and Calorimetry,* 145**,** 3125-3132.

DIJKSTRA, D., AUHL, D., BRUMMER, R., GABRIEL, C., MANGNUS, M., RUELLMANN, M., ZOETELIEF, W., HANDGE, U. & LAUN, M. 2014. Guidelines for checking performance and verifying accuracy of rotational rheometers: Viscosity measurements in steady and oscillatory shear (IUPAC Technical Report). *Pure and Applied Chemistry,* 86**,** 1945.

DJOKOVIĆ, V., MTSHALI, T. N. & LUYT, A. S. 2003. The influence of wax content on the physical properties of low-density polyethylene–wax blends. *Polymer International,* 52**,** 999-1004.

DROBNY, J. G. 2014. 3 - Additives. *In:* DROBNY, J. G. (ed.) *Handbook of Thermoplastic Elastomers (Second Edition).* Oxford: William Andrew Publishing.

DURU, R., AIRUEHIA, G. & OTAIGBE, J. 2013. Natural & synthetic wax emulsifications. *36th Annual international conference* Minna, Nigeria: Chemical Society of Nigeria.

ELLEITHY, R., ALI, I., AL-HAJ ALI, M. & AL-ZAHRANI, S. 2011. High density polyethylene/micro calcium carbonate composites: A study of the morphological, thermal, and viscoelastic properties. *Journal of Applied Polymer Science,* 117**,** 2413-2421.

ESMAEILZADE, R., SHARIF, F., RASHEDI, R. & DORDI NEJAD, A. 2022. Morphology, phase diagram, and properties of high-density

polyethylene/thermally treated waste polyethylene wax blends. *Journal of Applied Polymer Science,* 139**,** 51750.

EYRING, H. & HIRSCHFELDER, J. 1937. The theory of the liquid state. *The Journal of Physical Chemistry,* 41**,** 249-257.

FERNANDA, P. 2018. Chapter 11 - Methods used in the study of the physical properties of fats. *In:* MARANGONI, A. G. (ed.) *Structure-Function Analysis of Edible Fats (Second Edition).* AOCS Press.

FERRY, J. D. 1961. Viscoelastic properties of polymers. *Journal of the American Chemical Society,* 83**,** 4110-4111.

FERRY, J. D. 1980. *Viscoelastic properties of polymers*, John Wiley & Sons.

FETTERS, L., LOHSE, D. & COLBY, R. 2007. Chain dimensions and entanglement spacings. *In:* E, M. J. (ed.) *Physical Properties of Polymers Handbook.* New York, NY. : Springer.

FLORY, P. J. 1941. Thermodynamics of high polymer solutions. *The Journal of Chemical Physics,* 9**,** 660-661.

FLORY, P. J. 1962. On the morphology of the crystalline state in polymers. *Journal of the American Chemical Society,* 84**,** 2857-2867.

FOCKE, W. W., VAN DER WESTHUIZEN, I., MUSEE, N. & LOOTS, M. T. 2017. Kinetic interpretation of log-logistic dose-time response curves. *Scientific Reports,* 7**,** 1-7.

FOX, T. G. & FLORY, P. J. 1951. Further studies on the melt viscosity of polyisobutylene. *The Journal of Physical Chemistry,* 55**,** 221-234.

FRIEDMAN, E. M. & PORTER, R. S. 1975. Polymer viscosity-molecular weight distribution correlations via blending: for high molecular weight poly(dimethyl siloxanes) and for polystyrenes. *Trans Soc Rheol,* 19**,** 493-508.

GALE, M. 1997. Compounding with single-screw extruders. *Advances in Polymer Technology,* 16**,** 251-262.

GIDDE, R. & PAWAR, P. 2017. On effect of viscoelastic characteristics of polymers on performance of micropump. *Advances in Mechanical Engineering,* 9**,** 168781401769121.

GRÁNÁSY, L., PUSZTAI, T., TEGZE, G., WARREN, J. A. & DOUGLAS, J. F. 2005. Growth and form of spherulites. *Phys Rev E Stat Nonlin Soft Matter Phys,* 72**,** 011605.

GROENINCKX, G., HARRATS, C., VANNESTE, M. & EVERAERT, V. 2014. Crystallisation, micro- and nano-structure, and melting behaviour of polymer blends. *In:* UTRACKI, L. A. & WILKIE, C. A. (eds.) *Polymer Blends Handbook.* Dordrecht: Springer Netherlands.

GRUNBERG, L. & NISSAN, A. H. 1949. Mixture law for viscosity. *Nature,* 164**,** 799-800.

GUDIÑO RIVERA, J., HERNÁNDEZ GÁMEZ, J. F., BORJAS RAMOS, J. J., SALINAS HERNÁNDEZ, M. & SÁNCHEZ MARTÍNEZ, D. I. 2022. Effects of residual wax content on the thermal, rheological, and mechanical properties of high-density polyethylene. *Polymer Engineering & Science,* 62**,** 1867-1875.

GUMEDE, T. P., LUYT, A. S., PÉREZ-CAMARGO, R. A., ITURROSPE, A., ARBE, A., ZUBITUR, M., MUGICA, A. & MÜLLER, A. J. 2016. Plasticization and cocrystallisation in LLDPE/wax blends. *Journal of Polymer Science Part B: Polymer Physics,* 54**,** 1469-1482.

GUMEDE, T. P., LUYT, A. S., PÉREZ-CAMARGO, R. A. & MÜLLER, A. J. 2017. The influence of paraffin wax addition on the isothermal crystallisation of LLDPE. *Journal of Applied Polymer Science,* 134**,** 44398.

HAHLADAKIS, J. N., VELIS, C. A., WEBER, R., IACOVIDOU, E. & PURNELL, P. 2018. An overview of chemical additives present in plastics: Migration, release, fate and environmental impact during their use, disposal and recycling. *Journal of Hazardous Materials,* 344**,** 179-199.

HAN, C. D. 1988. Influence of molecular weight distribution on the linear viscoelastic properties of polymer blends. *Journal of Applied Polymer Science,* 35**,** 167-213.

HAN, C. D. & CHUANG, H. K. 1985. Criteria for rheological compatibility of polymer blends. *Journal of Applied Polymer Science,* 30**,** 4431-4454.

HAN, C. D. & JHON, M. S. 1986. Correlations of the first normal stress difference with shear stress and of the storage modulus with loss modulus for homopolymers. *Journal of Applied Polymer Science,* 32**,** 3809-3840.

HANDOO, J., SRIVASTAVA, S. P., AGRAWAL, K. M. & JOSHI, G. C. 1989. Thermal properties of some petroleum waxes in relation to their composition. *Fuel,* 68**,** 1346-1348.

HARTITZ, J. 1974. The effect of lubricants on the fusion of rigid poly(vinyl chloride). *Polymer Science and Engineering* 14(5)**,** 392-398.

HATO, M. J. & LUYT, A. S. 2007. Thermal fractionation and properties of different polyethylene/wax blends. *Journal of Applied Polymer Science,* 104**,** 2225-2236.

HAY, J. N. & ZHOU, X.-Q. 1993. The effect of mixing on the properties of polyethylene blends. *Polymer,* 34**,** 2282-2288.

HIGGINS, J., LIPSON, J. & WHITE, R. 2010. A simple approach to polymer mixture miscibility. *Philosophical Transactions. Series A, Mathematical, Physical, and Engineering Sciences,* 368**,** 1009-25.

HILL, A. V. 1910. The possible effects of the aggregation of the molecules of haemoglobin on its dissociation curves. *The Journal of Physiology,* 40**,** iv-vii.

HILL, M. J., BARHAM, P. J. & VAN RUITEN, J. 1993. Liquid-liquid phase segregation in blends of a linear polyethylene with a series of octene copolymers of differing branch content. *Polymer,* 34**,** 2975-2980.

HIND, R. K., MCLAUGHLIN, E. & UBBELOHDE, A. R. 1960. Structure and viscosity of liquids. Camphor + pyrene mixtures. *Transactions of the Faraday Society,* 56**,** 328-330.

HLANGOTHI, S. P., KRUPA, I., DJOKOVIĆ, V. & LUYT, A. S. 2003. Thermal and mechanical properties of cross-linked and uncross-linked linear low-density polyethylene–wax blends. *Polymer Degradation and Stability,* 79**,** 53-59.

HOFFMAN, J. D., FROLEN, L. J., ROSS, G. S. & LAURITZEN, J. I. 1975. On the growth rate of spherulites and axialites from the melt in polyethylene fractions: regime I and regime II crystallisation. *Journal of Research of the National Bureau of Standards. Section A, Physics and Chemistry,* 79A**,** 671-699.

HOFFMAN, J. D., GUTTMAN, C. M. & DIMARZIO, E. A. 1979. On the problem of crystallisation of polymers from the melt with chain folding. *Faraday Discussions of the Chemical Society,* 68**,** 177-197.

HÖHNE, G. W. H. & BLANKENHORN, K. 1994. High pressure DSC investigations on n-alkanes, n-alkane mixtures and polyethylene. *Thermochimica Acta,* 238**,** 351-370.

HONG, Y., COOMBS, S. J., COOPER-WHITE, J. J., MACKAY, M. E., HAWKER, C. J., MALMSTRÖM, E. & REHNBERG, N. 2000. Film blowing of linear low-density polyethylene blended with a novel hyperbranched polymer processing aid. *Polymer,* 41**,** 7705-7713.

HONG, Y., COOPER-WHITE, J., MACKAY, M., HAWKER, C., MALMSTRÖM, E. & REHNBERG, N. 1999. A novel processing aid for polymer extrusion: Rheology

and processing of polyethylene and hyperbranched polymer blends. *Journal of Rheology,* 43**,** 781-793.

HOSTOMSKY, J. & JONES, A. G. 1991. Calcium carbonate crystallisation, agglomeration and form during continuous precipitation from solution. *Journal of Physics D: Applied Physics,* 24**,** 165.

HOUGHTON, E. L., CARPENTER, P. W., COLLICOTT, S. H. & VALENTINE, D. T. 2013. Chapter 1 - basic concepts and definitions. *In:* HOUGHTON, E. L., CARPENTER, P. W., COLLICOTT, S. H. & VALENTINE, D. T. (eds.) *Aerodynamics for engineering students (Sixth Edition).* Boston: Butterworth-Heinemann.

HUGGINS, M. L. 1941. Solutions of long chain compounds. *The Journal of Chemical Physics,* 9**,** 440.

HULL, J. B. & JONES, A. R. 1996. Processing of liquid crystal polymers and blends. *In:* ACIERNO, D. & COLLYER, A. A. (eds.) *Rheology and processing of liquid crystal polymers.* Dordrecht: Springer Netherlands.

JAFARI ANSAROUDI, H. R., VAFAIE-SEFTI, M., MASOUDI, S., BEHBAHANI, T. J. & JAFARI, H. 2013. Study of the morphology of wax crystals in the presence of ethylene-co-vinyl acetate copolymer. *Petroleum Science and Technology,* 31**,** 643-651.

JIANG, L. & XU, X. 2017. Crystallisation behavior of cellulose nanocomposites and cellulose nanofibril-reinforced polymer nanocomposites. *In:* HANIEH KARGARZADEH, I. A., SABU THOMAS, ALAIN DUFRESNE (ed.) *Handbook of Nanocellulose and Cellulose Nanocomposites.* Germany: John Wiley & Sons, Incorporated.

KE, B. 1961. Differential thermal analysis of high polymers. II. Effects of diluents on melting behavior of polyethylenes. *Journal of Polymer Science,* 50**,** 79-86.

KEITH, H. D. & PADDEN, F. J. 1996. Banding in polyethylene and other spherulites. *Macromolecules,* 29**,** 7776-7786.

KHARCHENKO, S. B., MCGUIGGAN, P. M. & MIGLER, K. B. 2003. Flow induced coating of fluoropolymer additives: Development of frustrated total internal reflection imaging. *Journal of Rheology,* 47**,** 1523-1545.

KILIAN, H. G. 1985. The non-homogeneous thermodynamically autonomous and equivalent microphase. *In:* STEINKOPFF, J. (ed.) *Progress in Colloid & Polymer Science: Polymers as Colloid Systems. .* Springer.

KING, L. F. & NOËL, F. 1972. Characterisation of lubricants for polyvinyl chloride. *Polymer Engineering & Science,* 12**,** 112-119.

KONINGSVELD, R., KLEINTJENS, L. & SCHOFFELEERS, M. 1974. Thermodynamic aspects of polymer compatibility. *Pure and Applied Chemistry,* 39**,** 1-32.

KRUPA, I. & LUYT, A. S. 2000. Thermal properties of uncross-linked and cross-linked LLDPE/wax blends. *Polymer Degradation and Stability,* 70**,** 111-117.

KRUPA, I. & LUYT, A. S. 2001. Thermal and mechanical properties of extruded LLDPE/wax blends. *Polymer Degradation and Stability,* 73**,** 157-161.

KRUPA, I. & LUYT, A. S. 2001a. Physical properties of blends of LLDPE and an oxidized paraffin wax. *Polymer,* 42**,** 7285-7289.

KRUPA, I., MIKOVÁ, G. & LUYT, A. S. 2007. Phase change materials based on low-density polyethylene/paraffin wax blends. *European Polymer Journal,* 43**,** 4695-4705.

KUKALEVA, N., SIMON, G. P. & KOSIOR, E. 2003. Modification of recycled high-density polyethylene by low-density and linear-low-density polyethylenes. *Polymer Engineering & Science,* 43**,** 26-39.

KURYAKOV, V. N., IVANOVA, D. D., TKACHENKO, A. N. & SEDENKOV, P. N. 2020. Determination of phase transition temperatures (melting, crystallisation, rotator phases) of n-alkanes by the optical method. *IOP Conference Series: Materials Science and Engineering,* 848**,** 012044.

LAURITZEN, J. I., JR. & HOFFMAN, J. D. 1960. Theory of formation of polymer crystals with folded chains in dilute solution. *J Res Natl Bur Stand A Phys Chem,* 64a**,** 73-102.

LEDERER, E. 1931. Zur theorie der viskosität von flüssigkeiten. *Kolloid-Beihefte,* 34**,** 270-338.

LEE, C. D. 2002. Die-lip build-up in the extrusion of iighly filled low density polyethylene. *Annual Technical Conference ANTEC, Conference Proceedings 1.*

LEFEBVRE, J. & DOUBLIER, J.-L. 2006. Rheological behaviour of polysaccharides aqueous systems. *In:* DUMITRIU, S. (ed.) *Polysaccharides Structural Diversity and Functional Versatility, Second Edition.* New York: Taylor and Francis group.

LEYVA-PORRAS, C., CRUZ-ALCANTAR, P., ESPINOSA-SOLÍS, V., MARTÍNEZ-GUERRA, E., BALDERRAMA, C. I. P., MARTÍNEZ, I. C. & SAAVEDRA-LEOS, M. Z. 2019. Application of differential scanning calorimetry (DSC) and modulated differential scanning calorimetry (MDSC) in food and drug industries. *Polymers (Basel),* 12**,** 1-5.

LICHKUS, A. & HARRISON, I. 1992. LCP/PE blends for thin film applications. *ANTEC 92--Shaping the Future.,* 2**,** 2257-2259.

LIM, K. L. K., ISHAK, Z. A. M., ISHIAKU, U. S., FUAD, A. M. Y., YUSOF, A. H., CZIGANY, T., PUKANSZKY, B. & OGUNNIYI, D. S. 2005. High-density polyethylene/ultrahigh-molecular-weight polyethylene blend. I. The processing, thermal, and mechanical properties. *Journal of Applied Polymer Science,* 97**,** 413-425.

LIU, S.-L., CHEN, J.-Y. & CAO, Y. 2015. Effect of solid paraffin on the integrity of welded interfaces and properties of ultra-high molecular weight polyethylene. *Polymer Science Series A,* 57**,** 168-176.

LODGE, T., ROTSTEIN, N. & PRAGER, S. 1992. Dynamics of entangled polymer liquids: Do linear chains reptate? *Advances in chemical physics,* 79**,** 1-1.

LORENZO, A. T., ARNAL, M. L., ALBUERNE, J. & MÜLLER, A. J. 2007. DSC isothermal polymer crystallisation kinetics measurements and the use of the Avrami equation to fit the data: Guidelines to avoid common problems. *Polymer Testing,* 26**,** 222-231.

LUYT, A. S. & BRÜLL, R. 2004. Investigation of polyethylene-wax blends by CRYSTAF and SEC-FTIR. *Polymer Bulletin,* 52**,** 177-183.

LUYT, A. S. & KRUPA, I. 2002. PE/wax blends: interesting observations. *Macromolecular Symposia,* 178**,** 109-116.

LUYT, A. S. & KRUPA, I. 2008. Thermal behaviour of low and high molecular weight paraffin waxes used for designing phase change materials. *Thermochimica Acta,* 467**,** 117-120.

MANDELKERN, L. 2011. *Crystallisation of polymers: volume 1, equilibrium concepts,* New York, Cambridge University Press.

MAROTTA, A., SAIELLO, S., BRANDA, F. & BURI, A. 1982. Activation energy for the crystallisation of glass from DDTA curves. *Journal of Materials Science,* 17**,** 105-108.

MARTÍNEZ-SALAZAR, J., ALIZADEH, A., JIMÉNEZ, J. J. & PLANS, J. 1996. On the melting behaviour of polymer single crystals in a mixture with a compatible oligomer: 2. Polyethylene/paraffin. *Polymer,* 37**,** 2367-2371.

MARTÍNEZ-SALAZAR, J., CUESTA, M. S. & PLANS, J. 1991. On phase separation in high- and low-density polyethylene blends: 1. Melting-point depression analysis. *Polymer,* 32**,** 2984-2988.

MATSUSHITA, K. & SAKKA, S. 1981. Kinetic study on non-isothermal crystallisation of glass by thermal analysis (Commemoration issue dedicated to Professor Megumi Tashiro on the occation of his retirement). *Bulletin of the Institute for Chemical Research, Kyoto University,* 59**,** 159-171.

MCGUIRE, K. S., LAXMINARAYAN, A. & LLOYD, D. R. 1994. A simple method of extrapolating the coexistence curve and predicting the melting point depression curve from cloud point data for polymer-diluent systems. *Polymer,* 35**,** 4404-4407.

MCPHERSON, A., MALKIN, A. J. & KUZNETSOV, Y. G. 2000. Atomic force microscopy in the study of macromolecular crystal growth. *Annual Review of Biophysics and Biomolecular Structure,* 29**,** 361.

MNGOMEZULU, M. E., LUYT, A. S. & KRUPA, I. 2010. Structure and properties of phase change materials based on HDPE, soft Fischer-Tropsch paraffin wax, and wood flour. *Journal of Applied Polymer Science,* 118**,** 1541-1551.

MNGOMEZULU, M. E., LUYT, A. S. & KRUPA, I. 2011. Structure and properties of phase-change materials based on high-density polyethylene, hard Fischer–Tropsch paraffin wax, and wood flour. *Polymer Composites,* 32**,** 1155-1163.

MOFOKENG, T. G., RAY, S. S. & OJIJO, V. 2018. Influence of selectively localised nanoclay particles on non-isothermal crystallisation and degradation behaviour of PP/LDPE blend composites. *Polymers,* 10**,** 245.

MOHAMMADI, H., VINCENT, M. & MARAND, H. 2018. Investigating the equilibrium melting temperature of linear polyethylene using the non-linear Hoffman-Weeks approach. *Polymer,* 146**,** 344-360.

MOHAMMADI, M., YOUSEFI, A. & EHSANI, M. 2012. Thermorheological analysis of blend of high- and low-density polyethylenes. *Journal of Polymer Research,* 19**,** 9798

MOLEFI, J. A., LUYT, A. S. & KRUPA, I. 2010. Comparison of LDPE, LLDPE and HDPE as matrices for phase change materials based on a soft Fischer-Tropsch paraffin wax. *Thermochimica Acta,* 500**,** 88-92.

MORRIS, B. A. 2017. 4 - Commonly used resins and substrates in flexible packaging. *In:* MORRIS, B. A. (ed.) *The Science and Technology of Flexible Packaging.* Oxford: William Andrew Publishing.

MOTOOKA, M., MANTOKU, H. & TAKAO, O. 1986. *Process for producing stretched articles of ultrahigh-molecular-weight polyethylene*. 06/755,590.

MPANZA, H. S. & LUYT, A. S. 2006. Comparison of different waxes as processing agents for low-density polyethylene. *Polymer Testing,* 25**,** 436-442.

MPANZA, H. S. & LUYT, A. S. 2006a. Influence of different waxes on the physical properties of linear low-density polyethylene. *South African Journal of Chemistry,* 59**,** 48-54.

MTSHALI, T., SITTERT, C. V., DJOKOVJ , V. & LUYT, A. S. 2003. Binary mixtures of polyethylene and oxidized wax: Dependency of thermal and mechanical properties upon mixing procedure. *Journal of Applied Polymer Science,* 89**,** 2446-2456.

MTSHALI, T. N., KRUPA, I. & LUYT, A. S. 2001. The effect of cross-linking on the thermal properties of LDPE/wax blends. *Thermochimica Acta,* 380**,** 47-54.

MTSHALI, T. N., VAN SITTERT, C. G. C. E., DJOKOVIĆ, V. & LUYT, A. S. 2003a. Binary mixtures of polyethylene and oxidized wax: Dependency of thermal and mechanical properties upon mixing procedure. *Journal of Applied Polymer Science,* 89**,** 2446-2456.

MÜLHAUPT, R. 2003. Catalytic polymerization and post polymerization catalysis fifty years after the discovery of Ziegler's catalysts. *Macromolecular Chemistry and Physics,* 204**,** 289-327.

MÜLLER, A. J., BALSAMO, V., SILVA, F. D., ROSALES, C. M. & SÁEZ, A. E. 1994. Shear and elongational behavior of linear low-density and low-density polyethylene blends from capillary rheometry. *Polymer Engineering & Science,* 34**,** 1455-1463.

MUNARO, M. & AKCELRUD, L. 2008. Polyethylene blends: A correlation study between morphology and environmental resistance. *Polymer Degradation and Stability,* 93**,** 43-49.

MUSIL, J. & ZATLOUKAL, M. 2014. Historical review of die drool phenomenon in plastics extrusion. *Polymer Reviews,* 54**,** 139-184.

MUSIL, J., ZATLOUKAL, M., GOUGH, T. & MARTYN, M. T. 2011. Experimental investigation of die drool and slip-stick phenomena during HDPE polymer melt extrusion. *AIP Conference Proceedings,* 1375**,** 26-42.

NAKAJIMA, A. & HAMADA, F. 1965. Estimation of thermodynamic interactions between polyethylene and n-alkanes by means of melting point measurements. *Kolloid-Zeitschrift und Zeitschrift für Polymere,* 205**,** 55-61.

NICHETTI, D. & MANAS-ZLOCZOWER, I. 1998. Viscosity model for polydisperse polymer melts. *Journal of Rheology,* 42**,** 951-969.

OGAH, O. 2012. The effects of linear low-density polyethylene (LLDPE) on the mechanical properties of high-density polyethylene (HDPE) film blends. *International Journal of Engineering and Management Sciences,* 3**,** 85-90.

PADDING, J. & BRIELS, W. 2002. Time and length scales of polymer melts studied by coarse-grained molecular dynamics simulations. *The Journal of Chemical Physics,* 117**,** 925-943.

PAK, J. & WUNDERLICH, B. 2001. Melting and crystallisation of polyethylene of different molar mass by calorimetry. *Macromolecules,* 34**,** 4492-4503.

PATEL, R. M. 2012. Crystallisation kinetics modeling of high density and linear low density polyethylene resins. *Journal of Applied Polymer Science,* 124**,** 1542-1552.

PATTERSON, D. & ROBARD, A. 1978. Thermodynamics of polymer compatibility. *Macromolecules,* 11**,** 690-695.

PLASTICSSA 2020/2021. Plastic, people and planet: An annual review.

RAGAERT, K., DELVA, L., VAN DAMME, N., KUZMANOVIC, M., HUBO, S. & CARDON, L. 2016. Microstructural foundations of the strength and resilience of LLDPE artificial turf yarn. *Journal of Applied Polymer Science,* 133**,** 44080

RAIMO, M. 2015. Growth of spherulites: foundation of the DSC analysis of solidification. *ChemTexts,* 1**,** 13.

RAIMO, M. 2019. An optical test to unveil twisting of birefringent crystals in spherulites. *Royal Society Open Science,* 6**,** 181215.

RATHOD, M. K. & BANERJEE, J. 2013. Thermal stability of phase change materials used in latent heat energy storage systems: A review. *Renewable and Sustainable Energy Reviews,* 18**,** 246-258.

RETIEF, J. J. & LE ROUX, J. H. 1983. Crystallographic investigation of a paraffinic Fischer-Tropsch wax in relation to a theory of wax structure and behaviour. *South African Journal of Science,* 79**,** 234-239.

ROBESON, L. 2014. Historical perspective of advances in the science and technology of polymer blends. *Polymers,* 6**,** 1251-1265.

ROBESON, L. M. 2007. *Polymer Blends: A Comprehensive Review*, Hanser.

ROEGIERS, M. & ROEGIERS, L. 1947. La viscosité des mélanges de" fluides normaux". *Submitted in 1947 in Gand by Impr AA Hoste*.

SALYER, I. O. 1996. Thermoplastic, moldable, non-exuding phase change materials. University of Dayton: European patents.

SAVILLE, B. P. 1989. Polarized light: qualitative microscopy. *In:* HEMSLEY, D. A. (ed.) *Applied Polymer Light Microscopy.* Dordrecht: Springer Netherlands.

SCHELLENBERG, J. & FIENHOLD, G. 1998. Environmental stress cracking resistance of blends of high-density polyethylene with other polyethylenes. *Polymer Engineering & Science,* 38**,** 1413-1419.

SHEN, L., SEVERN, J. & BASTIAANSEN, C. W. M. 2018. Drawing behavior and mechanical properties of ultra-high molecular weight polyethylene blends with a linear polyethylene wax. *Polymer,* 153**,** 354-361.

SHILPA KASARGOD NAGARAJ, S. S., NITHIN KUNDACHIRA SUBRAMANI AND HATNA & SIDDARAMAIAH 2016. Revisiting powder X-ray diffraction

technique: A powerful tool to characterise polymers and their composite films. *Journal of Material Science,* 4**,** 1-5.

SOTOMAYOR, M. E., KRUPA, I., VÁREZ, A. & LEVENFELD, B. 2014. Thermal and mechanical characterisation of injection moulded high density polyethylene/paraffin wax blends as phase change materials. *Renewable Energy,* 68**,** 140-145.

SRIVASTAVA, S. P., HANDOO, J., AGRAWAL, K. M. & JOSHI, G. C. 1993. Phase-transition studies in n-alkanes and petroleum-related waxes—A review. *Journal of Physics and Chemistry of Solids,* 54**,** 639-670.

STADLER, F. J., PIEL, C., KASCHTA, J., RULHOFF, S., KAMINSKY, W. & MÜNSTEDT, H. 2006. Dependence of the zero shear-rate viscosity and the viscosity function of linear high-density polyethylenes on the mass-average molar mass and polydispersity. *Rheologica Acta,* 45**,** 755-764.

TANNIRU, M. & MISRA, R. D. K. 2005. On enhanced impact strength of calcium carbonate-reinforced high-density polyethylene composites. *Materials Science and Engineering: A,* 405**,** 178-193.

TURNER, W. R., BROWN, D. S. & HARRISON, D. V. 1955. Properties of paraffin waxes. *Industrial & Engineering Chemistry,* 47**,** 1219-1226.

UNGAR, G., STEJNY, J., KELLER, A., BIDD, I. & WHITING, M. C. 1985. The crystallisation of ultralong normal paraffins: the onset of chain folding. *Science,* 229**,** 386-9.

UTRACKI, L. A. & SCHLUND, B. 1987. Linear low density polyethylenes and their blends: Part 2. Shear flow of LLDPE's. *Polymer Engineering & Science,* 27**,** 367-379.

VADALIA, H. C., LEE, H. K., MYERSON, A. S. & LEVON, K. 1994. Thermally induced phase separation in ternary crystallisable polymer solutions. *Journal of Membrane Science,* 89**,** 37-50.

WATANABE, H. 1999. Viscoelasticity and dynamics of entangled polymers. *Progress in Polymer Science,* 24**,** 1253-1403.

WEBBER, G. V. 2009. *The origin of multiple DSC melting peaks of Fischer-Tropsch hard waxes.* University of Cape Town.

WEEKS, J. J. 1963. Melting temperature and change of lamellar thickness with time for bulk polyethylene. *Journal of research of the National Bureau of Standards. Section A, Physics and chemistry,* 67A**,** 441-451.

WEI, H. & XIAOYA, F. 2012. An overview of wax production, requirement and supply in the world market. *European Chemical Bulletin,* 1**,** 266-268.

WHALEY, J. K., TEMPLETON, C. & ANVARI, M. 2019. Rheological testing for semisolid foods: traditional rheometry. *In:* JOYNER, H. S. (ed.) *Rheology of Semisolid Foods.* Cham: Springer International Publishing.

WUNDERLICH, B. 2013. *Macromolecular Physics,* New York, Academic Press.

WUNDERLICH, B. & CZORNYJ, G. 1977. A study of equilibrium melting of polyethylene. *Macromolecules,* 10**,** 906-913.

XU, J., XIA, T., ZHAO, L., YIN, B. & YANG, M. 2018. Correlation between phase separation and rheological behavior in bitumen/SBS/PE blends. *RSC Advances,* 8**,** 41713-41721.

ZACHMANN, H. G. & WUTZ, C. 1993. Studies of the mechanism of crystallisation by means of WAXS and SAXS employing synchrotron radiation. *In:* DOSIÈRE, M. (ed.) *Crystallisation of Polymers.* Dordrecht: Springer Netherlands.

ZALBA, B., MARíN, J. M., CABEZA, L. F. & MEHLING, H. 2003. Review on thermal energy storage with phase change: materials, heat transfer analysis and applications. *Applied Thermal Engineering,* 23**,** 251-283.

ZHAO, L. & CHOI, P. 2006. A review of the miscibility of polyethylene blends. *Materials and Manufacturing Processes,* 21**,** 135-142.

ZHMUD, B. 2014. Viscosity blending equations. *Lube-Tech,* 93**,** 22-27.

APPENDIX A: PUBLICATIONS

JOURNAL ARTICLES

Phillips, J., Weldhagen, M., **Mhlabeni, T**., Radebe, L., Ramjee, S., Wesley-Smith, J., Atanasova, M. & Focke, W. W. 2021. Thermal characterisation of metal stearate lubricant mixtures for polymer compounding applications. *Thermochimica Acta*, 699, 178906.

Mhlabeni, T., Ngobese, C., Ramjee, S., & Focke, W. W. 2023. Rheological characterisation of linear low-density polyethylene–Fischer–Tropsch wax blends. *Journal of Vinyl & Additive Technology*, 1.

Mhlabeni, T., Ramjee, S., López, J., Díaz-Díaz, A.-M., Artiaga, R. & Focke, W. 2023. Thermal and rheological properties of Fischer–Tropsch wax/high-flow LLDPE blends. *Macromolecular Materials and Engineering,* n/a**,** 2300125.

APPENDIX B: MATERIAL DATA SHEET

WAX RESINS DATA SHEET

Referred to as L-WAX in text

sasol

product data sheet

Sasolwax M3B

Code 1388 ***Revision 4*** ***31 May 2018***

Properties	*Test method*	*Units*	*Specification*	*Typical values*
Congealing point	*ASTM D 938*	*°C*	*58 - 64*	*62*
Penetration at 25°C	*ASTM D1321*	*0.1 mm*	*17 - 23*	*20*
Oil Content	*ASTM D721*	*mass %*	*4.2 max*	*3.8*
Colour	*Sasol 2000*	*Saybolt*	*+ 17min*	*+27*
Appearance	*Sasol 1074*	*-*	*Clear at 90°C*	*Clear*
Water crackle test	*Sasol 1087*	*-*	*Pass splutter test*	*Pass*
Centrifuge test	*Sasol 1052*	*-*	*Free from foreign material*	*Pass*

Packaging
Sasolwax M3B is supplied as Liquid, pastilles or powder in 20kg polyethylenen bags or in boxes as 25kg slabs.

Note
To obtain the best performance from the product, we recommend use within 5 years from sample date on the Certificate of Analysis. Product should be stored under standard warehousing conditions, at least in a clean dry place, in its original packing at a temperature not exceeding 35°C

Notice ***This product information is indicative and does not include any guarantee***

Sasol Chemicals a division of Sasol South Africa (Pty) Ltd.
ISO 9001/ISO 14001

Referred to as H-WAX in text

sasol

product data sheet

Sasolwax H1

Code 1550 **Revision 18** **27 March 2019**

Properties	Test method	Units	Specification	Typical values
Congealing point	ASTM D 938	°C	96-100	97
Drop melting point	ASTM D 3954	°C	-	112
Penetration at 25°C	ASTM D 1321	0.1 mm	1 max	1
Penetration at 65°C	ASTM D 1321	0.1 mm	20 max	18
Acid Value	ASTM D 1386/7	mg KOH/g	-	<0.1
Saponification value	ASTM D 1386/7	mg KOH/g	-	<0.5
Brookfield viscosity at 135°C	Sasol 1010	cP	6-10	8
Bromine value	Sasol 3016	g Br/100g	-	0.1
Colour	Sasol 2000	Saybolt	+15 min	+22
Oil content	ASTM D 721	mass %	-	0.2
MIBK solubles	Sasol 4036	mass %	1.5 max	0.8
Centrifuge test	Sasol 1052		Free from foreign material	Pass
Molecular weight	-	Dalton	-	880
UV absorptivity @290 nm	ASTM D2008-12	L/g.cm	-	<0.01

Compliance

F&DA *This product complies with the requirements of 21 Code of Federal Regulations: Parts 172.615 (Chewing gum base), 175.105 (Adhesives), 175.250 (Paraffin, synthetic), 175.125 (Pressure sensitive adhesive), 175.300 (Resinous & Polymeric coatings), 175.320 (Resinous & Polymeric coatings for Film), 176.170 (Components of Paper & Paperboard, Wet), 176.180 (Components of Paper & Paperboard, Dry), 177.1200 (Cellophane), 177.1390 (Laminate Structures) and 177.1210 (Closures with sealing gaskets for food containers).*

BfR recommendation: *This product complies with BfR requirement XXV, Part C, (Synthetische Hartparaffine)*

Packaging

Sasolwax H1 is supplied in the form of pastilles packed in 20kg paper bags and 700kg and coarse powder packed in 20kg paper bags or 600kg.

Note

To obtain the best performance from the product, we recommend use within 20 years from sample date on the Certificate of Analysis. Product should be stored under standard warehousing conditions, at least in a clean dry place, in its original packing at a temperature not exceeding 35°C.

Notice **This product information is indicative and does not include any guarantee**

Sasol Chemicals a division of Sasol South Africa (Pty) Ltd.
ISO 9001/ISO 14001

POLYMER RESIN DATA SHEET

Referred to as L-LLDPE in text

SABIC® LLDPE M500026

Linear low density polyethylene for masterbatch compounding

Description

SABIC® LLDPE M500026 is a high flow linear low density polyethylene copolymer grade with a narrow molecular weight distribution.

Application

SABIC® LLDPE M500026 resin is recommended for injection moulding masterbatch where a high filler acceptance is required, combined with a good flow.

Processing conditions

Typical moulding conditions for SABIC® LLDPE M500026 are: material temperature 180 - 230 °C (355 - 450 °F).

Mechanical properties

Test specimen is prepared from compression moulded sheet made according to ASTM D-1928, procedure C.

Typical data. Revision 20060418

Properties	Units SI	Values	Test methods
Polymer properties			
Melt flow rate (MFR) at 190 °C and 2.16 kg	g/10 min	**50**	ASTM D 1238
Density	kg/m³	**926**	ASTM D 1505
Mechanical properties			
Tensile test			ASTM D 638
stress at yield	MPa	**13**	
stress at break	MPa	**12.4**	
strain at break	%	**120**	
secant modulus at 1% elongation	MPa	**354**	
Izod impact notched at 23 °C	J/m	**450**	ASTM D 256
Hardness Shore D	-	**55**	ASTM D 2240
ESCR	h	**2**	ASTM D 1693
Thermal properties			
Vicat softening temperature at 10 N (VST/A)	°C	**88**	ASTM D 1525
Brittleness temperature	°C	**<-75**	ASTM D 746

internet www.SABIC-europe.com
email TCC.TM-PE@SABIC-europe.com

SABIC® LLDPE M500026

Linear low density polyethylene for masterbatch compounding

General information. SABIC® LLDPE grades are available in a wide range of viscosities. Supplementary to this, various grades are also available in powder form. This unique combination makes SABIC® LLDPE grades extremely suitable for masterbatch and compounding applications.
The SABIC® LLDPE portfolio offers an excellent choice to find a good base resin for both additives, black, white and colour masterbatches, with varying amounts of additives and pigments.

Health, Safety and Food Contact regulations. Detailed information is provided in the relevant Material Safety Datasheet and or Standard Food Declaration, available on the Internet (www.SABIC-europe.com). Additional specific information can be requested via your local Sales Office.

Quality. SABIC Europe is fully certified in accordance with the internationally accepted quality standard ISO 9001-2000. It is SABIC Europe's policy to supply materials that meet customers specifications and needs and to keep up its reputation as a pre-eminent, reliable supplier of e.g. polyethylenes.

Storage and handling. Polyethylenes resins (in pelletised or powder form) should be stored in such a way that it prevents exposure to direct sunlight and/or heat, as this may lead to quality deterioration. The storage location should also be dry, dust free and the ambient temperature should not exceed 50 °C. Not complying with these precautionary measures can lead to a degradation of the product which can result in colour changes, bad smell and inadequate product performance. It is also advisable to process polyethylene resins (in pelletised or powder form) within 6 months after delivery, this because also excessive aging of polyethylene can lead to a deterioration in quality.

Environment and recycling. The environmental aspects of any packaging material do not only imply waste issues but have to be considered in relation with the use of natural resources, the preservations of foodstuffs, etc. SABIC Europe considers polyethylene to be an environmentally efficient packaging material. Its low specific energy consumption and insignificant emissions to air and water designate polyethylene as the ecological alternative in comparison with the traditional packaging materials. Recycling of packaging materials is supported by SABIC Europe whenever ecological and social benefits are achieved and where a social infrastructure for selective collecting and sorting of packaging is fostered. Whenever 'thermal' recycling of packaging (i.e. incineration with energy recovery) is carried out, polyethylene -with its fairly simple molecular structure and low amount of additives- is considered to be a trouble-free fuel.

internet www.SABIC-europe.com
email TCC.TM-PE@SABIC-europe.com

Referred to as H-LLDPE in text

PRODUCT DATA SHEET

sasol

LLDPE LLDPE LLDPE LLDPE LLDPE LLDPE LLDPE LLDPE LLDPE LLDPE

Linear Low Density Polyethylene

HM2420

Technical support:
Polymer Technology Services Centre
22 Pressburg Road,
Modderfontein, 1645
South Africa

Tel: +27 (0)11 458 0700
Fax: +27 (0)11 458 0734

Sales office:
Sasol Base Chemicals
PO Box 5486
Johannesburg, 2000
South Africa

Tel: +27 (0) 10 344 5000
polymers@sasol.com

Date of issue: March 2017

www.sasol.com

Melt Index: 20 g/10min

Density: 0.924 g/cm³

Features
- High gloss
- Excellent low temperature impact strength
- Good ESCR
- Hexene copolymer

Applications
- Injection moulded containers and lids
- Base polymer for masterbatch

Additives
- Antioxidant

Typical properties (not to be construed as specifications)		Value (SI)	Value (English)	Method
Resin Properties	Melt Index (190°C/2.16kg)	20 g/10min	20 g/10min	ASTM D1238
	Density	0.924 g/cm³	0.924 g/cm³	ASTM D1505
Product Properties	Tensile strength at yield	15 MPa	2 175 psi	ASTM D638[1)]
	Tensile strength at break	18 MPa	2 610 psi	ASTM D638[1)]
	Elongation at break	900 %	900 %	ASTM D638[1)]
	Flexural modulus	440 MPa	63 800 psi	ASTM D790
	ESCR	> 50 hr	> 50 hr	ASTM D1693[2)]
	Impact energy at -40°C	20 J/mm	44 ft/lbs	ASTM D5628[3)]
	Shore D hardness	56	56	ASTM D2240
	Vicat softening temperature	97 °C	97 °C	ASTM D1525

1) **Crosshead speed 50 mm/min**
2) **100% Igepal CO630**
3) **Tested on 3mm compression moulded samples**

PRODUCT DATA SHEET

sasol

LLDPE LLDPE LLDPE LLDPE LLDPE LLDPE LLDPE LLDPE LLDPE LLDPE

Injection moulding

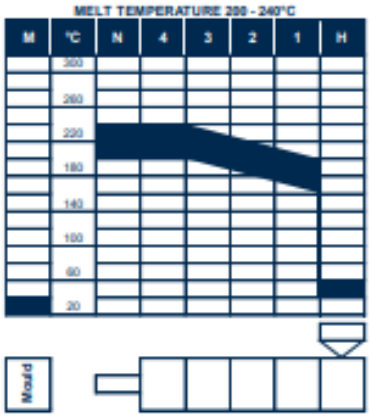

Processing – Injection moulding

HM2420 can be processed over a wide range of temperatures. Typical melt temperatures are 200°C to 240°C. HM2420 can be demoulded at fairly high temperatures due to its higher melting point, which can benefit cycle times.

Processing – Masterbatch

HM440 processes over a wide range of temperatures. Typical melt temperatures are 180°C to 250°C. HM2420 can be used for various pigment concentrations due to its high flow properties.

Handling

Workers should be protected from the possibility of skin or eye contact with molten polymer. Safety glasses are suggested as a minimal protection to prevent possible mechanical or thermal injury to the eyes. Fabrication areas should be ventilated to carry away fumes or vapours. Please consult the material safety data sheet (SDS) for more detailed information.

Storage

As ultraviolet light may cause a change in the material, all resins should be protected from direct sunlight during storage. If stored in cool (<25°C), dry area with low ambient light levels, polyolefin resins are expected to maintain their original material and processing properties for at least 12 months.

Combustibility

Polyethylene resins will burn when supplied adequate heat and oxygen. They should be handled and stored away from contact with direct flames and/or other ignition sources. In burning, polyethylene resins contribute high heat and may generate a dense black smoke. Fires can be extinguished by conventional means with water and water mist preferred. In enclosed areas, fire fighters should be provided with self contained breathing apparatus.

Conveying

Conveying equipment should be designed to prevent accumulation of fines and dust particles that are contained in all polyethylene resins. The fines and dust particles can, under certain conditions, pose an explosion hazard. We recommend that the conveying system used:

- be equipped with adequate filters
- is operated and maintained in such a manner to ensure no leaks develop
- that adequate grounding exists at all times

It is further recommended that good housekeeping is practiced throughout the facility.

Regulatory & Legal Compliance

This material complies with FDA regulation 21 CFR 177.1520 when used unmodified and according to good manufacturing practices for food contact applications. Refer to applicable food contact compliance statement which is available on request.
This material is not medically approved and should therefore not be used in any such application.

APPENDIX C: CHARACTERISATION OF NEAT WAXES AND LLDPES

GAS AND SIZE EXCLUSION CHROMATOGRAPHY ANALYSIS

METHOD

Two waxes were used in this study and their molar mass distributions were determined by Cirrebelle (Randburg, South Africa) using a standard gas chromatography (GC) method. The carbon number distributions were determined using Perkin Elmer Clarus Gas Chromatography 4000. Xylene AR was used as the mobile phase. It was required that the sample vials be heated to above 70 °C to ensure complete solubility of the sample which was injected at this temperature. The waxes comprise of mainly *n*-paraffins with other different types of hydrocarbon molecules including iso-alkanes, alpha-olefins, alcohols and oxygenates present in small amounts. Table C.1 and Figure C.1 shows a breakdown of these components in L-Wax and H-Wax according to GC analysis.

Table C.1: Components in L-Wax and H-Wax according to GC analysis

Component (%)	**L-Wax**	**H-Wax**
***n*-paraffins**	86.69	98.41
Iso-paraffins	12.66	-
olefins	0.59	-
OH	0.12	-
Total (%)	100	98.41

Two different polymer materials were used, and their molar mass distributions were determined by the Department of Chemistry and Polymer Science, University of Stellenbosch, using size exclusion chromatography (SEC). Results of the molecular mass distribution are shown in figure C.2 and Table C.2

RESULTS

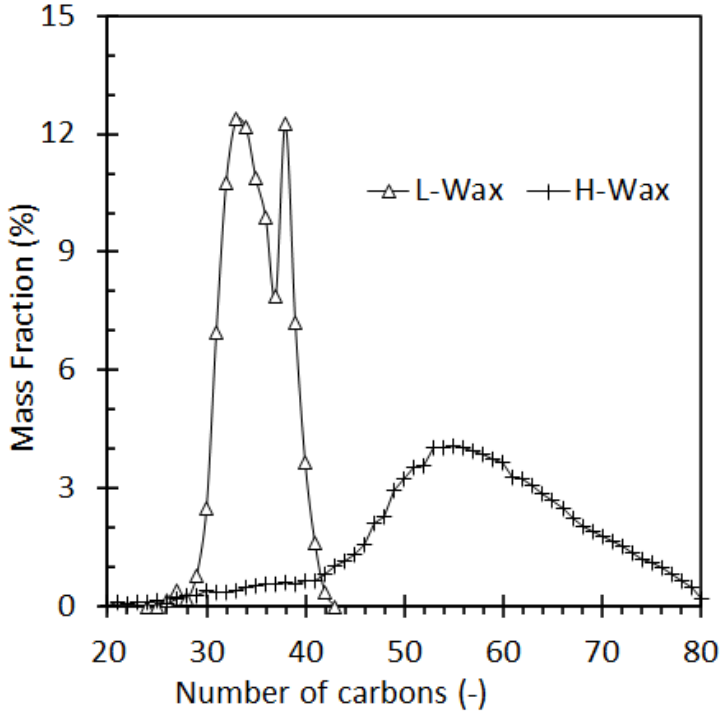

Figure C.1: Molecular mass distribution of L-Wax and H-Wax

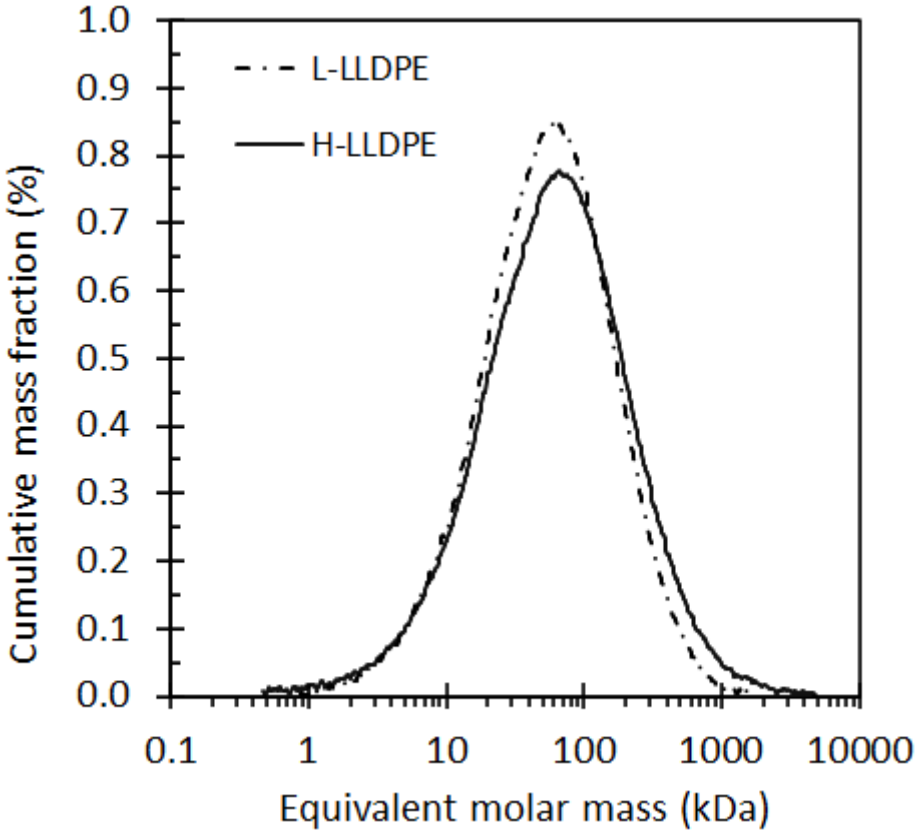

Figure C.2: Molecular mass distribution of L-LLDPE and H-LLDPE

Table C.2: Composition and molecular mass distribution of the F-T waxes and LLDPE are summarized

Sample	M (Da)	M_n (Da)	PDI
L-Wax	493	490	1.00
H-Wax	786	776	1.01
L-LLDPE	92390	26460	3.49
H-LLDPE	129100	23530	5.49

*PDI - dispersity

FOURIER TRANSFORM INFRARED SPECTROSCOPY

METHOD

To study the chemical composition and possibility of oxidation of the waxes attenuated total reflectance (ATR) Fourier transform infrared (FT-IR) spectroscopy using a Perkin-Elmer Spectrum 100 spectrometer in the wavelength region of between 550 and 3200 cm^{-1} was used. The instrument resolution was set on 4 cm^{-1} with a data interval of 1 cm^{-1}. The instrument is fitted with a MIR source, optical KBr beamsplitter and windows and a $LiTaO_3$ source.

RESULTS

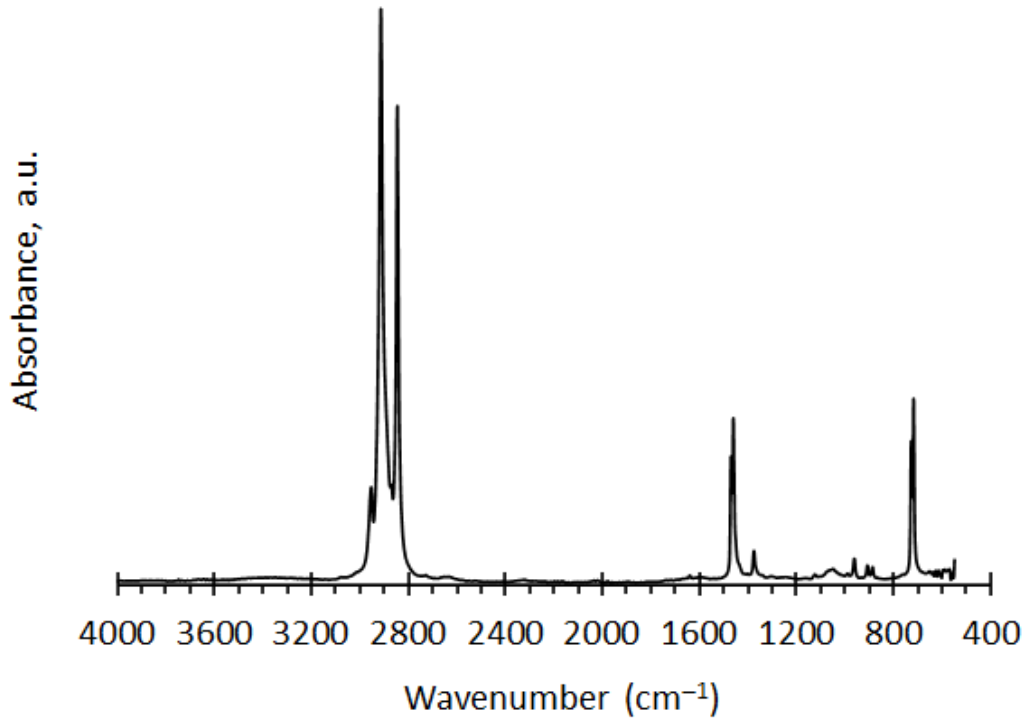

Figure C.3: FTIR spectrum of L-Wax

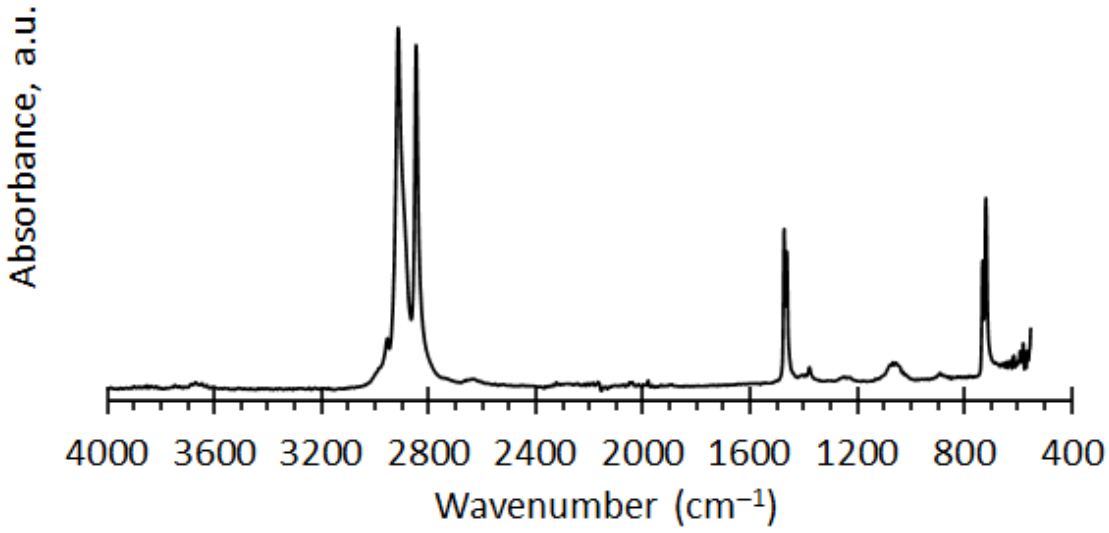

Figure C.4: FTIR spectrum of H-Wax

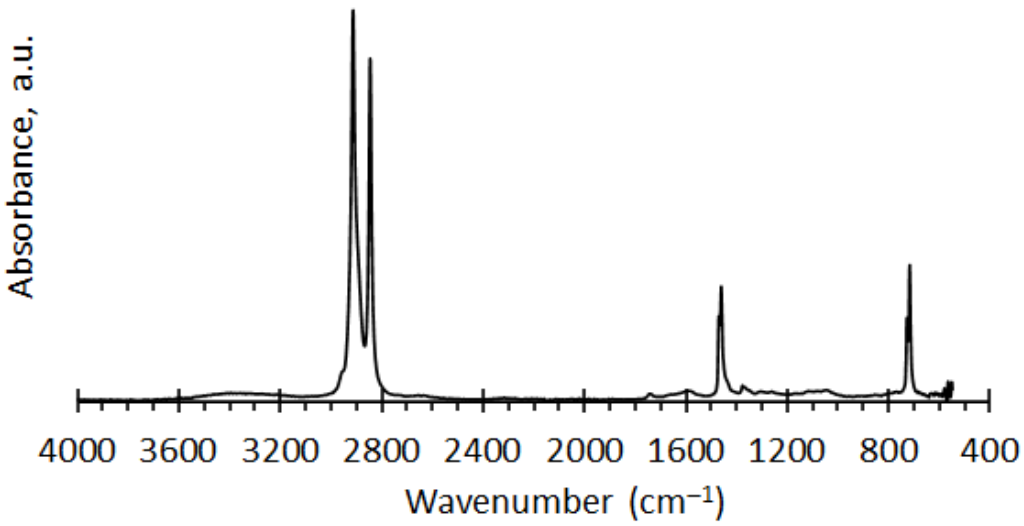

Figure C.5: FTIR spectrum of L-LLDPE

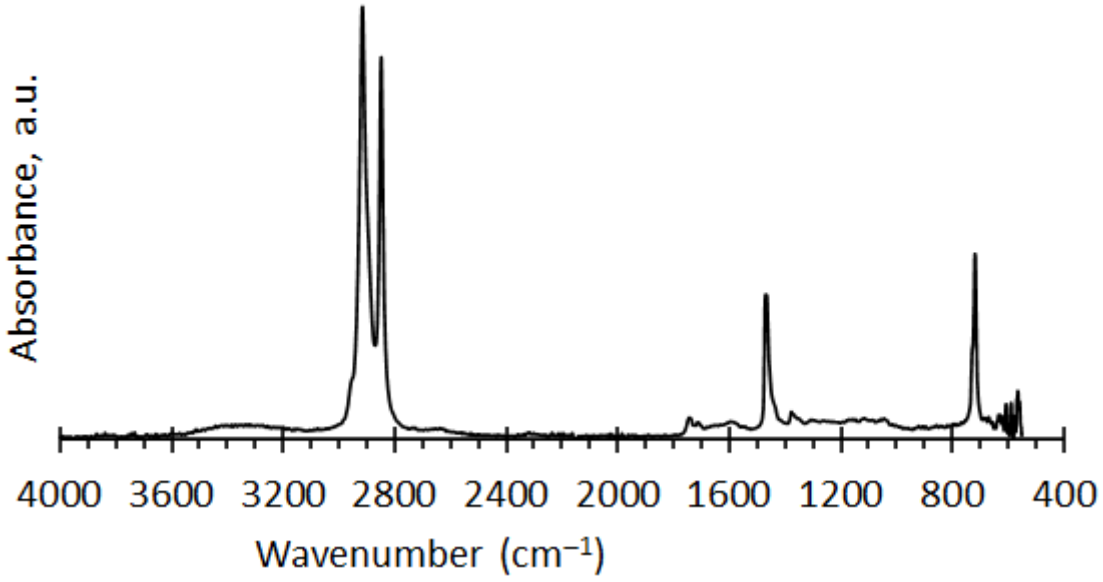

Figure C.6: FTIR spectrum of H-LLDPE

THERMOGRAVIMETRIC ANALYSIS

METHOD

The wax samples were subjected to thermogravimetric analysis in an inert atmosphere of nitrogen. The thermograms were obtained at heating rates 10 °C min^{-1} up to 600 °C, 50 ml min^{-1} N_2 flow rate, to avoid unwanted oxidation of the sample. An average mass range of 10-20 mg was used in this study.

RESULTS

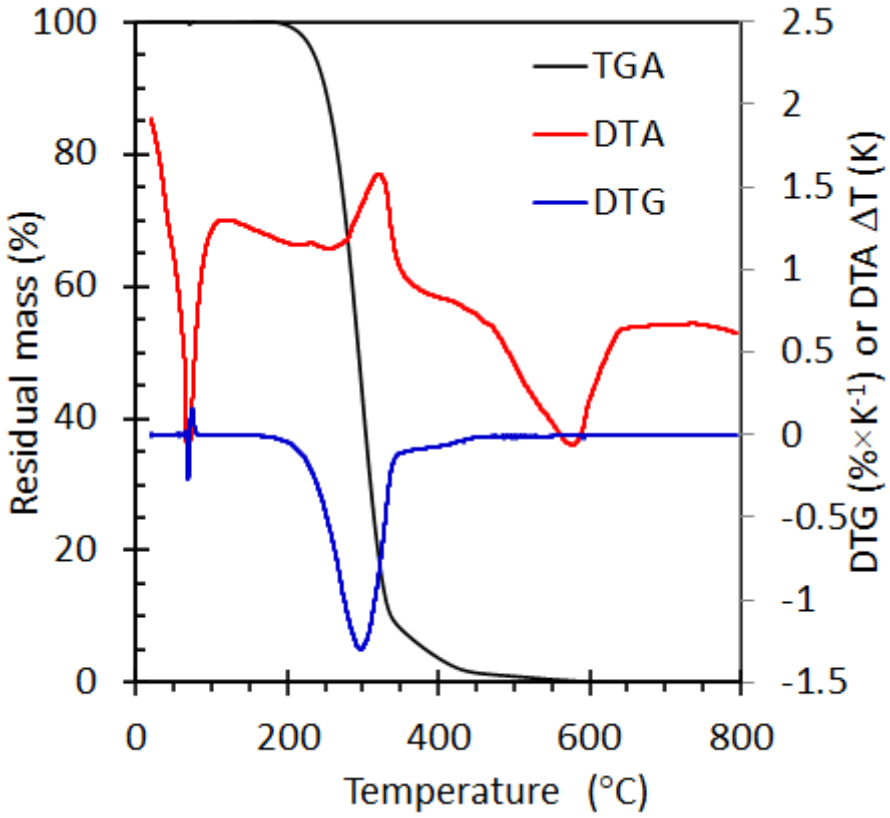

Figure C.7: TGA analysis in nitrogen atmosphere of L-Wax

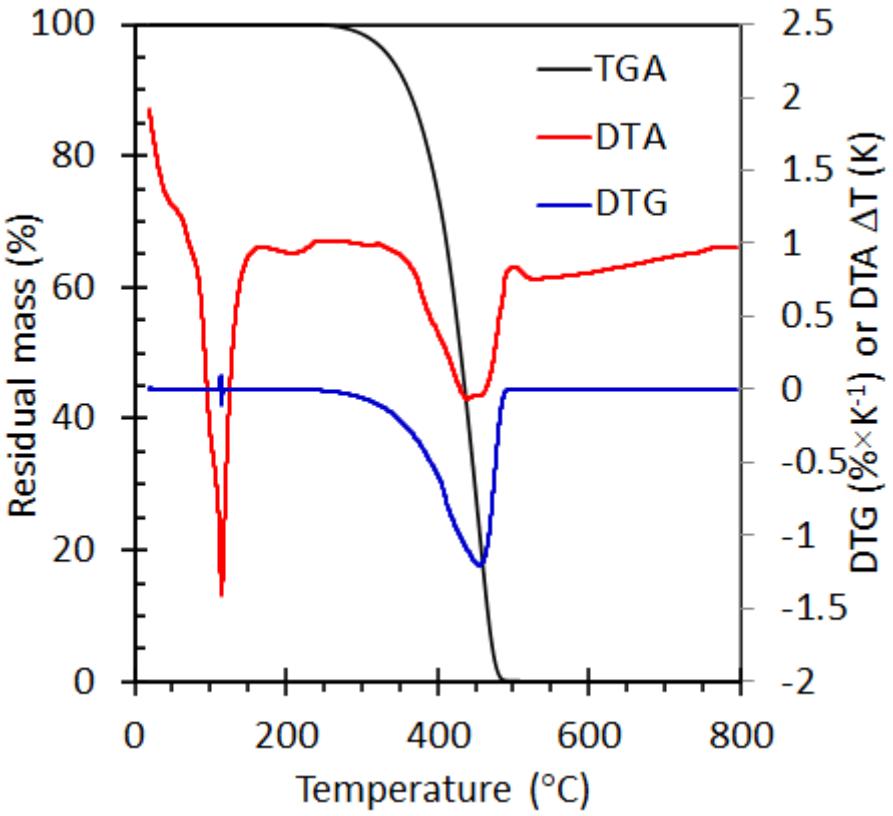

Figure C.8: TGA analysis in nitrogen atmosphere of H-Wax

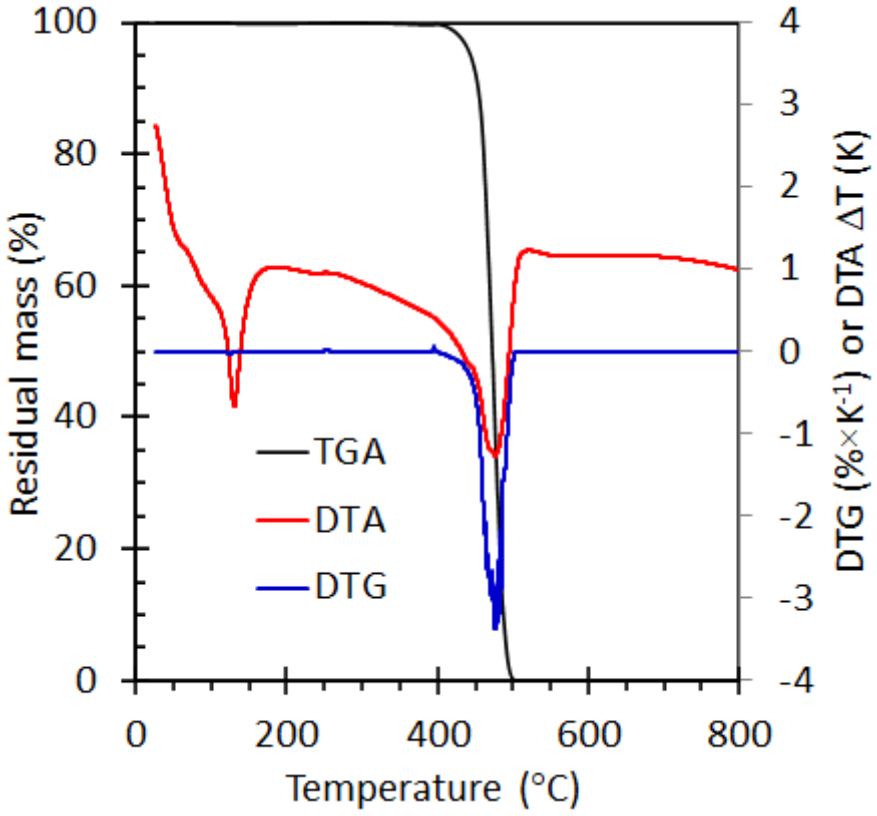

Figure C.9: TGA analysis in nitrogen atmosphere of L-LLDPE

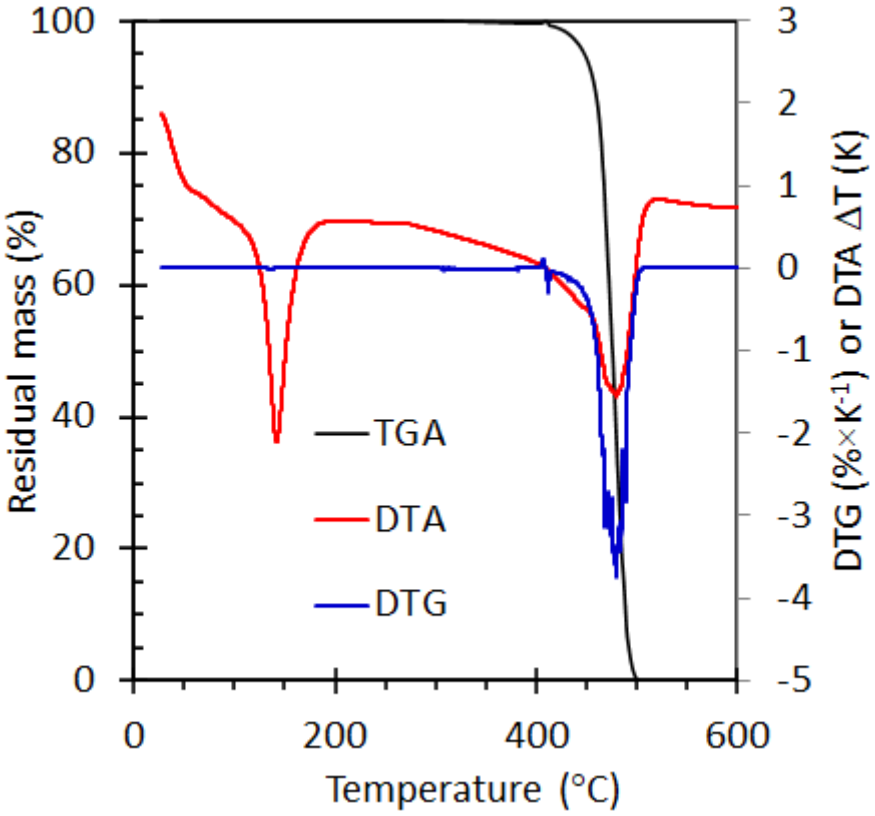

Figure C.10: TGA analysis in nitrogen atmosphere of H-LLDPE

Table C.3: Thermal stability of the neat waxes in terms of 5 %, 50 % and maximum degradation temperatures

Wax sample	$T_{5\ \%}$ (°C)	$T_{50\ \%}$(°C)	T_{max} (°C)
L-Wax	235.4	294.0	299.2
H-Wax	337.4	430.3	459.1
L-LLDPE	355.2	445.0	470.1
H-LLDPE	320.9	424.3	453.0

APPENDIX D: FORMULA DERIVATIONS

Effect of molar mass on zero-shear viscosity of wax/LLDPE melts

Consider blends of compounds of similar chemical structure. The only difference is in the length of the molecules involved. Combinations of hydrocarbon waxes, e.g., Fischer-Tropsch waxes and polyethylene are a good example. At low molar mass, the melt viscosity increases linearly with molar mass. This applies to the wax. Therefore

$$\eta_{o,w} = K_w M_w \tag{1}$$

Above a critical molar mass, the polymer chains become entangled and the zero-shear melt viscosity increases with the 3.4th power of weight-average molar mass (Bernard and Noolandi, 1982). This applies to the LLDPE. Therefore:

$$\eta_{o,p} = K_p M^{\alpha} \tag{2}$$

where the exponent takes on a universal value of α = 3.4.

The weight average molar mass of a blend is given by:

$$M = w_w M_w + w_p M_p \tag{3}$$

where w_w and w_p represent the weight fractions wax and polymer respectively in the binary blend.

The following constraint applies:

$$w_w + w_p = 1 \tag{4}$$

If a blend of two low molar mass compounds is considered, combination of equation (1) with equation (3) leads to the following mixing rule, which should apply if one mixes two waxes:

$$\eta = w_1\eta_1 + w_2\eta_2 \tag{5}$$

If, instead a blend of two polymers are considered, combining equation (2) and (3) leads to the Friedman and Porter (1975) mixing rule:

$$\eta = \left(w_1\eta_1^{1/\alpha} + w_2\eta_2^{1/\alpha} \right)^{\alpha} \tag{6}$$

Note that this is equivalent to a weighted power-mean of order $p = 1/\alpha$. For the wax/polymer blends, the temperature dependence of Equation (6) was “removed” or at least “diminished” by scaling with the viscosity of the neat polymer:

Different, more general approach:

$$M = w_1M_1 + w_2M_2 \tag{7}$$

with $\eta_1 = K_1M_1^{\beta}$ and $\eta_2 = K_2M_2^{\alpha}$ (8)

$$M = w_1\left(\frac{\eta_1}{K_1}\right)^{\frac{1}{\beta}} + w_2\left(\frac{\eta_2}{K_2}\right)^{\frac{1}{\alpha}} \tag{9}$$

At concentrations approaching pure component 1 the viscosity of the blend should follow a dependence that approaches the dependence defined by component 1:

$$\left(\frac{\eta}{K_2}\right)^{\frac{1}{\alpha}} = w_1\left(\frac{\eta_1}{K_1}\right)^{\frac{1}{\beta}} + w_2\left(\frac{\eta_2}{K_2}\right)^{\frac{1}{\alpha}} \tag{10}$$

$$\eta = K_2 \left[w_1 \left(\frac{\eta_1}{K_1} \right)^{\frac{1}{\beta}} + w_2 \left(\frac{\eta_2}{K_2} \right)^{\frac{1}{\alpha}} \right]^{\alpha} \tag{11}$$

At concentrations approaching pure component 2 the viscosity of the blend should follow a concentration dependence that approaches that of component 2. By analogy to equation (11):

$$\eta = K_1 \left[w_1 \left(\frac{\eta_1}{K_1} \right)^{\frac{1}{\beta}} + w_2 \left(\frac{\eta_2}{K_2} \right)^{\frac{1}{\alpha}} \right]^{\beta} \tag{12}$$

The two limiting forms can be combined as a weighted power mean in order to define the viscosity trend. A power-mean of order p = 1 corresponds to the arithmetic mean:

$$\eta = w_1 K_1 \left[w_1 \left(\frac{\eta_1}{K_1} \right)^{\frac{1}{\beta}} + w_2 \left(\frac{\eta_2}{K_2} \right)^{\frac{1}{\alpha}} \right]^{\beta} + w_2 K_2 \left[w_1 \left(\frac{\eta_1}{K_1} \right)^{\frac{1}{\beta}} + w_2 \left(\frac{\eta_2}{K_2} \right)^{\frac{1}{\alpha}} \right]^{\alpha} \tag{13}$$

Note that the terms in the square brackets are equal to the weight average molar mass of the blends. Simplifying:

$$\eta = w_1 K_1 M^{\beta} + w_2 K_2 M^{\alpha} \tag{14}$$

Note that, if the exponents and the constants K_i are the same, equation (14) reduces to either equation (5) or equation (6) depending on the value of the exponents.

Proof:

$$\eta = w_1 K_1 M^{\beta} + w_2 K_2 M^{\alpha} = w_1 K M^{\alpha} + w_2 K M^{\alpha} = \left(w_1 + w_2 \right) K M^{\alpha} = K M^{\alpha}$$

From equation (9): $M = w_1\left(\frac{\eta_1}{K}\right)^{\frac{1}{\alpha}} + w_2\left(\frac{\eta_2}{K}\right)^{\frac{1}{\alpha}}$

$$\eta = KM^{\alpha} = K\left[w_1\left(\frac{\eta_1}{K}\right)^{\frac{1}{\alpha}} + w_2\left(\frac{\eta_2}{K}\right)^{\frac{1}{\alpha}}\right]^{\alpha} = \left(w_1\eta_1^{\frac{1}{\alpha}} + w_2\eta_2^{\frac{1}{\alpha}}\right)^{\alpha}$$

Substituting the K_i values using equation (8) yields the general mixing rule:

$$\eta = w_1\eta_1\left(\frac{M}{M_1}\right)^{\beta} + w_2\eta_2\left(\frac{M}{M_2}\right)^{\alpha} \qquad (15)$$

Applied to the present situation, let the wax be represented by component 1 and the polymer by component 2. Then it follows that β = 1 and α = 3.4

$$\eta = w_w\eta_w\left(\frac{M}{M_w}\right) + w_p\eta_p\left(\frac{M}{M_p}\right)^{3.4} \qquad (16)$$

Data was generated at three different temperatures, i.e., 160 °C, 170 °C and 180 °C. Viscosity is a strong function of temperature. Therefore, in order to suppress the temperature dependence, the experimental data was plotted as η/η_0:

$$\frac{\eta}{\eta_p} = w_w\left(\frac{\eta_w M}{\eta_p M_w}\right) + w_p\left(\frac{M}{M_p}\right)^{3.4} \qquad (17)$$

The figure shows that the fully predictive equation (17) provided a good fit of the experimental data trends.

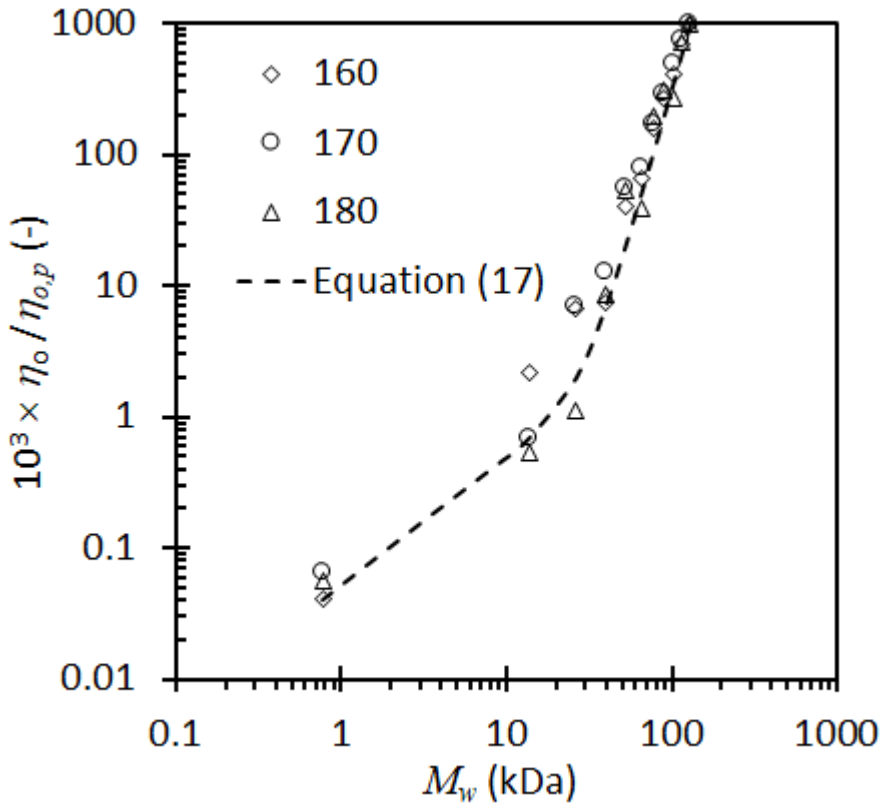

Figure: Test of the novel zero-shear viscosity mixing rule for F-T wax/LLDPE blends. The data were generated at temperatures of 160 °C, 170 °C and 180 °C.

Notes:

Critical molar mass

At the critical molar mass (M_c), equation (1) and equation (2) predict the same zero-shear viscosity. This condition links the values of the two viscosity constants:

$$K_w = K_p M_c^{\alpha-1} \tag{18}$$

It is sometimes stated that the critical molar mass is a fixed quantity. If that is indeed the case, it implies that the ratio K_w/K_p is temperature independent.

Athermal mixtures of chemically dissimilar polymers

It is expected that Equation (15) should also hold for blends of two polymers of different chemistry provided the unlike interactions and like interactions are the same:

$$\eta = \left(\frac{w_1 \eta_1}{M_1^{\alpha}} + \frac{w_2 \eta_2}{M_2^{\alpha}} \right) M^{\alpha} \tag{19}$$

or

$$\eta = \left(w_1 \eta_1 M_2^{\alpha} + w_2 \eta_2 M_1^{\alpha} \right) \left(\frac{M}{M_1 M_2} \right)^{\alpha} \tag{20}$$

Power mean

$$\eta = w_1 \left[\left(K_1 M^{\beta} \right)^p + w_2 \left(K_2 M^{\alpha} \right)^p \right]^{1/p}$$

$$\eta = \left[w_1 \left(\eta_1 \left(\frac{M}{M_1} \right)^{\beta} \right)^p + w_2 \left(\eta_2 \left(\frac{M}{M_2} \right)^{\alpha} \right)^p \right]^{1/p}$$

Simple mixing rules proposed for liquid viscosity

Grunberg and Nissan (1949) model: $\ell n \eta = w_1^2 \ell n \eta_1 + 2 w_1 w_2 \ell n \eta_{12} + w_2^2 \ell n \eta_2$

Hind et al. (1960) model: $\eta = \eta_1 w_1^2 + 2 \eta_{12} w_1 w_2 + \eta_2 w_2^2$

Combining rules provides a way to express binary parameters in terms of pure component properties. Consider the following possibilities for these models:

Linear combining rule: $\eta_{12} = (\eta_1 + \eta_2)/2$

Geometric combining rule: $\eta_{12} = \sqrt{\eta_1 \eta_2}$

Harmonic combining rule: $\eta_{12} = 1/\left(1/\eta_1 + 1/\eta_2\right)$

Sotomayor et al. (2014) studied blends of high-density polyethylene with a soft paraffin wax. They assumed the Grunberg and Nissan model with combining rule

$$\ln \eta_{12} = \left(\ln \eta_1 + \ln \eta_2\right)/2$$

Substituting in the Grunberg-Nissan model:

$$\begin{aligned}
\ell n \eta &= w_1^2 \ell n \eta_1 + 2 w_1 w_2 \ell n \eta_{12} + w_2^2 \ell n \eta_2 \\
&= w_1^2 \ell n \eta_1 + w_1 w_2 \left(\ln \eta_1 + \ln \eta_2\right) + w_2^2 \ell n \eta_2 \\
&= w_1^2 \ell n \eta_1 + w_1 w_2 \ln \eta_1 + w_1 w_2 \ln \eta_2 + w_2^2 \ell n \eta_2 \\
&= w_1 \left(w_1 + w_2\right) \ln \eta_1 + w_2 \left(w_1 + w_2\right) \ell n \eta_2 \\
&= w_1 \ln \eta_1 + w_2 \ell n \eta_2
\end{aligned}$$

“Ideal” viscosity

$$\ell n \eta = w_1 \ln \eta_1 + w_2 \ell n \eta_2$$

$$\eta = \eta_1^{w_1} \eta_2^{w_2}$$

$$\Delta \eta = \eta - \eta_1^{w_1} \eta_2^{w_2}$$

where η is the measured viscosity and η_1 and η_2 are the viscosities of the pure components 1 and 2, respectively.

To get rid of the temperature dependence, a normalized expression can be used:

$$\frac{\Delta \eta}{\eta_1^{w_1} \eta_2^{w_2}} = \frac{\eta}{\eta_1^{w_1} \eta_2^{w_2}} - 1$$

Theoretically, if the Friedman and Porter (1975) model applies, the experimental data should track the following expression

$$\Delta\eta = \left(w_1\eta_1^{1/\alpha} + w_2\eta_2^{1/\alpha}\right)^{\alpha} - \eta_1^{w_1}\eta_2^{w_2}$$

$$\frac{\Delta\eta}{\eta_1^{w_1}\eta_2^{w_2}} = \frac{\left(w_1\eta_1^{1/\alpha} + w_2\eta_2^{1/\alpha}\right)^{\alpha}}{\eta_1^{w_1}\eta_2^{w_2}} - 1$$

$$\Delta\eta \Big/ \left(\eta_1^{w_1}\eta_2^{w_2}\right)$$

Problem: We were unable to measure the pure wax viscosity! So, it had to be estimated assuming the same activation energy holds

Derivation of the Lederer model

(Lederer, 1931) model:

$$\ell n\eta = \frac{x_1}{x_1 + ax_2}\ell n\eta_1 + \frac{ax_2}{x_1 + ax_2}\ell n\eta_2$$

From $w_1 = \frac{M_1 x_1}{M_1 x_1 + M_2 x_2}$ $w_2 = \frac{M_2 x_2}{M_1 x_1 + M_2 x_2}$ $M = M_1 x_1 + M_2 x_2$

$$w_1 = \frac{M_1 x_1}{M_1 x_1 + M_2 x_2}$$
$$w_1 M_1 x_1 + w_1 M_2 (1 - x_1) = M_1 x_1$$
$$w_1 M_1 x_1 + w_1 M_2 - x_1 w_1 M_2 = M_1 x_1$$
$$M_1 x_1 + x_1 w_1 M_2 - w_1 M_1 x_1 = w_1 M_2$$
$$(M_1 + w_1 M_2 - w_1 M_1) x_1 = w_1 M_2$$
$$x_1 = \frac{w_1 M_2}{M_1 + w_1 M_2 - w_1 M_1}$$
$$x_1 = \frac{w_1 M_2}{M_1 (w_1 + w_2) + w_1 M_2 - w_1 M_1}$$
$$x_1 = \frac{w_1 M_2}{w_1 M_2 + w_2 M_1}$$

Therefore: $x_1 = \frac{w_1 M_2}{w_1 M_2 + w_2 M_1}$ and $x_2 = \frac{w_2 M_1}{w_1 M_2 + w_2 M_1}$

$$\frac{x_1}{x_1 + a x_2} = \frac{\frac{w_1 M_2}{w_1 M_2 + w_2 M_1}}{\frac{w_1 M_2}{w_1 M_2 + w_2 M_1} + \frac{a w_2 M_1}{w_1 M_2 + w_2 M_1}} = \frac{w_1 M_2}{w_1 M_2 + a w_2 M_1} = \frac{w_1}{w_1 + a \frac{M_1}{M_2} w_2}$$

$$a x_2 = \frac{w_2 a M_1}{w_1 M_2 + w_2 M_1}$$

$$\frac{a x_2}{x_1 + a x_2} = \frac{\frac{w_2 a M_1}{w_1 M_2 + w_2 M_1}}{\frac{w_1 M_2}{w_1 M_2 + w_2 M_1} + \frac{w_2 a M_1}{w_1 M_2 + w_2 M_1}} = \frac{w_2 a M_1}{w_1 M_2 + w_2 a M_1} = \frac{w_2 \frac{a M_1}{M_2}}{w_1 + w_2 \frac{a M_1}{M_2}}$$

Define $aM_1/M_2 = b$, then the Lederer equation can be recast to look the same in mass fractions:

$$\ell n \eta = \frac{w_1}{w_1 + b w_2} \ell n \eta_1 + \frac{b w_2}{w_1 + b w_2} \ell n \eta_2$$